Fall 2012

Development and demonstration of an automated method for deriving novel morphometric indices of cerebral aneurysms

Benjamin Micah Berkowitz
University of Iowa

DEVELOPMENT AND DEMONSTRATION OF AN AUTOMATED METHOD FOR DERIVING NOVEL MORPHOMETRIC INDICES OF CEREBRAL ANEURYSMS

by

Benjamin Micah Berkowitz

A thesis submitted in partial fulfillment
of the requirements for the Master of
Science degree in Biomedical Engineering
in the Graduate College of
The University of Iowa

December 2012

Thesis Supervisor: Professor Madhavan L. Raghavan

Graduate College
The University of Iowa
Iowa City, Iowa

CERTIFICATE OF APPROVAL

MASTER'S THESIS

This is to certify that the Master's thesis of

Benjamin Micah Berkowitz

has been approved by the Examining Committee
for the thesis requirement for the Master of Science
degree in Biomedical Engineering at the December 2012 graduation.

Thesis Committee: _____
Madhavan Raghavan, Thesis Supervisor

_____
Joseph Reinhardt

_____
Krishnan Chandran

_____
Gary Christensen

_____
Sarah Vigmostad

To my family.

ACKNOWLEDGMENTS

I would like to thank first and foremost my advisor, Dr. M.L. Raghavan. He has provided me with a fantastic opportunity to expand my mind and professional capabilities through his lab's research. This research was supported by funding from the NIH/NHLBI grant #HL083475 to Dr. Raghavan.

Additionally, I would like to thank my committee members for setting aside their time and for providing their advice. Dr. Luca Antiga, who tirelessly assisted with the implementation of VMTK in my project, and Dr. Marina Piccinelli for assisting with the implementation of the parent vessel reconstruction algorithm, also deserve my thanks. I would also like to thank Dr. Bob Harbaugh, Dr. David Hasan, Dr. Christopher Ogilvy, Dr. Robert Rosenwasser, and Dr. Manasi Ramachandran for assistance with patient recruitment; Ben Dickerhoff, Kevin Johnson, and Steve Lin for their help with performing isolations; and Rohini Retarekar and Dr. Ryan Amelon for their frequent philosophical assistance.

Most of all, I would like to thank my friends and family for supporting me through my education, from pre-school to graduate school. I couldn't have done it without them.

ABSTRACT

Cerebral aneurysm rupture is a major cause of death and permanent disability. Rupture rate, however, is low; therefore, a physician must weigh the risk of rupture against treatment risk. In order to help physicians determine the rupture risk of any particular case, studies have previously explored morphology as an indicator for mechanical and hemodynamic characteristics of rupture-prone aneurysms. Morphological characteristics of the aneurysms in these studies are often quantified with morphometric indices, or normalized measures of specific geometric traits. This study introduces several novel morphometric indices. These include tissue stretch ratio, which characterizes the amount of deformation which aneurysm tissue may have undergone; neck-to-vessel ratio, which may have hemodynamic implications and is derived from the ratio of the diameter of the ostium to the diameter of the parent vessel; ellipticity index, which may indicate increased wall tension due to an elliptical shape; and non-sphericity index, which may indicate the presence of stress concentrations due to a non-spherical shape. In order to extrapolate these morphological measures, the aneurysm must first be separated from the parent vasculature. A novel method for aneurysm sac isolation is presented, which uses an approximation of the healthy parent vessel to remove all non-aneurysmal portions of a vascular model. This approach results in a more complete extraction of the aneurysm geometry than is possible using previous standard techniques. The repeatability of the isolation process is analyzed, as well as mesh-independence and the agreement of the resulting aneurysm sac model to a known geometry.

TABLE OF CONTENTS

LIST OF TABLES

LIST OF FIGURES

CHAPTER 1

BACKGROUND AND INTRODUCTION

Cerebral Aneurysm

Cerebral aneurysms are a relatively common condition with a prevalence of approximately 3.6 to 6 percent in the general population. Although aneurysm rupture occurs in only approximately 1.9 percent for those patients presenting with an aneurysm (Rinkel et al., 1998), the risk of short-term death from the associated hemorrhage upon rupture is high (10 to 20 percent). An additional number (12 to 30 percent) never recover from the initial bleed (Hop et al., 1997).

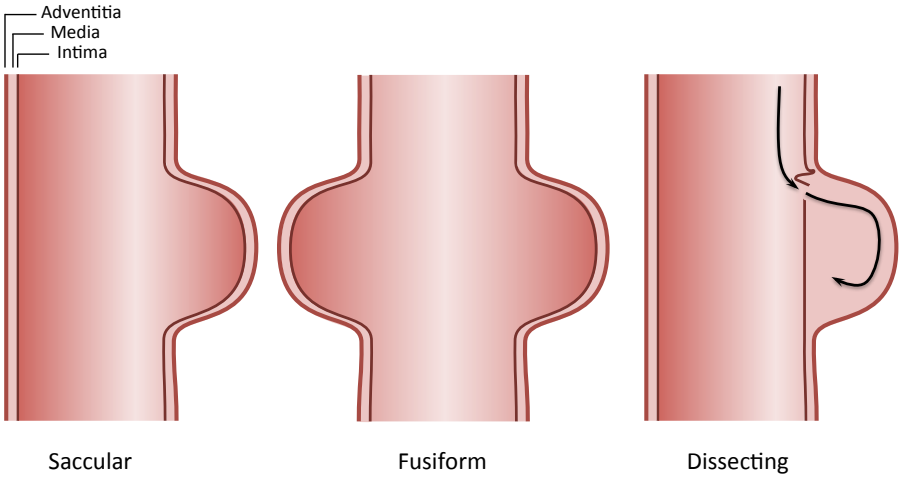

Figure 1. Types of cerebral aneurysms

Cerebral aneurysms are characterized by a ballooning of the arterial wall outward from the original lumen volume. Approximately 90 percent of all cerebral aneurysms occur in a saccular form (Vega et al., 2002), and more rarely in a fusiform or dissecting manner, as shown in Figure 1. Saccular aneurysms, which will be focused upon in this work, form as a consequence of a weakening of the internal elastic lamina. The exact

etiology of any particular cerebral aneurysm's formation varies from case to case. However, hereditary traits (including Marfan syndrome, previous familial occurrence, and female gender) and acquired risk factors (such as age over 50 years, tobacco use, and hypertension) may indicate a higher risk for aneurysm manifestation (Vega et al., 2002).

Treatment Options

Four clinical options currently exist for aneurysm patients including three treatment methods, or long-term clinical observation. Traditionally, the most common treatment procedure has been surgical clipping of the aneurysm neck, which involves a craniotomy to access the affected vessel. Complication risk is a concern because of the invasiveness of the surgery, which will naturally exclude many patients from this treatment option. However, given an eligible patient the surgery is generally very effective, with complete occlusion rates reported around 93% (Raftopoulos et al., 2003).

The growing treatment of choice in recent years is endovascular coil embolization. The first endovascular coiling device approved by the FDA for general use was the Guglielmi detachable coil in 1991 (Guglielmi et al., 1991). This is an outpatient procedure that has relatively low associated complication risk and a short recovery period. The International Subarachnoid Aneurysm Trial (ISAT), a European study involving 2,143 patients across 42 neurosurgical centers, found that endovascular coiling provided absolute risk reduction of 6.9% and relative risk reduction of 22.6% over surgical clipping in risk of death or dependence (van den Berg et al., 2003). However, endovascular coiling outcomes are highly dependent on aneurysm sac geometry. Studies have shown that the rate of complete aneurysm occlusion is anywhere from 75-85% with initial treatment and aneurysm sac recanalization and continued growth occurs in 22-42% of endovascular coil-treated cases (Grunwald et al., 2007; Sluzewski et al., 2003). Treatment with endovascular coils by nature requires that an aneurysm exhibit a neck of smaller diameter than the main body of the aneurysm sac. In one study, a significant

increase in operative success with a sac-to-neck ratio of 2 to 1 was shown (Gonzalez et al., 2008). However, interventionists have also conceived ad-hoc solutions in order to treat cases with sub-optimal geometry, such as using the technique known as stent-assisted coiling. In this technique a stent is placed through the parent lumen beneath an aneurysm sac and in numerous configurations in terminal aneurysms in order to allow for successful treatment of wide-necked aneurysms (Wakhloo et al., 1998).

Flow diverters are a more recent development for cerebral aneurysm treatment. Arterial stents, such as those used in conjunction with cerebral aneurysm coils or to maintain patency of an atherosclerotic artery had previously been observed to occlude aneurysms by diverting flow away from the aneurysm sac (Wakhloo et al., 1994). Flow diverters take this idea beyond the observation of this phenomenon and bring it to clinical use. The mesh porosity is optimized for use specifically to occlude cerebral aneurysms while maintaining patency of perforating and branching arteries that are covered by the device. These devices are very new to the market having been approved in mid-2011, and are only indicated for the treatment of large or giant aneurysms located on specific portions of the internal carotid artery (ICA) (Federal Drug Administration, 2011). This, unfortunately, precludes treatment of a large number of patients.

For many cerebral aneurysm patients, considering their poor health and age, there is a large enough risk for complication that even endovascular treatment is not an option. Therefore, a fourth option of clinical observation and management is presented to patients upon clinical consultation. The treating physician will recommend this based on his or her clinical opinion, in which statistical risk of complication from treatment is weighed against statistically predicted rupture risk based on size and aneurysm location. Observation will likely be recommended to patients for whom risk of rupture is higher than risk from treatment (Wiebers, 2003). These patients will return on a semi-annual or annual basis for clinical follow-up and image-based evaluation to assess the aneurysm for signs of growth.

Studies on Factors of Rupture Risk

The risk associated with surgery or intervention is not only present for elderly and complication-prone patients, but for all patients who would undergo treatment. Therefore the capability to accurately discern an inherently low-risk aneurysm from one that may shortly rupture is crucial.

The International Study of Unruptured Intracranial Aneurysms (ISUIA) was conducted to assess the risk of rupture in relation to certain concurrent factors. The ISUIA was conducted beginning in 1991 and followed 5,500 cerebral aneurysm patients over the course of the following 10 years. This study found that several factors contribute significantly to rupture risk, namely aneurysm location on the posterior circulation and increasing risk with size (Wiebers, 2003, 2006).

Given the answers provided by the ISUIA study, questions still persist. It is currently unknown why, although generally considered low risk, aneurysms of small sizes are still seen to rupture (Villablanca, 2002). Additionally, some risk factors simply cannot be measured on a patient-by-patient basis. For instance, direct blood pressure is a measure that would give insight into the stress that an aneurysm dome sees given its geometry. Although a clinical systemic blood pressure measurement is available for most patients, these measurements are somewhat uninformative because of the fact that blood pressure can change rapidly and frequently for any person given his or her current activity level (Bowker et al., 2010). Studies have also been performed to characterize pressures within specific arteries throughout the cerebral circulation in relation to systemic blood pressure. These measurements were derived from flow phantoms constructed using population-average artery diameter measurements (Cieslicki et al., 2005). However, ascertaining the range of activity level and the resulting blood pressure change for any specific patient, especially the hundreds or thousands of patients included in some of the previously mentioned studies would be nearly impossible.

Tissue thickness of an aneurysm is a measurement that might give insight into weaknesses of an aneurysm wall that could lead to rupture, but is also generally immeasurable from image data. Tissue thickness of an aneurysm dome ranges from 16 to 400 μm (Kadasi et al., 2012). Because even the thickest tissue in this range is on the order of only one voxel with standard computed tomography (CT) and magnetic resonance imaging (MRI), it is unlikely that any information about the thickness of an aneurysm dome can be measured in-vivo using conventional medical imaging techniques, and therefore is another limitation in evaluating rupture risk in any large clinical study.

Previous Morphological Studies

Although location-based and size-related risk factors have been shown to correlate well with cerebral aneurysm rupture risk, cases of exception are still seen on a somewhat widespread basis. In order to explain these cases, other clinical treatment indicators such as geometric factors have been explored as well. Early studies explored simple morphological factors. For instance in 1998, Hademenos et al. showed that the presence of multilobular geometry and neck size were significant discriminating factors for retrospectively determining ruptured versus unruptured aneurysms. Measurements were performed by hand on two-dimensional angiograms. Ujii et al., in 2001, measured aspect ratio by hand on two-dimensional angiogram. This was performed in a retrospective manner, and found that the aspect ratio demonstrated the ability to discriminate ruptured from unruptured aneurysms. In direct contrast to these studies, however, was the earlier study by Wiebers et al., published in 1981. This study took a prospective approach to data collection, and analyzed several of the same morphological indices again using hand measurements on two-dimensional angiograms. The differing conclusions of these studies opened the door for controversy, and many concurrent studies have also produced results that disagree with Wiebers' 1981 report.

With the introduction and common practice of three-dimensional imaging modalities, the possibilities for the in-depth analysis of the geometric features of cerebral aneurysms have subsequently increased dramatically. In 2004 and 2005, respectively, Ma et al. and Raghavan et al. introduced several shape parameters that take into consideration not only two-dimensional measurements or the presence of these shape features, but the gestalt sac geometry as well. The papers included new definitions for the derivation of measurements from three-dimensional aneurysm geometries, and morphological indices that provide a relative scale on which to quantify specific features of an aneurysm's geometry. Undulation Index (UI) was introduced as a descriptor of the undulation present in the dome of the aneurysm. It is computed by comparing the volume of the aneurysm to the volume of its convex hull (a similar geometry from which the concavities are removed). It was thought that these undulations could represent stress concentrations and weakened inhomogeneous regions within the aneurysm dome. Aspect Ratio (AR) was introduced to describe the ratio of the aneurysm neck to its height as measured perpendicularly from the neck plane. This was intended as one measure of an aneurysm's similarity of a shape to an elliptical geometry, which would indicate an inhomogeneous stress distribution leading to generally higher peak stresses than a spherical geometry. Ellipticity Index (EI) was another index seeking to measure the ellipticity of an aneurysm. It was measured from a ratio of the surface area to the volume, for which a sphere would produce a value of 0, and an elliptically shaped aneurysm producing an indicial value near 1. Nonsphericity Index (NSI) was introduced to describe the overall deviation from a spherical geometry. Similarly to Ellipticity Index it was measured from a ratio of surface area to volume, but differed in that these values were calculated from the aneurysm geometry directly. In this way, it combined non-spherical characteristics from elliptical shape as well as surface undulation. Conicity parameter was introduced to describe a potential measure of the location of growth of an aneurysm. The location of the cross-section of largest diameter was compared to the

midpoint from the neck to the maximal height. In this way if an aneurysm's largest cross section was located near to the neck, the growth would be assumed to be near to the neck; if the cross section were located near the top of the dome, the growth would be assumed to be near the top of the dome. Bottleneck factor (BF) was introduced as a potential indicator for increased hemodynamic abnormalities. It was calculated as the ratio of the maximum diameter of the aneurysm to the diameter of the neck. Several surface curvature-based indices were also introduced. In 2012, Ramachandran performed a prospective cohort study of these indices in which 198 aneurysms were collected and followed. Rupture did not occur in any of the aneurysms; however, physicians indicated 20 of the 198 aneurysms as grown or unstable. There was no significant difference found in the morphological index calculations between the stable and unstable groups.

In 2005, Banatwala et al. introduced the use of Legendre polynomials as a method for modeling an aneurysm surface in order to more generally obtain the surface curvature. Ma et al. showed in 2004 that the surface curvature of a surface mesh is highly affected by small mesh-based variations. To this effect, a Legendre polynomial model is meant to extract a more generalized shape from which to measure curvature. In 2007, Millán et al. demonstrated the use of geometric and Zernike moment invariants to characterize the geometry of aneurysms. In 2010, Rahman et al. found in a case-control study that the ratio between the aneurysm's largest diameter and its parent vessel diameter corresponded with rupture status. In 2008, Dhar et al. explored the relation between aneurysm to parent vessel angle and rupture risk and found correlation in retrospective data. In 2011, Yasuda et al. and Ryu et al. introduced volume-to-ostium ratio and volume-to-neck ratio, respectively, which were new hemodynamically-driven geometric measures of the ratio of the volume of the aneurysm sac to the surface area of the ostium that were shown to be as effective as aspect ratio in discriminating ruptured versus unruptured status aneurysms. In 2011, Lauric et al. described the use of the writhe number in discriminating ruptured and unruptured aneurysms. The writhe number, in this

case, was used to describe the symmetry of an aneurysm surface model, as well as the likelihood that all points on the aneurysm mesh are in mechanical equilibrium. In 2011, Lauric et al. also introduced the centroid-radii model. The centroid-radii model computes the distance from an aneurysm model's centroid to the points on its surface mesh, and subsequently computes its entropy. This model was able to discriminate between ruptured and unruptured aneurysms with reasonable accuracy. In 2012, Piccinelli et al. explored several novel methods for computationally obtaining measurements from aneurysm sacs, including the introduction of the Voronoi diagram core – a hypothetical representation of the largest and most stable portions of the aneurysm sac, a centerline-based sac diameter measurement, and best-fit ellipsoid.

In light of these studies, it would seem as though that despite the importance of aneurysm size in a clinical diagnostic decision, it is only one piece of the puzzle. It is conceivable as well that size, geometry, and orientation of an aneurysm all play a part in the complex interaction between hemodynamics and tissue solid mechanics that may contribute to the growth and rupture of cerebral aneurysms. Additionally, no conclusive evidence has been yet presented to prospectively correlate any morphological index except for size ratio. The importance of the prospective study of aneurysm rupture risk in relation to any index is important to show the predictive capabilities in clinic, and not only the ability of the index to discern ruptured from unruptured that is explored by retrospective studies.

Necessity of Automation

The limitations of image resolution inherent to current medical imaging capabilities in comparison to the feature size of cerebral aneurysms creates a certain amount of ambiguity in the segmentation of cerebral aneurysm geometries. This uncertainty is compounded by the fact that any individual user may choose different threshold levels, seed and target points for various segmentation algorithms, or leave out

entire portions of the surrounding vasculature based upon his or her perception of the important image features. Individual differences in feature perception are also seen when manually isolating aneurysm sacs from the parent vasculature.

A recent study showed that two reviewers who segmented and isolated the same patient image data would obtain slightly different results. In some cases, poor image quality contributed to large differences in final geometry following segmentation. In others, the ambiguous or non-planar nature of an aneurysm's neck plane also contributed greatly to variability of the isolated aneurysm sac between users (Ramachandran, 2012).

Because of the differences between user preferences, any choice that is determined using a computer-automated protocol removes the chance for human user-induced inconsistencies and bias. In order to address this, Piccinelli et al. (Piccinelli et al., 2012) attempted to automate the choice of clipping plane placement and orientation. After definition of the aneurysmal region and approximation of the original healthy parent vessel (Ford et al., 2009), an optimal cutting plane would be algorithmically chosen that successfully isolates the aneurysm sac. This automatic neck plane definition was found to successfully produce low inter-user variability.

Objectives

This work seeks to improve the tools and methods available to researchers in the search for morphological factors of cerebral aneurysms that contribute to risk of growth and rupture. The first specific area of the field of cerebral aneurysm research that this work seeks to improve is the automation of cerebral aneurysm sac isolation and morphological characterization. Secondly, this work aims to improve the capacity of aneurysm morphology by describing a more complete method for isolating the aneurysm sac. This new method should provide a more appropriate isolation than a clipping plane could provide. Third, in order to take advantage of the more complete aneurysm geometry provided by this new isolation technique, novel morphometric indices should

be developed. Finally, in order to provide evidence as to the extents to which these novel methods could improve this particular field of research, the efficacy of the isolation method and the morphological indices should be evaluated.

CHAPTER 2

ANEURYSM SAC ISOLATION

Geometric Data

In morphological studies of cerebral aneurysms involving patient-specific models, aneurysm and vascular geometry is generally obtained from medical imaging data via level-set segmentation techniques. Since segmentation was not the focus of this work, it will not be addressed in great detail. The experiments that were conducted included both patient-specific segmentations from CT and MR imaging and computer generated hypothetical models. Both sources of data are valid inputs to the isolation and analysis methods described in the following sections. For many of the subroutines within the software libraries used to process the geometric data, a triangular surface mesh is required. Therefore, the data involved in this study was meshed using triangular elements.

Key Concepts

Programming Environment

The algorithm outlined in this study was developed using the Python programming language, the Visualization Toolkit (VTK) framework and the Vascular Modeling Toolkit (VMTK). VTK is open-source software, programmed in C++, and nearly all of the classes in its library are available wrapped in Python. It is used mainly for visualization of medical and scientific data, and has classes for numerical data manipulation, image data visualization, mesh processing, and many other uses. VTK is widely used among the academic community due to its open nature, and many of its functions are based upon published work (Kitware, 2006). VMTK is open-source as well, and is built upon a foundation laid by VTK and the Insight Segmentation and Registration Toolkit (ITK). It is programmed using both Python and C++ languages,

with the main focus of its functionality on image segmentation and mesh processing of vascular structures.

Applications of the Voronoi Diagram

Much of the mesh processing functions within VMTK are focused upon triangular surface meshes. As opposed to tetrahedral volume meshes, triangular surface meshes reduce computational expense enormously. VMTK provides robust methods for surface mesh processing and analysis by utilizing the concept of the Voronoi diagram.

The Voronoi diagram forms the basis for robust meshing schemes and surface analysis methods. In VMTK, Voronoi diagrams are used to define medial axes, or centerlines, for blood vessels. It is simplest to think of this concept first in two dimensions. For any set of points P, it is possible to circumscribe subsets of three points from P so that all points are circumscribed and each circumcircle encloses no points not within of the subset. This is referred to as the Delaunay criterion. When each set of circumscribed points is connected in a triangle, the Delaunay tessellation is formed. Connecting the circumcenters of neighboring tessellated triangles forms the corresponding Voronoi diagram, as demonstrated in Figure 2 (Antiga, 2002).

A similar approach is utilized in three dimensions. Spheres are circumscribed about sets of three points in set P so that the Delaunay criterion is satisfied (analog in three dimensions to the dotted circles in Figure 2). These are referred to as Voronoi spheres. Additionally, because the three-dimensional Delaunay tessellation of a set of points will always results in a convex surface, a convex hull of a surface may be extracted in this manner (Antiga, 2002).

A Voronoi diagram by nature is defined in all space internal and external to a surface. In applications involving closed surfaces, an additional criterion is imposed so that all Voronoi spheres external to a surface (as defined by their relation to the surface normal) are not included in the construction of the Voronoi diagram. This internal

portion of the Voronoi diagram is referred to as the embedded Voronoi diagram as shown in Figure 3.

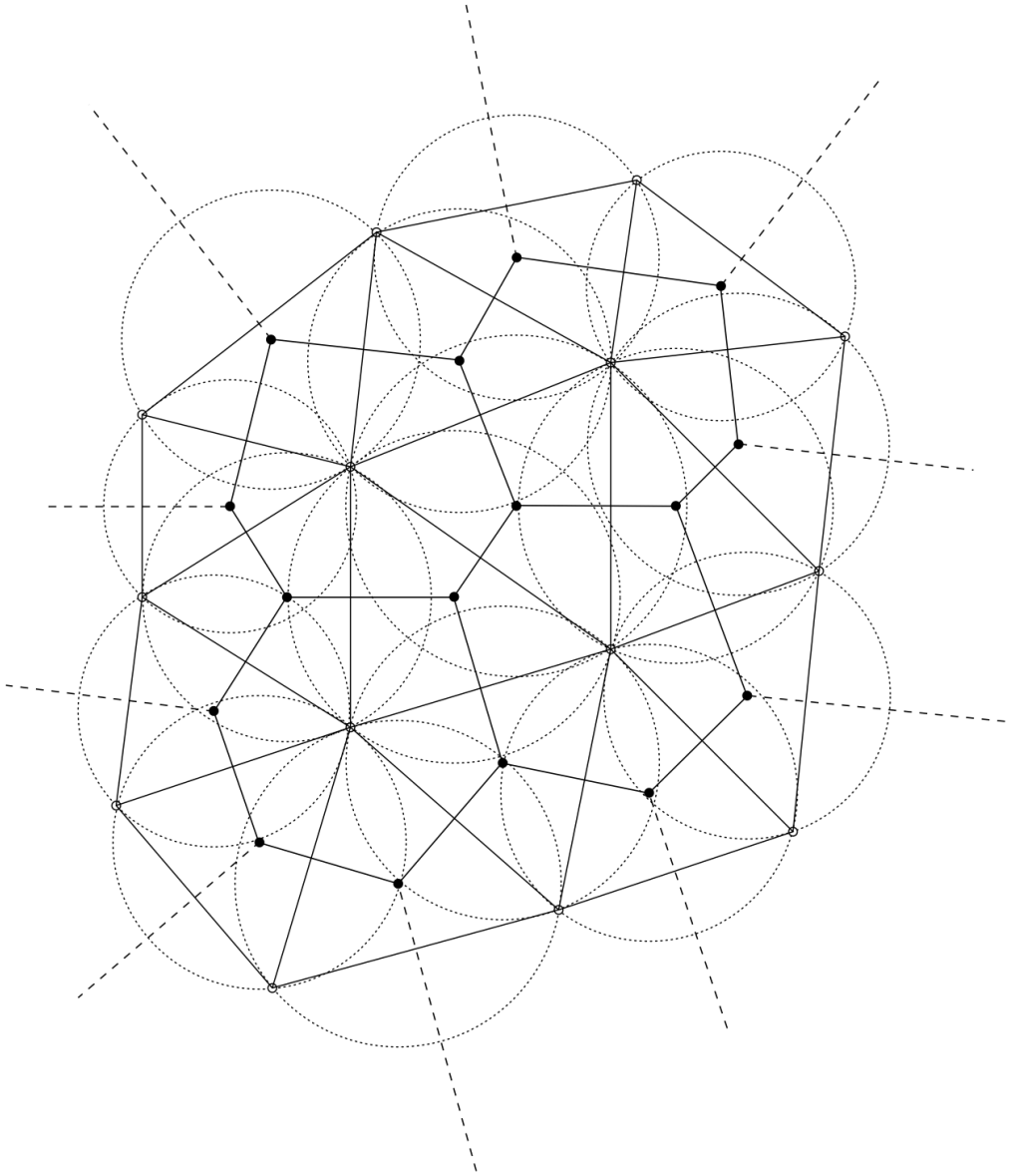

Figure 2. Demonstration of the Delaunay tessellation (thin lines), Voronoi diagram (thick lines), and Voronoi vertices (filled dots) of a point set P (open dots) and its circumcircles fitting the Delaunay criterion (dotted lines) (Antiga, 2002).

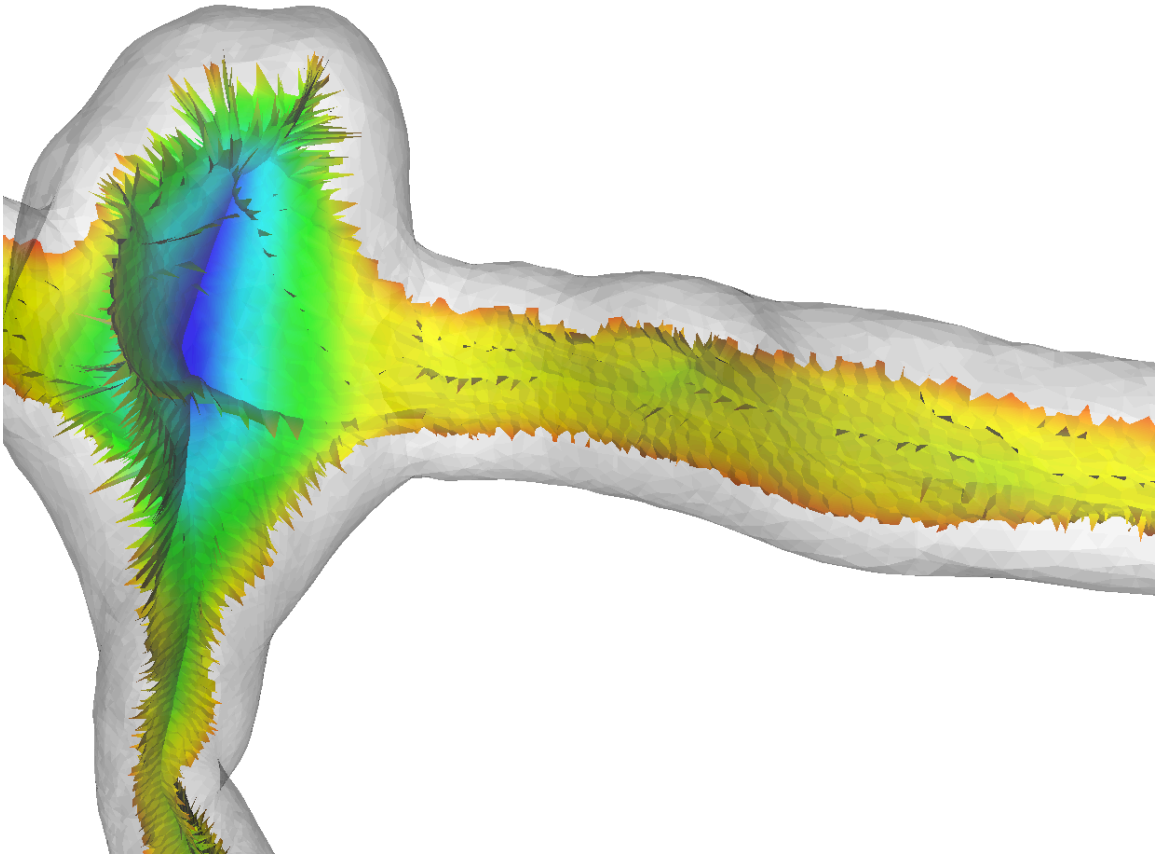

Figure 3. Embedded Voronoi diagram (colored) of a cerebral artery and aneurysm (transparent).

Voronoi Spheres

The Voronoi spheres of a closed surface, as an aggregate, form a structure similar to the original surface. Thus, in the same way, a surface can be constructed from a newly created or modified Voronoi sphere set. A three-dimensional point-sampling grid in conjunction with the implicit sphere functions of the Voronoi sphere set is then used to define a voxel grid. The zero-level can then be extracted using a marching cubes algorithm to replicate the surface represented by the Voronoi sphere set, as shown in Figure 4.

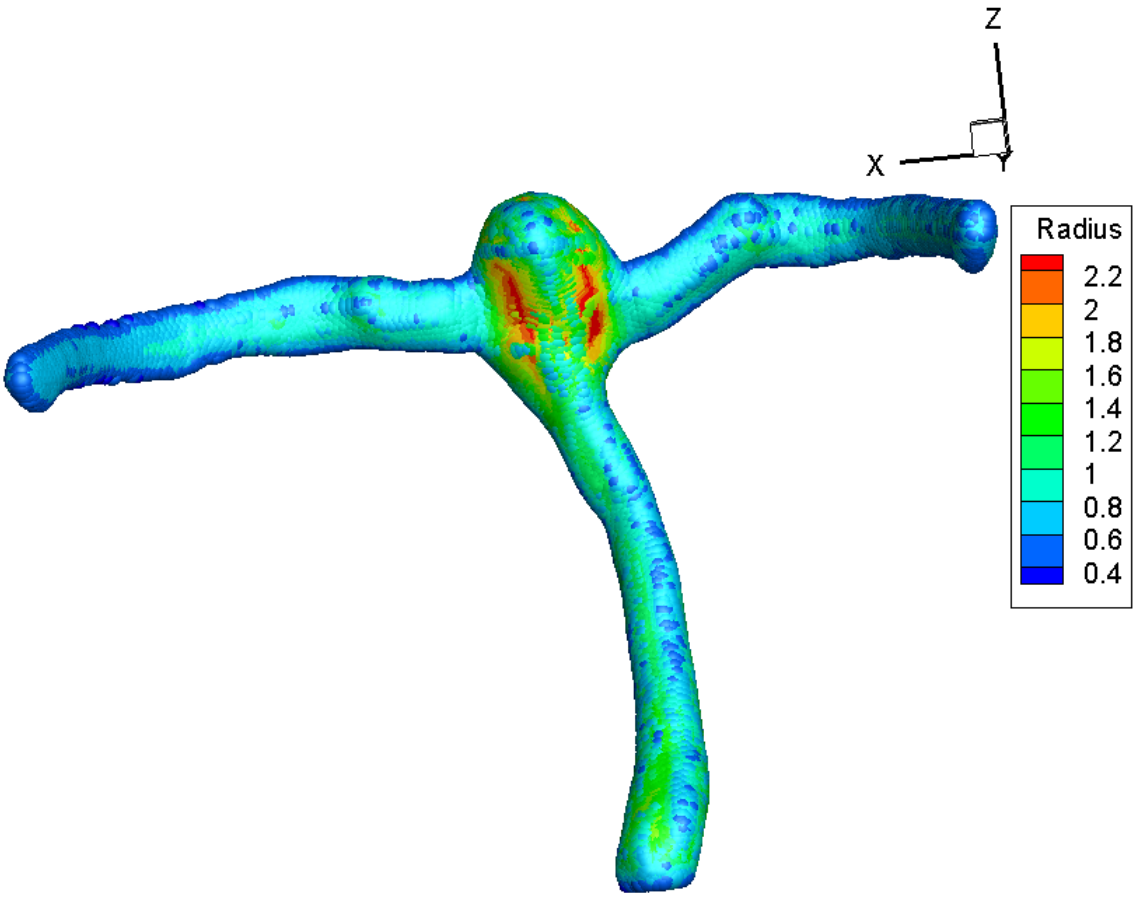

Figure 4. All Voronoi spheres of a surface mesh, which together form the dual of the surface itself.

The medial axis, which is representative of the centerline of a tubular object, can also be obtained from the Voronoi diagram. Maximal inscribed spheres are defined as Voronoi spheres that are fully contained by no other Voronoi sphere. The centers of these maximal inscribed spheres form the medial axis of the object, and can be considered the centerline in vascular structures (Antiga, 2002).

Parent Vessel Reconstruction

To isolate the aneurysm sac geometry, the aneurysmal features must first be distinguished from that of the healthy cerebral vasculature. To accomplish this, the parent vessel is first approximated using the algorithm detailed by Ford et al. in 2009. This algorithm takes as its input a vessel surface model, its Voronoi diagram, and several sets of centerlines. The centerlines are created by defining the inlet, outlet(s), and a point on the aneurysm dome, and propagating along the artery from inlet to outlet and subsequently outlet to inlet as shown in Figure 5a. The point where the centerline of the vessel diverges to follow the medial axis of the aneurysm sac to the user-defined target point as shown in Figure 5a is designated the diverging point. Centerline clipping points are then defined one maximal-inscribed sphere radius proximal and distal to the diverging points along the centerline, as shown in figure 3a. The aneurysmal segment is then designated as the region between the clipping points.

Subsequent to defining the clipping points, the portion of the centerline within the aneurysmal region is removed and then interpolated using a cardinal cubic Hermite spline function, as shown in Figure 5b. The Voronoi diagram sphere centers are also removed between the centerline normal planes at each clipping point. A portion of the sphere centers within a specific distance adjacent to each clipping normal plane is interpolated linearly across the aneurysmal region, accounting for position and sphere radius. A surface may then be created from the extent of the Voronoi sphere set as described in the previous section of this chapter and as demonstrated in Figure 5c. This method is defined for both terminal aneurysms (aneurysms that form at a vessel bifurcation) and lateral aneurysms (aneurysms that form on the side of a vessel wall).

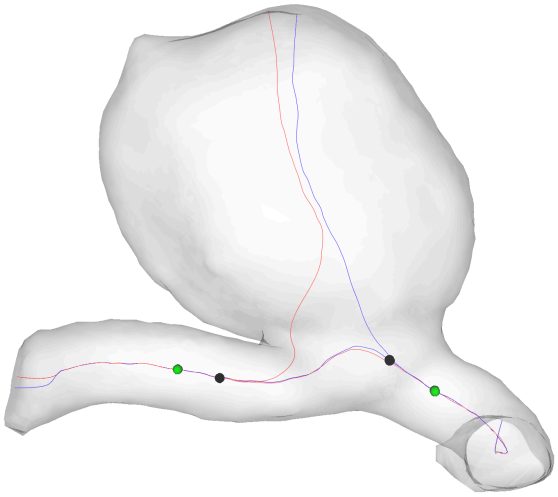

Figure 5a.

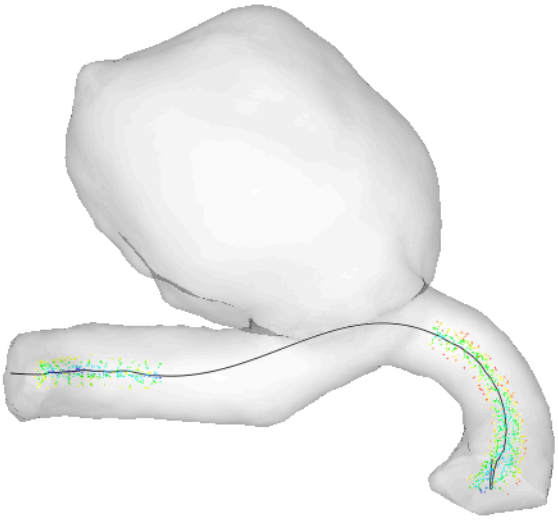

Figure 5b.

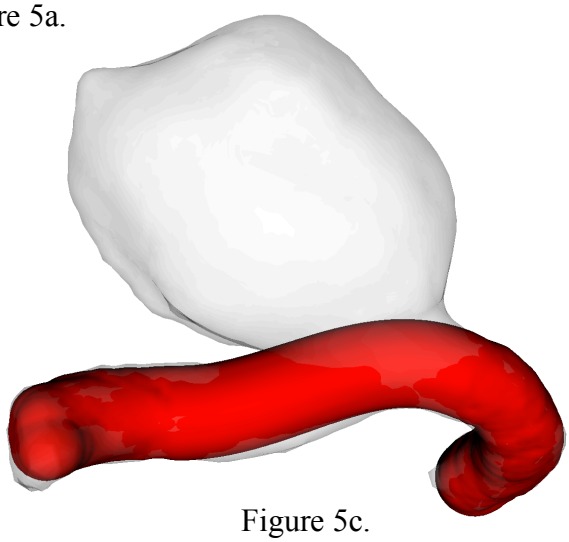

Figure 5c.

Figure 5. Parent vessel reconstruction process. (a) Surface model of aneurysmal vessel segment (grey) with forward centerline (red), backward centerline (blue), clipping points (green), and diverging points (black). (b) Interpolated centerline (black) with clipped Voronoi diagram (multicolored) within original surface model (grey). (c) Reconstructed parent vessel (red) shown within original surface model (grey).

Expansion of the Reconstructed Parent Vessel

The surface extracted from the reconstruction of the parent vessel will always be internal to the non-aneurysmal portion of the original surface because it is constructed from inscribed spheres. The healthy parent vasculature will eventually be removed from the aneurysmal surface model by means of a Boolean subtraction; therefore, in order to isolate the aneurysm successfully, the reconstruction of the parent vessel must be expanded in diameter.

To determine the optimal degree of expansion, the boundary of the aneurysm dome must first be found. Similar to the procedure outlined by Piccinelli et al. in 2012, the Voronoi sphere centers of the original surface model internal to the parent vessel reconstruction are removed. The residual Voronoi spheres are checked for connectivity with the user-defined aneurysm dome target point and subsequently deleted if the connectivity criterion is not met. The aggregate of the remaining Voronoi spheres forms an approximate representation of the aneurysm volume, shown in Figure 6. The point-wise minimum distance values are then determined on the original surface model in relation to both the parent vessel reconstruction and the aneurysm Voronoi diagram. The distance values from the original surface to the aneurysm volume is then subtracted from the distance value from the original surface to the parent vessel reconstruction, creating a scalar value at each point within the original surface mesh that is negative for portions of the surface that are closer to the reconstructed parent vessel, and positive for portions of the surface that are closer to the aneurysm volume. A contour line is created from the largest continuous zero level, shown in Figure 7, and represents the boundary on the original surface between the aneurysm and the non-aneurysmal vasculature. The largest minimum point-wise distance between the contour line and the reconstructed parent vessel is then determined, which corresponds to the distance that the reconstructed parent vessel must be expanded to cover the entire aneurysm neck boundary, ***D***. The average radius of the aneurysmal section of the reconstructed parent vessel, ***R***, is then determined.

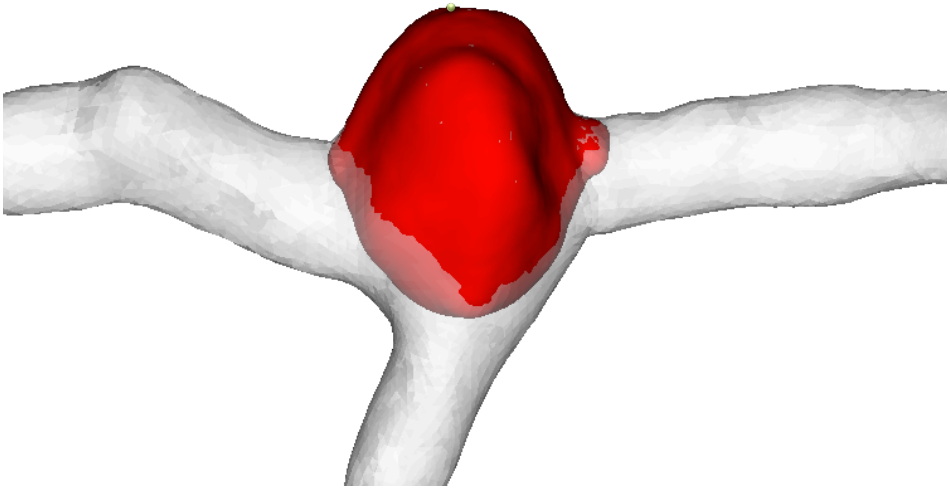

Figure 6. Surface encompassing the approximated volume of the aneurysm dome shown in red. Original parent vessel is shown in grey, and target point used to define aneurysm volume is shown in green.

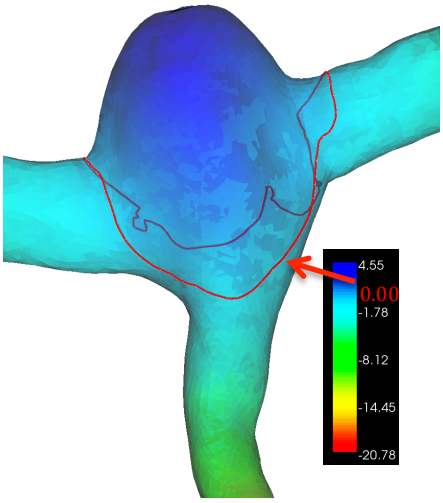

Figure 7. Distance difference contour plot (multicolored), with zero-level contour line (white) and contour line point of maximum distance from parent vessel (red).

Once the values ***D*** and ***R*** are determined, each Voronoi sphere radius within the Voronoi sphere set of the reconstructed parent vessel is scaled by a factor of $\frac{R+D}{R}$. A surface mesh is then created from the newly scaled Voronoi sphere set, creating a uniformly expanded parent vessel that encompasses the entire neck boundary contour line. This process ensures complete isolation of the sac and a minimal amount of volume loss.

Subtraction of the Parent Vasculature

The expanded parent vessel reconstruction is next subtracted from the original surface mesh using a Boolean subtraction algorithm (Kitware, 2006). This results in a surface mesh of the entire volume of all aneurysmal features of the original surface. This isolated aneurysm surface contains identical elements on the outer lumen surface, and elements from the parent vessel reconstruction on the inner neck surface. Because of this, the expanded parent vessel reconstruction is re-meshed to eliminate any errors in the Boolean operation that may arise from sub-optimal element geometry. The resolution of the original surface mesh and expanded parent vessel reconstruction mesh should be similar in order to avoid skewed elements at their interface.

Separation of the Neck Surface

The neck surface of the aneurysm must be distinguished from the newly isolated aneurysm surface in order to analyze certain morphological characteristics. To accomplish this, three quantities are calculated. The first quantity is the surface normal vectors for the isolated aneurysm surface mesh. Next, the minimum point-wise distance scalars from the isolated aneurysm surface mesh to the expanded parent vessel reconstruction surface mesh are calculated to indicate the region in the vicinity of the neck. Finally the minimum point-wise distance vectors from the isolated aneurysm

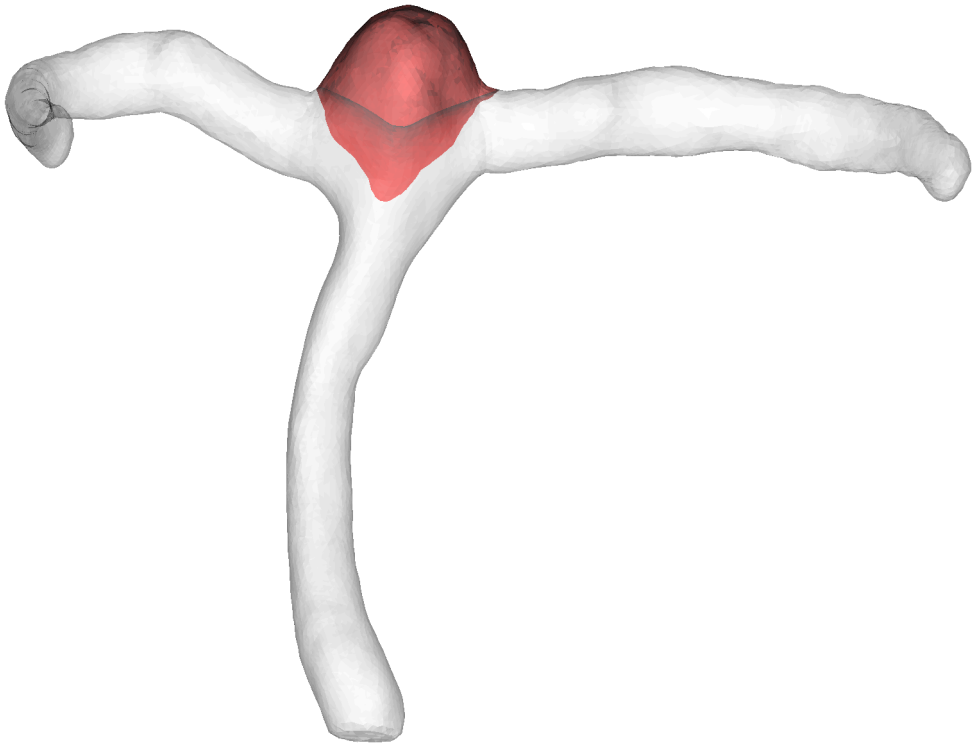

Figure 8. Completed aneurysm sac isolation (red) from original model (grey).

surface mesh to the original reconstructed parent vessel surface mesh are calculated. The distance vectors are three-dimensional vectors that represent the distance and direction from each point on the first surface mesh to the closest point on the second surface mesh. Because each of these quantities will ultimately be used to distinguish the elements of the mesh rather than the points, the point values are converted to element-centered values using a VMTK class.

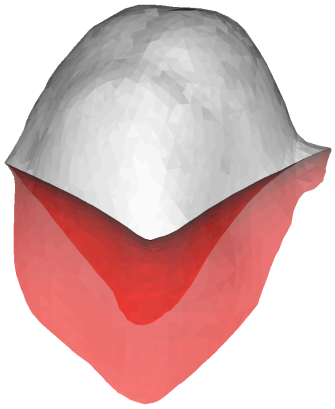

Figure 9. Separation of the aneurysm neck surface (red) from the aneurysm dome (grey).

The neck surface is distinguished from the rest of the isolated aneurysm surface mesh by defining two criteria for each element, which must be met to distinguish the element as a neck element. First, the angle between the distance vector and the normal vector are compared. Because the neck surface is a replication of the expanded parent vessel, the minimum distance element on the reconstructed parent vessel (to which the distance vector points) will be adjacent to the corresponding neck element at a distance equal to the expansion distance. Because of this, the distance vector will be nearly normal to the element, and the first criteria for inclusion in the neck surface will be satisfied if the angle between the normal vector and the distance vector is less than the tolerance to allow for slight mesh-related variations. Second, the distance scalar value from the element to the minimal-distance corresponding element on the expanded parent vessel reconstruction surface mesh should be nearly 0. If the distance between the element on the isolated aneurysm surface mesh and the corresponding minimal distance element on the expanded parent vessel reconstruction is below the tolerance to allow for slight mesh-related differences, then the element will meet the second criteria. If both

criteria are met, the element is then separated as a member of the neck surface. The criteria are demonstrated in Figure 10.

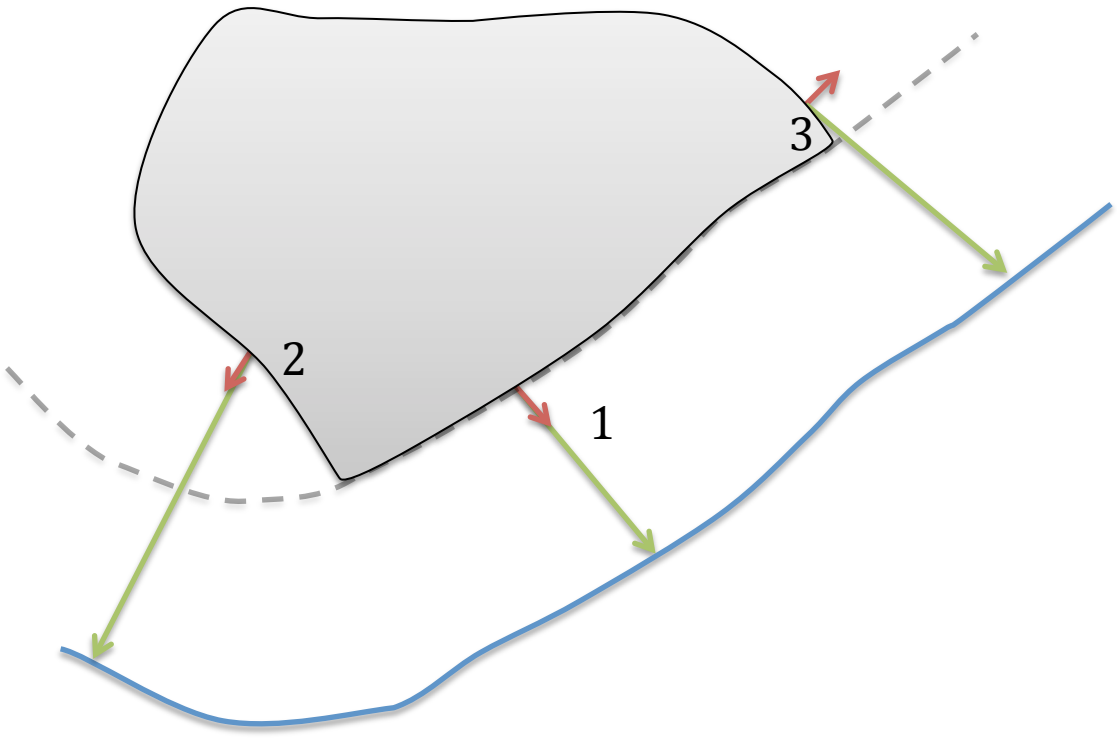

Figure 10. Aneurysm dome (grey) is shown with normal vectors (red), distance vectors (green), parent vessel reconstruction surface (blue), and expanded parent vessel reconstruction surface (dotted grey). An element at location 1 is included in the neck, while an element at location 2 is excluded based on the distance criteria, and an element at location 3 is excluded based on the angle criteria.

CHAPTER 3

MORPHOLOGICAL CHARACTERIZATION

Many shape metrics have been derived in an attempt to exhaustively describe an aneurysm's morphology, as evidenced by the literature review on the subject. However, because of the novel sac isolation method outlined in the previous chapter, new approaches must now be employed. Because of the lack of a planar neck surface several measures must now be determined in a new manner, such as maximum aneurysm diameter, which previously was calculated as the largest measurement across planar cross-sections parallel to the neck (Ma et al., 2004). Additionally, new parameters can now be defined because of the inclusion of a neck surface that is representative of the pre-aneurysmal parent vessel lumen.

Geometric Measurements

Volume of the interior of the isolated aneurysm surface is measured using the vtkMassProperties class (Alyassin et al., 1994; Kitware, 2006), which uses a discrete form of the divergence theorem to calculate volume and surface area. Surface area was also measured in this manner. The measurements from this algorithm were crosschecked using Rhinoceros 3D, and agreement was confirmed in all cases.

Maximum diameter is a one-dimensional quantity that is measured as the maximum distance across all points within the isolated aneurysm surface mesh. It is measured point-by-point in the mesh, and does not discriminate against points within the neck region; however, by the nature of the geometry involved in the isolation operation, the maximum diameter will not be measured from within the neck surface.

Neck diameter is derived from the isolated neck surface. The neck of the aneurysm is first isolated using the method discussed in the previous chapter, and the perimeter is then extracted. The centroid of the perimeter is next determined by averaging the positions of all perimeter points, and the average distance from the centroid

to all perimeter points is determined and multiplied by two to serve as a diameter. This quantity is illustrated in Figure 11.

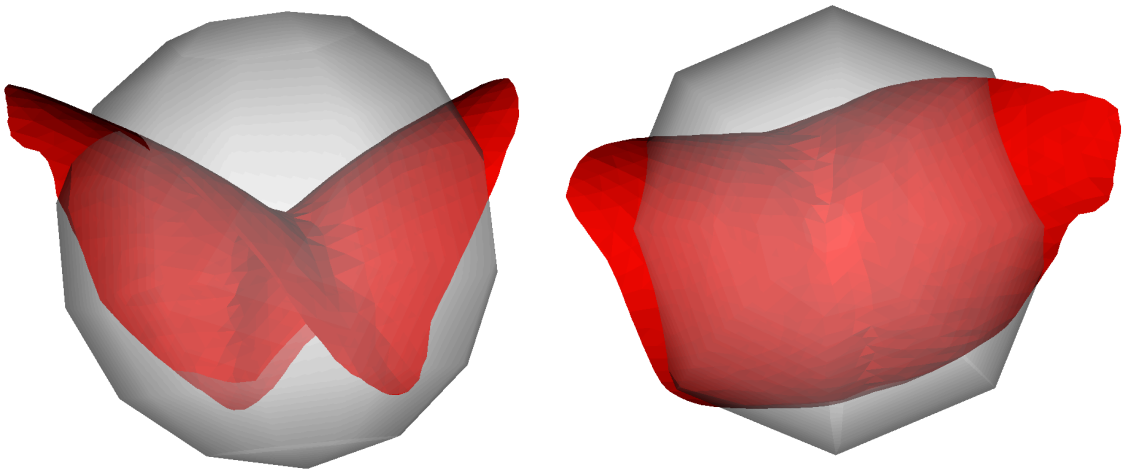

Figure 11. A sphere of diameter equal to the neck diameter calculation (grey) overlaid onto the separated neck surface (red). Two orthogonal views are shown.

Vessel diameter is defined as the average radius of the maximal inscribed spheres at the clipping points, as shown in Figure 18. Because the hypothetical parent vessel reconstruction is merely a linearly interpolated set of Voronoi spheres, this is a reasonable simplification. Piccinelli et al. in 2012 and used similar approaches in their morphological studies.

Morphometric Indices

Six morphometric indices are explored in this paper. Several have been described previously in literature, including Bottleneck Factor, Size Ratio, Ellipticity Index,

Undulation Index, and Nonsphericity Index. However, because of the different limitations and advantages posed by the novel isolation method introduced in this project, Ellipticity Index, Nonsphericity Index are defined in a completely novel manner, and Bottleneck Ratio and Size Ratio are both defined using the novel measurement techniques introduced in the previous section. Additionally, two completely novel indices, Tissue Stretch Ratio and Neck to Vessel Ratio are introduced.

Neck to Vessel Ratio

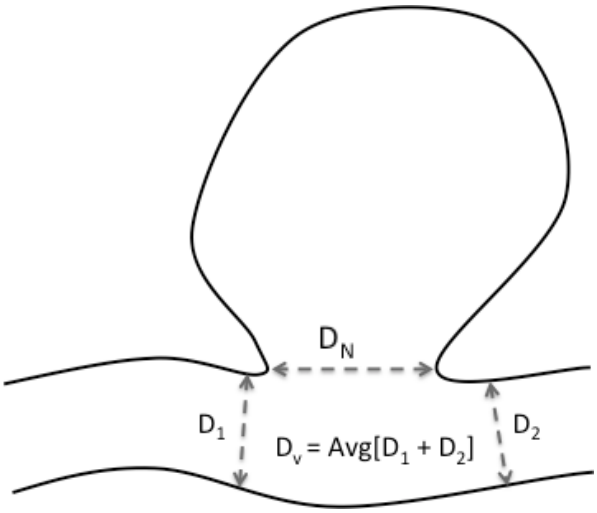

Figure 12. Demonstration of the measures contributing to the Neck to Vessel Ratio.

Neck to Vessel Ratio (NVR) is a novel index defined as the ratio of the neck diameter (D_N) to the vessel diameter under the aneurysm sac (D_V), $NVR = \frac{D_N}{D_V}$. Many geometric indices such as this are developed in order to describe characteristics of the local hemodynamics that could affect an aneurysm. This index seeks to describe the relationship between the cross-sectional area through which blood may flow and the area through which blood may enter the aneurysm sac. If the value of this index is higher than 1 then the cross-sectional diameter of an aneurysm neck is higher than that of the feeding

vessel, and may contribute to slower entry flow in that aneurysm relative to one that has a lower indicial value.

Tissue Stretch Ratio

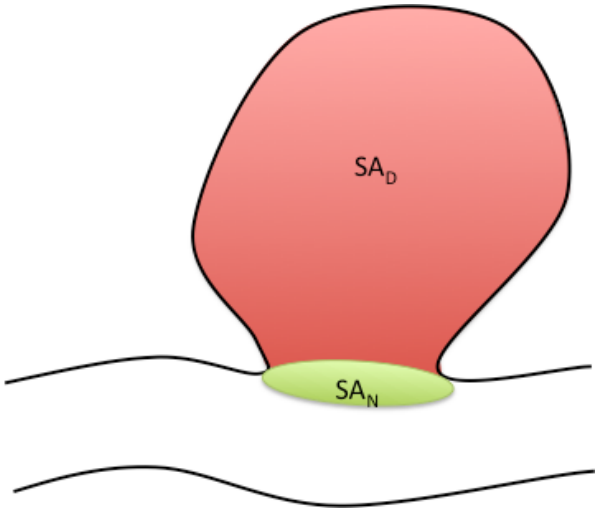

Figure 13. Demonstration of the measures contributing to the Tissue Stretch Ratio.

Tissue Stretch Ratio (TSR) is defined as the ratio of the surface area of the neck (SA_N) surface to the surface area of the aneurysm dome surface (SA_D), $TSR = 1 - \frac{SA_N}{SA_D}$. The neck surface as defined in this work is the area from which the reconstructed parent vessel tissue would have hypothetically deformed toward the aneurysmal geometry. Therefore, this ratio of areas may be representative of the amount of stretch encountered by the aneurysm dome, and subsequently provides insight into the relative amount of aggregate strain throughout the aneurysm dome. This index is calculated by detaching the neck surface from the isolated aneurysm surface as previously described and separately measuring the surface area of the neck and the aneurysm dome. The range of

this index is bounded between 0 and 1, with a value of 0 indicative of a very small difference in neck surface area compared to dome surface area.

Bottleneck Factor

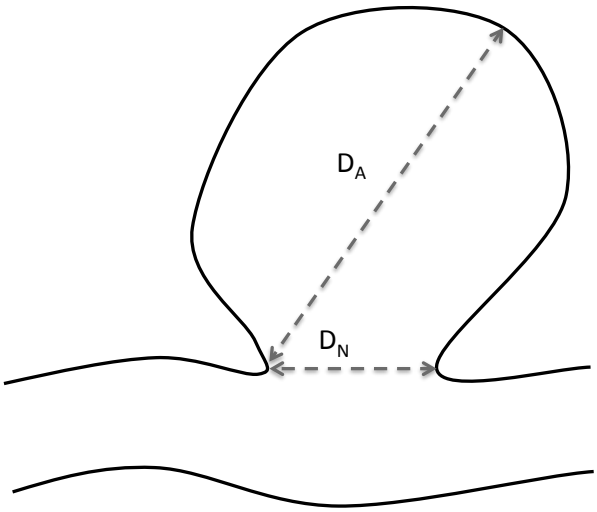

Figure 14. Demonstration of the measures contributing to the Bottleneck Factor.

Bottleneck Factor (BF) is defined as the ratio of the neck diameter (D_N) to the maximum aneurysm diameter (D_A), $BF = \frac{D_N}{D_A}$ (Raghavan, Ma, & Harbaugh, 2005). It is thought that a smaller neck in relation to a larger aneurysm would indicate a larger tissue stretch, and therefore a larger chance for weakening of the aneurysm tissue. It is calculated by dividing the neck diameter, as defined in the previous section, by the maximum diameter, as defined in the previous section. The range for this index in all cases is between 0 and 1, with a lower number corresponding to a large maximum diameter in relation to neck diameter.

Size Ratio

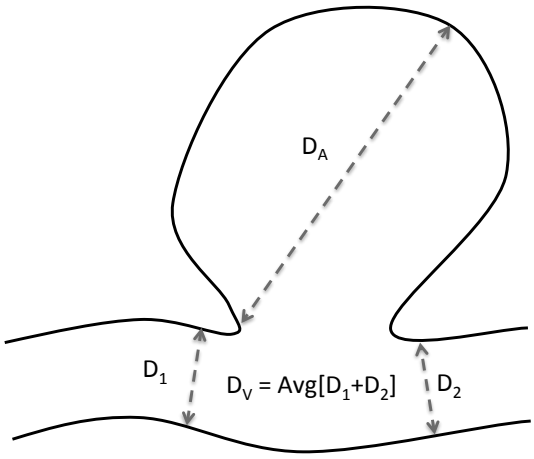

Figure 15. Demonstration of the measures contributing to the Size Ratio.

Size ratio (SR) is defined as the ratio of the maximum aneurysm diameter (D_A) to the vessel diameter (D_V), $SR = \frac{D_A}{D_V}$. This index has been described in the past, and has been shown to correlate prospectively with rupture risk (Rahman, 2010). However, it is now defined using the parent vessel reconstruction, which may be a more accurate measure of vessel diameter. This is particularly true in terminal aneurysms where it may be relatively unclear from where to measure each diameter, and where a distinction between the aneurysm and vessel is sometimes less clearly defined.

Undulation Index

Undulation Index (UI) is a measure of the difference in volume of the aneurysm sac (V_A) and its convex hull (V_{CH}), $UI = 1 - \frac{V_A}{V_{CH}}$ (Ma et al., 2004; Raghavan et al., 2005). Aneurysm sac geometries with neck surfaces that lack concavity, such as planar neck surfaces used in past morphological studies, will by nature introduce no measurement error of dome surface undulation. However, because of the three-

dimensional, concave nature of the neck surfaces resulting from the novel isolation method outlined in this work, inaccuracies in undulation measurements will always be present without modification of the convex hull. The convex hull of an aneurysm is first obtained using the native Delaunay tessellation of the aneurysm surface point set. The excess volume within the convex hull resulting from the concavity of the neck region is then eliminated by means of a Boolean subtraction of the expanded parent vessel reconstruction from the convex hull. This is performed in the same manner as the isolation of the aneurysm sac. It is notable that this index will range between 0 and 1, with a completely convex aneurysm resulting in a measurement of 1. This is demonstrated in Figure 17.

Ellipticity and Nonsphericity Indices

In 2005, Raghavan et al. originally proposed ellipticity index (EI) and nonsphericity index (NSI) as three-dimensional morphometric indices intended to describe, respectively, the similarity of an aneurysm sac to a spherical shape with disregard to surface undulation and concavities, and the general similarity of an aneurysm sac to a sphere with respect to surface undulation, concavities, and general shape. These parameters were originally extrapolated using a relationship between volume and surface area. While this approach may theoretically act as a complete descriptor of these properties, in actuality small surface undulations due to image noise or other tenuous sources will cause large increases in surface area measurements yet small or negative changes in volume measurements compared to an otherwise similar model. To demonstrate this, a sphere of radius 1 cm was created in Rhinoceros 3D, as shown in Figure 16(a). Small undulations of a radius 5% that of the sphere were then added to simulate surface noise, as shown in Figure 16(b). While no change in volume was observed, a 4% change in surface area was seen as a result of the undulations.

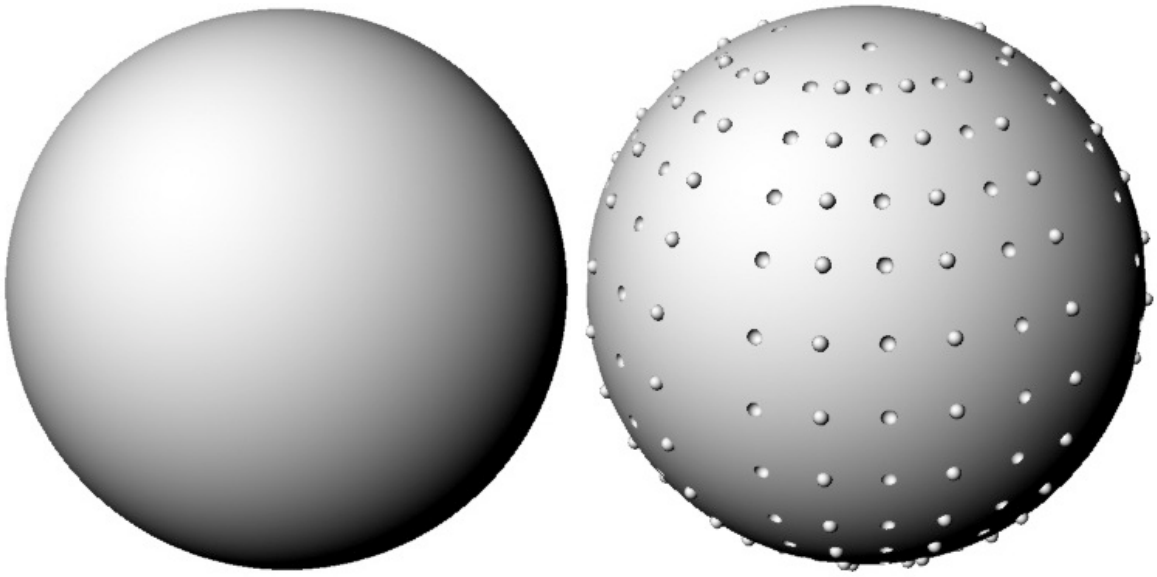

(a) (b)

Figure 16. Demonstration of surface area measurements obtained before (a) and after (b) small surface undulations were applied to an otherwise similar surface model created in Rhinoceros 3D. No volume change was observed despite a 4% change in surface area.

To perhaps improve upon these otherwise solid concepts, new definitions have been proposed for EI and NSI, as well as an accommodation for the now three-dimensional neck surface when measuring undulation of a surface.

EI is a measure of the general likeness of an aneurysm sac to a spherical shape while disregarding surface undulations and daughter sacs. Originally defined using the formula $EI = 1 - (18\pi)^{\frac{1}{3}}\frac{V_{CH}{}^{\frac{2}{3}}}{SA_{CH}}$ (Raghavan et al., 2005), in which V_{CH} is the volume of the convex hull of the aneurysm, and SA_{CH} is the surface area of the convex hull of the aneurysm, the index is now derived using only volumetric measurements. The convex hull of the isolated aneurysm sac is first extracted in the manner described in the previous paragraph, shown in Figure 17. The Voronoi diagram is then extracted and the volume of the largest Voronoi sphere of the convex hull, V_{CHLVS}, computed. This is the largest

spherical volume and theoretically the most stable portion of the aneurysm. This is then compared to the volume of the convex hull with the formula $EI = 1 - \frac{V_{CHLVS}}{V_{CH}}$. Because all Voronoi spheres are internal to their respective surface, this index will range from 0 to 1 in all cases, with values of 1 resulting from completely spherical convex hull geometries.

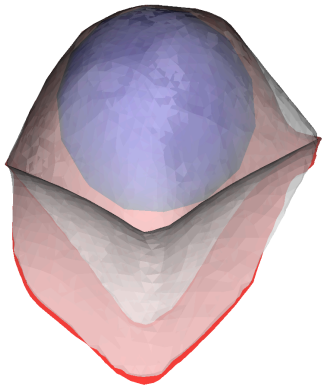

Figure 17. Isolated aneurysm (red) shown within its convex hull (white). Also shown is the maximal inscribed sphere of the convex hull (blue).

NSI is a measure of the overall similarity of an aneurysm sac surface to a sphere with respect to surface undulation, daughter sacs, and overall geometry. It was originally computed using the formula $NSI = 1 - (18\pi)^{\frac{1}{3}}\frac{V^{\frac{2}{3}}}{SA}$ (Raghavan et al., 2005); however, as in the new method for calculation of EI it is now defined using only volumetric measurements. The Voronoi diagram of the isolated aneurysm surface is computed, and the volume of the largest Voronoi sphere (V_{LVS}) is calculated, as seen in Figure 18. This volume is compared to that of the aneurysm sac (V_A) using the formula $NSI = 1 - \frac{V_{LVS}}{V_A}$.

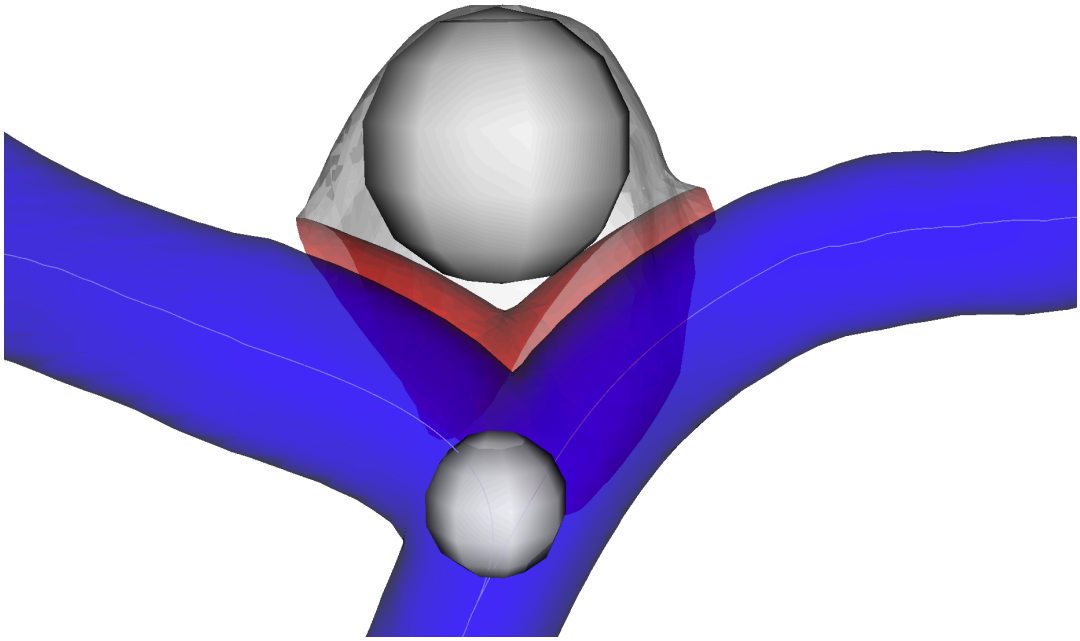

Figure 18. Isolated aneurysm dome (grey), neck surface (red), maximal inscribed sphere (large grey sphere), and sphere representing the average vessel diameter (small grey sphere). The diameter appears inaccurate because the original vessels were not spherical, thus the minor axis of the cross-section is represented.

CHAPTER 4

ANALYSIS OF THE METHODS

Three experiments were performed to analyze the variability induced by multiple users on the isolation of the aneurysm sac, the general efficacy of the shape analysis algorithms, and the effect of surface mesh resolution on the results of the morphological analysis. These experiments contributed to the general understanding of the efficacy of the isolation method and the morphological indices.

Analysis of Repeatability of Isolation and Shape Analysis

Methods

Because of the large sample size and time constraints of many of the morphological studies conducted recently, it is necessary to have multiple scientists working to segment and analyze patient data. Depending on the protocol of a particular study, some steps of the segmentation, sac isolation, and morphological analysis are computer automated and therefore consistent between users; however, the manually executed remainder of the process may leave room for discrepancies. A recent study investigated the variability induced in several cases by multiple users of both the segmentation and sac isolation protocol. It was found that much variation came not only from the differences in image segmentation between the two users, but also in some cases from the differing opinion on cutting plane placement (Ramachandran, 2012).

This study investigated segmentation independently in addition to segmentation and sac isolation simultaneously. However, because sac isolation was not independently investigated a new study was needed. This study was performed using the same patient data sets. In order to control for variations due to user variability from segmentation, only one out of the two segmentation sets were utilized.

Two isolation methods were investigated for comparison of overall user-induced variability: the cutting-plane method using the protocol in the above-mentioned study, and the isolation method outlined in the methods section of this work. Two separate users each isolated the sac using both methods, and were blinded from the sac isolation results of the previous study by the passing of a sufficient amount of time. Each user was also blinded from the other user's isolation results. The resulting models were analyzed using the morphometric indices described in the methods section of this study (although to determine parent vessel-based indices for cases isolated using the clipping plane method, the parent vessel reconstruction from only user 2 of the Boolean isolation method was used), and compared statistically. The repeatability of each index was characterized with a coefficient of repeatability (CR), defined as the maximum difference, with 95% confidence, seen in any results produced by two users or two repetitions by a single user. A Spearman coefficient, which is defined as the Pearson coefficient of the rank, was also produced for each index.

Results

Two users of each isolation method isolated nine aneurysm surface models (one case was excluded because of a meshing error in the original segmentation data). The original full-vasculature models, aneurysm models isolated by clipping plane, and aneurysm models isolated by parent-vessel reconstruction are shown in Figure 19, Figure 20, and Figure 21 respectively. The morphometric indices were calculated for each case, and the coefficient of repeatability was determined for each index. Figure 22 shows the correlation plots and R^2 values and Table 1 shows the coefficient of repeatability for each index.

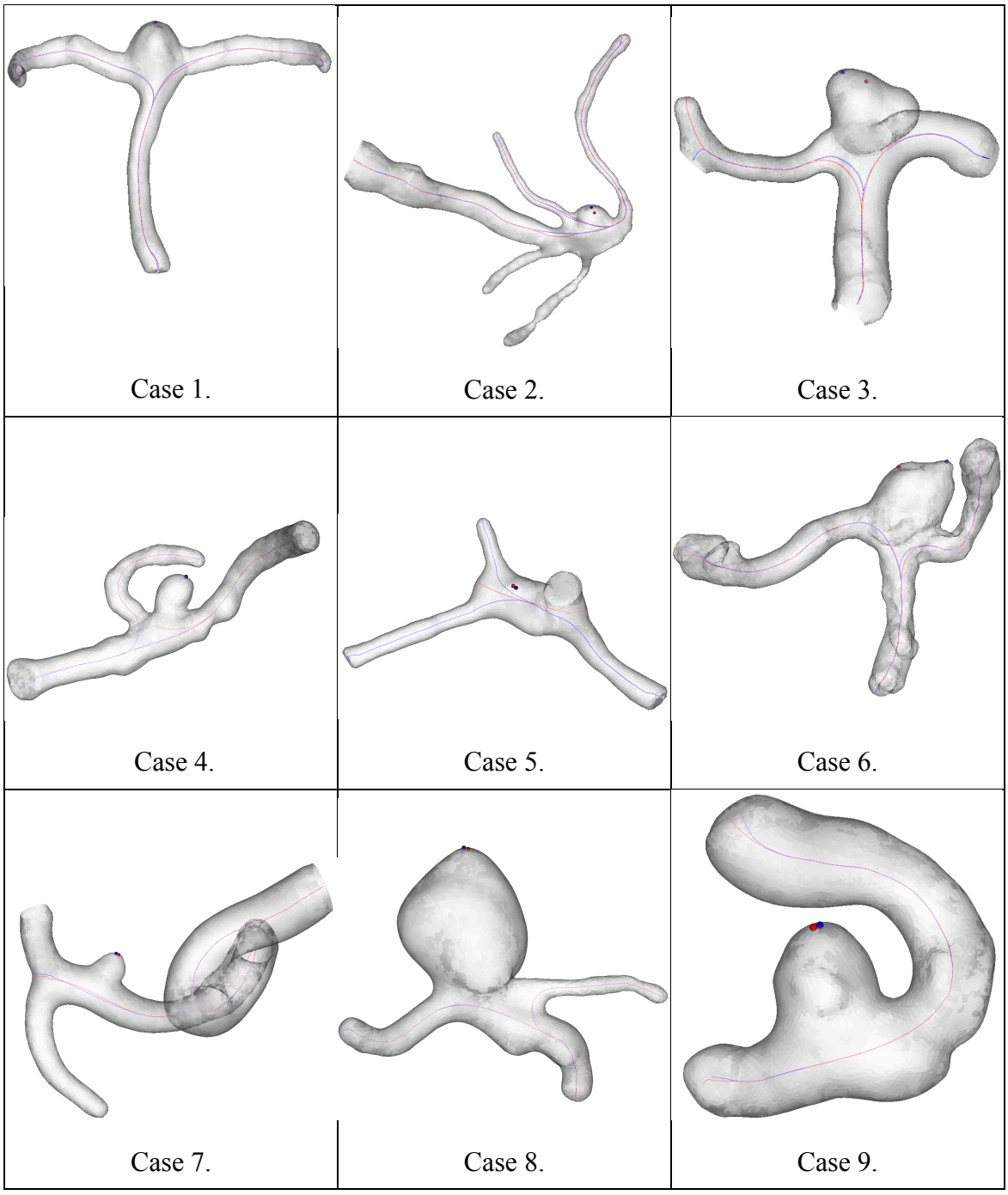

Figure 19. Original full-vasculature surface models, before sac isolation. Dome target points and reconstructed parent centerlines (red by user 1 and blue by user 2) from each user's isolation are represented on the surface.

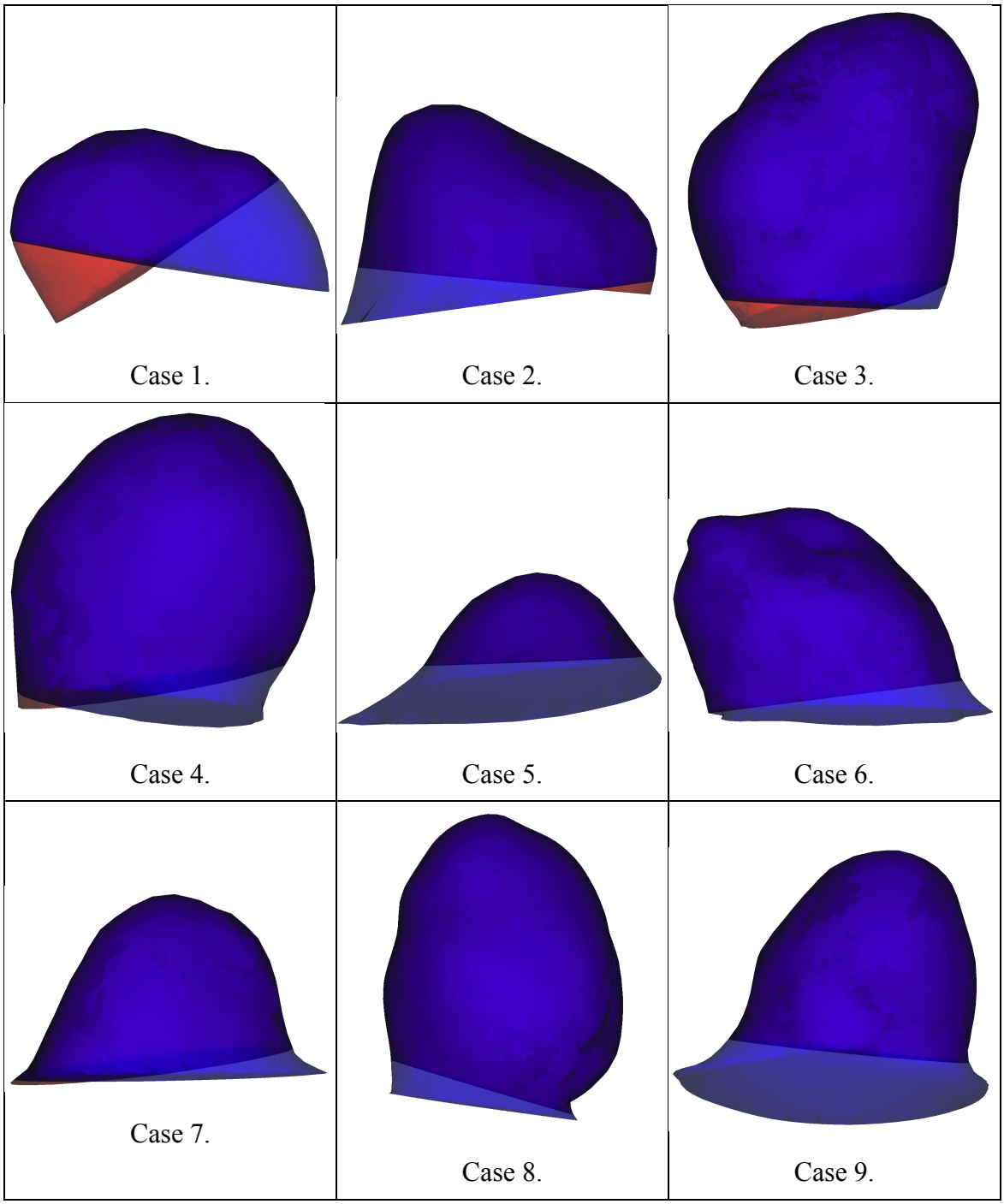

Figure 20. Aneurysm sacs isolated using clipping plane. User 1 isolated the red geometry and user 2 isolated the blue geometry.

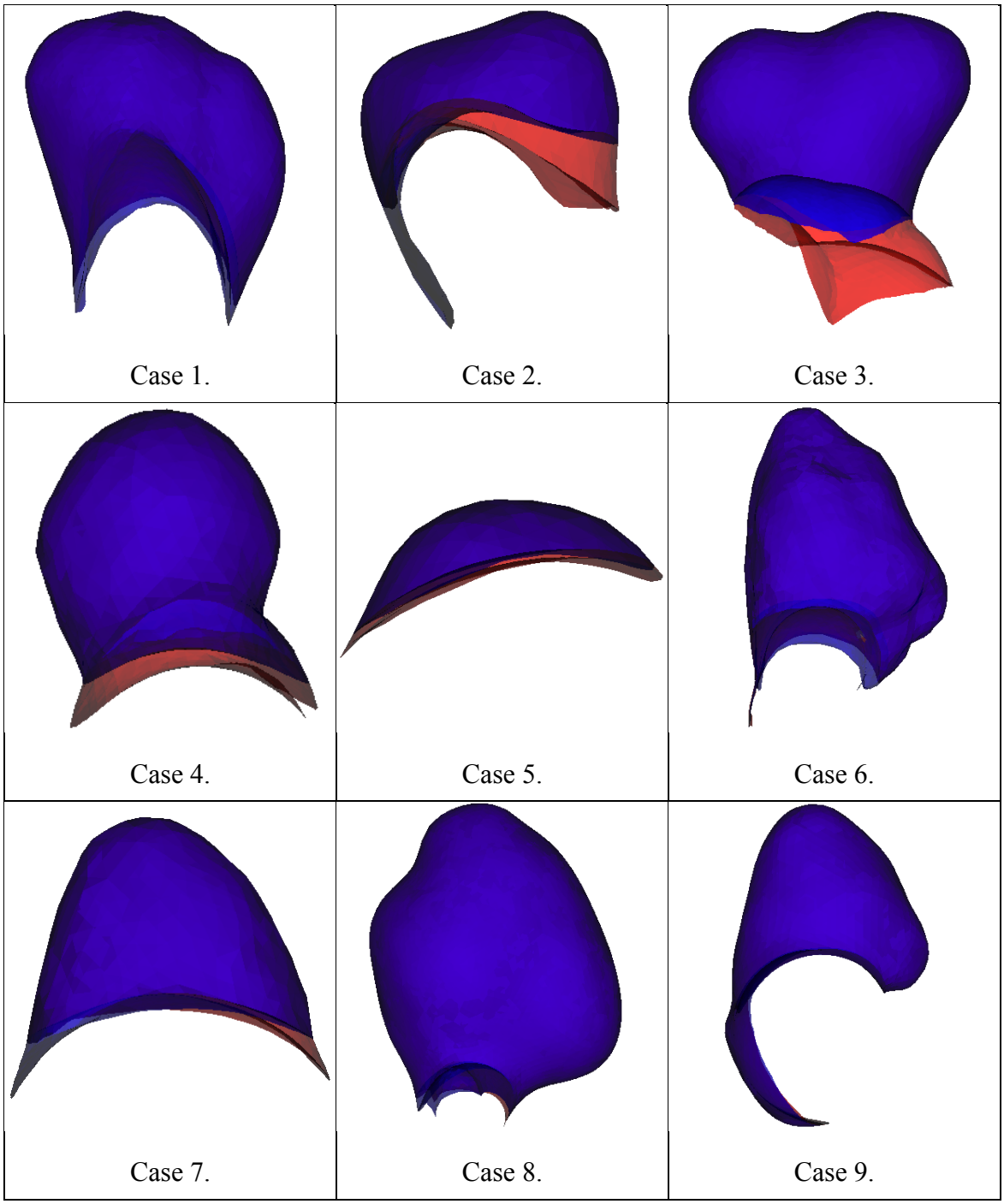

Figure 21. Aneurysm sacs isolated using parent vessel reconstruction and Boolean subtraction. User 1 isolated the red geometry and user 2 isolated the Blue geometry.

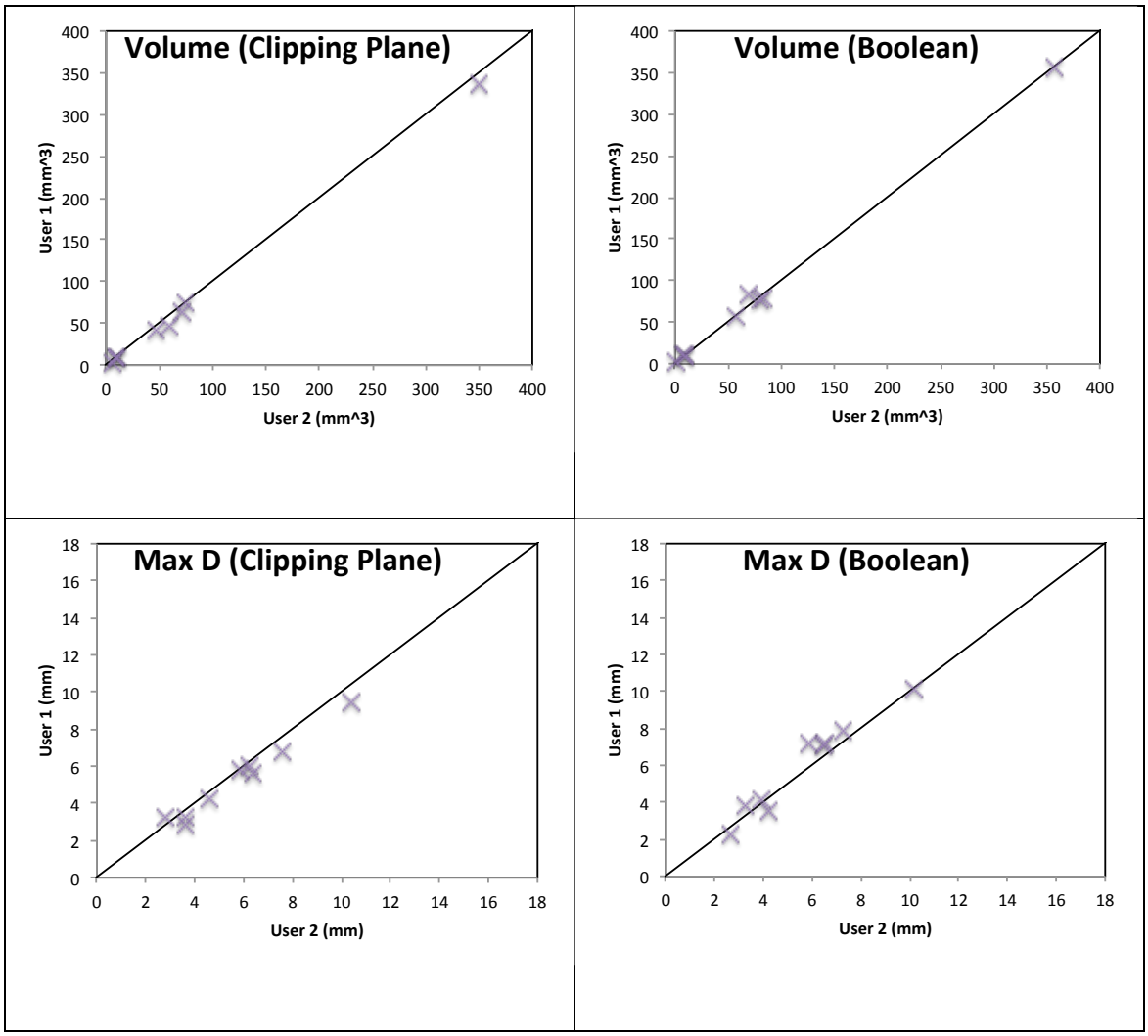

Figure 22. Correlation plots for each index and isolation method.

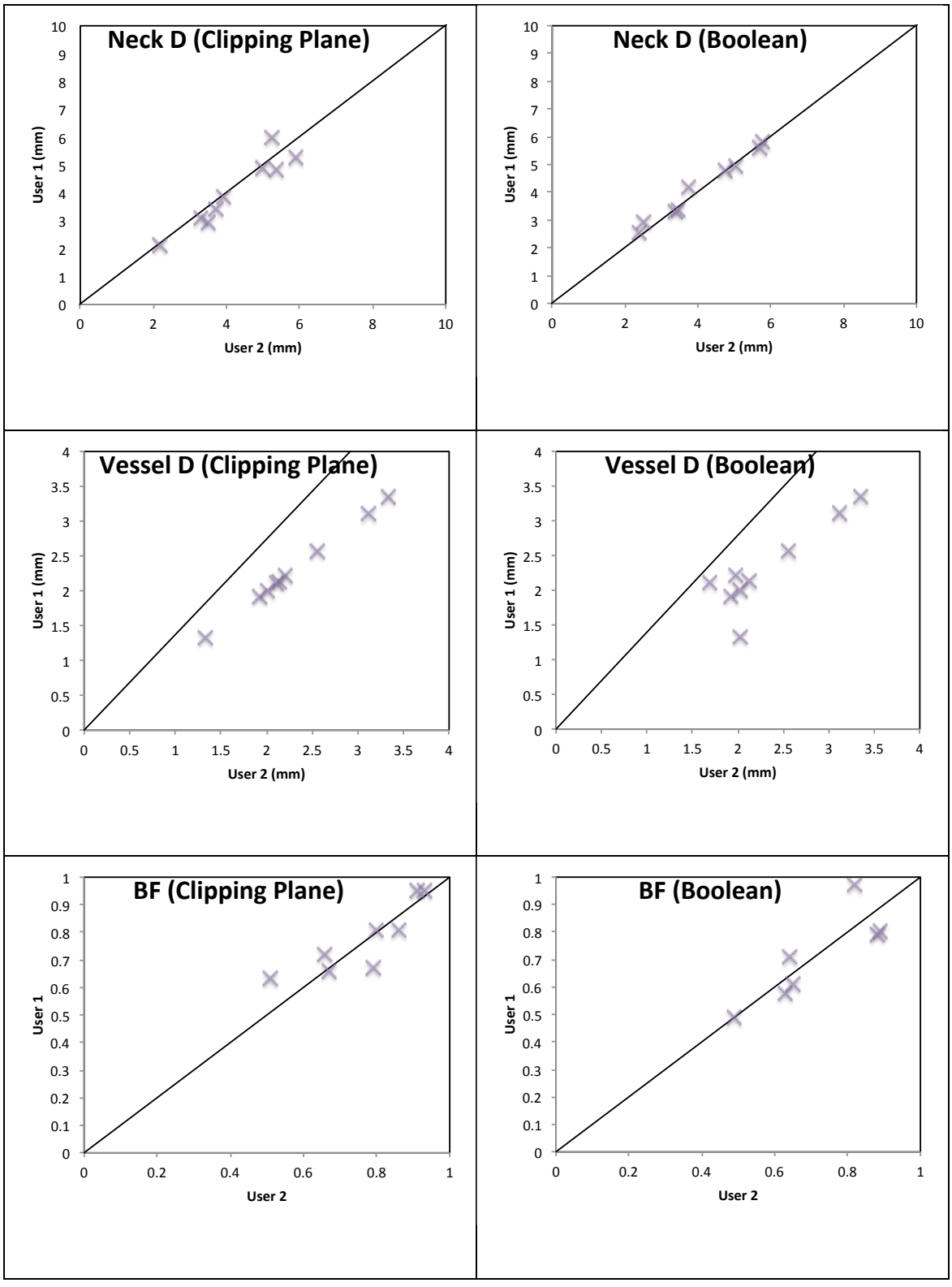

Figure 22 – continued

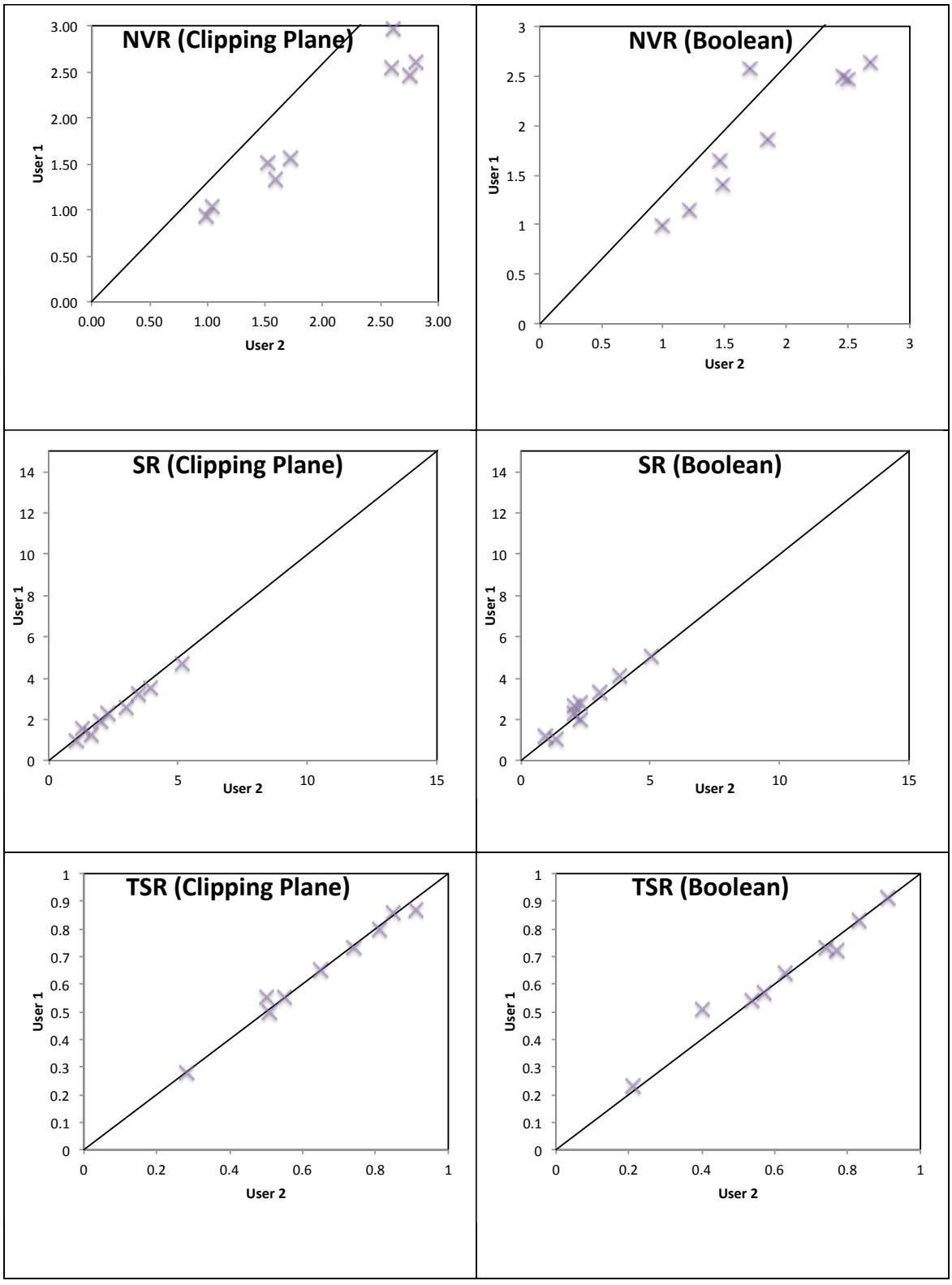

Figure 22 – continued

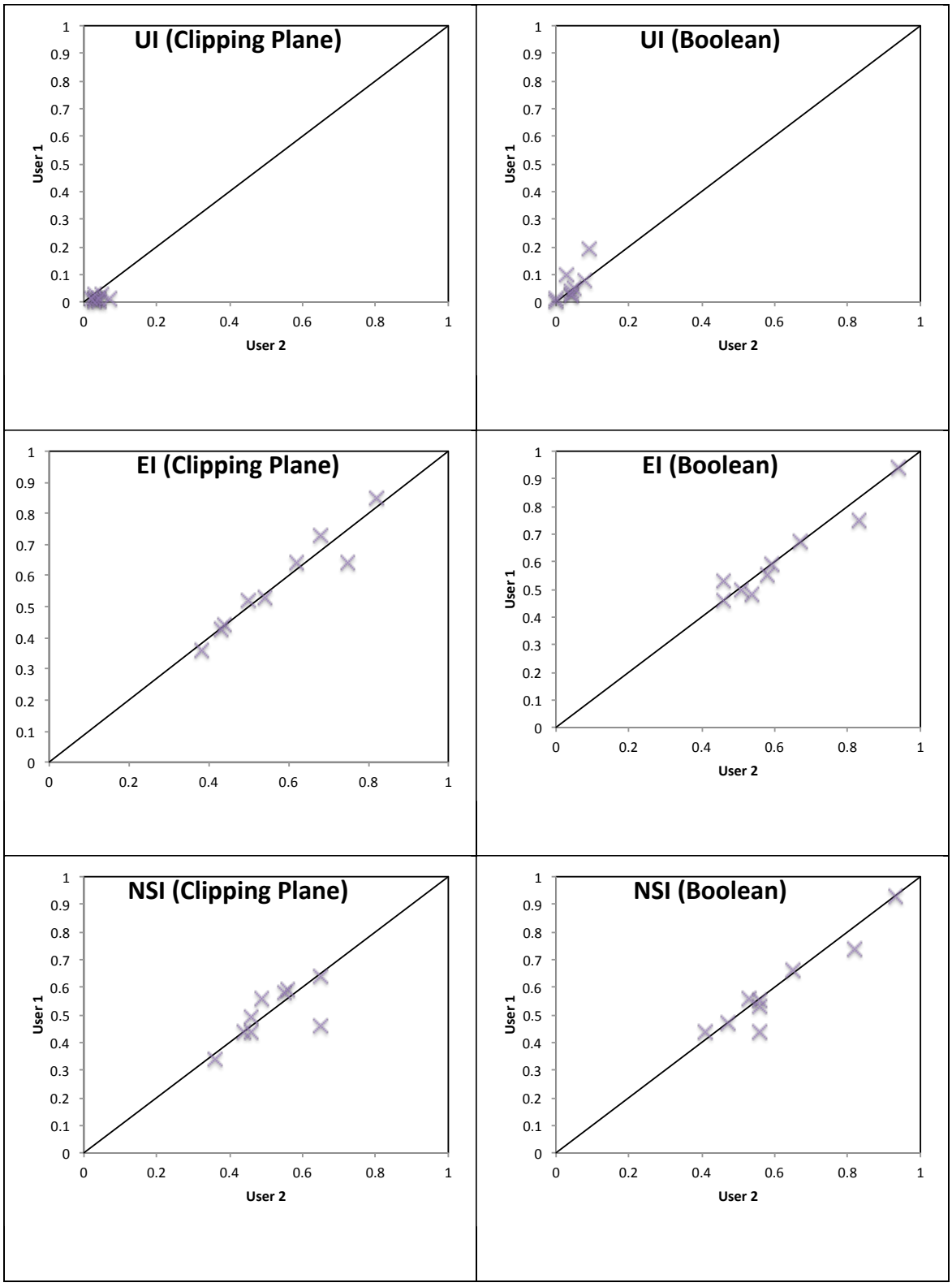

Figure 22 – continued

Table 1. Coefficient of repeatability (CR) for each index and aneurysm sac isolation method.

	Clipping Plane Isolation (CPI) CR	**Boolean Isolation (BI) CR**
Volume	10.18	9.47
Max Diameter	0.89	1.22
Neck Diameter	0.78	0.42
Vessel Diameter	0.00	0.59
BF	0.14	0.25
NVR	0.37	0.59
SR	0.44	0.63
TSR	0.05	0.08
EI	0.09	0.08
UI	0.03	0.08
NSI	0.15	0.10

Table 2. Spearman rank coefficient (SRC) for each index and aneurysm isolation method.

	Clipping Plane Isolation (CPI) SRC	**Boolean Isolation (BI) SRC**
Volume	0.983	0.933
Max Diameter	0.900	0.933
Neck Diameter	0.900	1.000
Vessel Diameter	1.000	0.700
BF	0.941	0.833
NVR	0.900	0.867
SR	0.983	0.890
TSR	0.959	0.983
EI	0.977	0.923
UI	0.014	0.643
NSI	0.741	0.722

Discussion

Clipping of the aneurysm sac by a single plane is the standard aneurysm isolation method in current morphological research. Therefore, clipping plane isolation (CPI) was compared against the novel Boolean isolation (BI) method. After morphometric analysis, the results were compared. Both methods generally had high Spearman coefficients, indicating a high agreement between users. However, mixed results were seen when comparing the user-induced variation between isolation methods. The CR did not

demonstrate a high tendency overall towards a lower window of variability. It should be noted that the Vessel Diameter and any related morphometric indices had no associated user variability for the clipping plane method. This is because the same parent vessel reconstruction was used for both. These indices were NVR and SR, which both resulted in much smaller coefficients of repeatability for the clipping plane method.

The Spearman coefficient was high for all but the UI for both methods, indicating strong agreement between users in all other indices. The generally poor agreement in UI for both the CPI and BI methods is likely due to the very small spread in values and the sensitivity of the index to differences at the neck region, which is discussed in the conclusion.

Analysis of the Efficacy of the Sac Isolation and Morphometric Indices

The purpose of the morphometric indices introduced in this study is to ultimately classify cerebral aneurysms by geometric characteristics. Thus, not only must a morphometric index be able to distinguish two different geometries, but also the measurements with which it is defined must be accurately obtained. This section explores how effectively the aneurysm sac is isolated, as well as how effectively the analysis techniques analyze aneurysm sacs of varying sizes and shapes. Aneurysm models between the diameters of 2 mm and 10 mm were created in order to coincide with the range of aneurysms seen in the Analysis of Repeatability.

Methods

In this study, a total of 14 hypothetical idealized vascular models were created using Rhinoceros 3D. This dataset was composed of 2 mm, 4 mm, 6 mm, 8 mm, and 10 mm spherical aneurysms, an irregular oblate ellipsoidal aneurysm, and an irregular prolate ellipsoidal aneurysm. Each model was placed in both a lateral and terminal configuration on a basilar terminus vessel segment and an internal carotid artery vessel

segment. The aneurysm models were created in Rhinoceros 3D (McNeel, Seattle, WA), and the arterial segments were extracted from a pre-existing model of the cerebral vasculature (Berkowitz et al., 2009). Each model was first re-meshed with a target element area of 0.05 mm. The parent vessel was the reconstructed according to the protocol, and isolated using the Boolean subtraction isolation method. Morphometric indices were calculated for each case.

For comparative purposes, isolation was performed directly in Rhinoceros 3D for all 14 models. In these cases, the parent vessel did not need to be expanded in order to isolate the sac because the parent vessel and aneurysm surface were innately defined as separate surfaces. These models were meshed within Rhinoceros 3D and analyzed directly in 13 of the 14 cases. In 1 of the 14 cases (the 8mm terminal spherical aneruysm), numerical errors related to the Rhinoceros-generated mesh required the model to be re-meshed in VMTK. The processed isolated models were then compared to the direct NURBS Boolean subtraction performed by Rhinoceros 3D. The similarity was evaluated by means of a Spearman's rank coefficient.

Results

The 14 vascular models and corresponding aneurysm models are shown in Figure 23 and Figure 24, respectively. The morphometric indices were calculated for the 14 aneurysm models. These are shown below for laterally oriented aneurysm models, **Error! Reference source not found.**, and for terminally oriented aneurysm models, **Error! Reference source not found.**. The Spearman rank coefficients for each index and method are shown in Table 3.

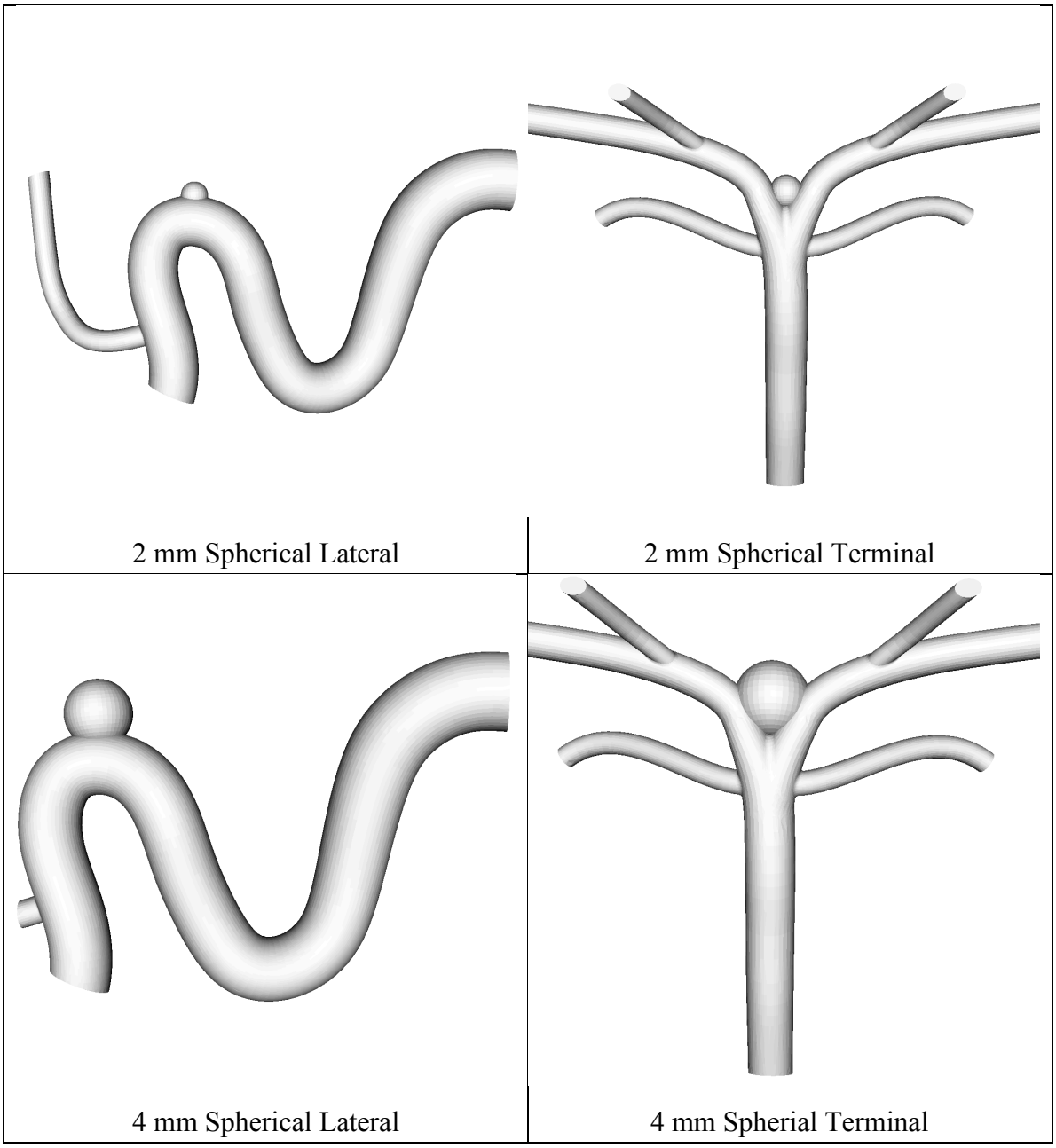

Figure 23. Original vascular models produced in Rhinoceros 3D and re-meshed using a 0.05 mm target area in VMTK.

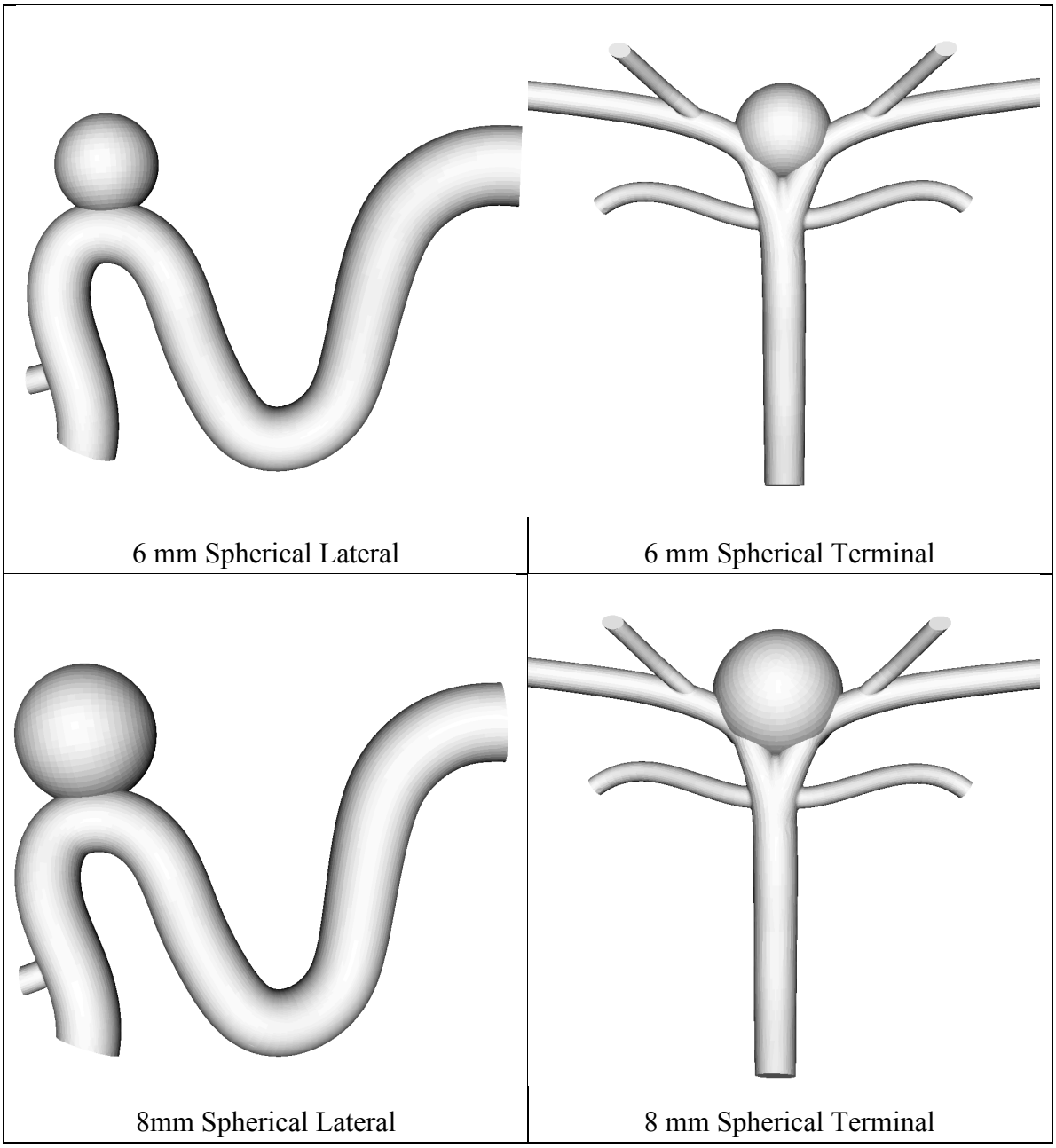

Figure 23 – continued

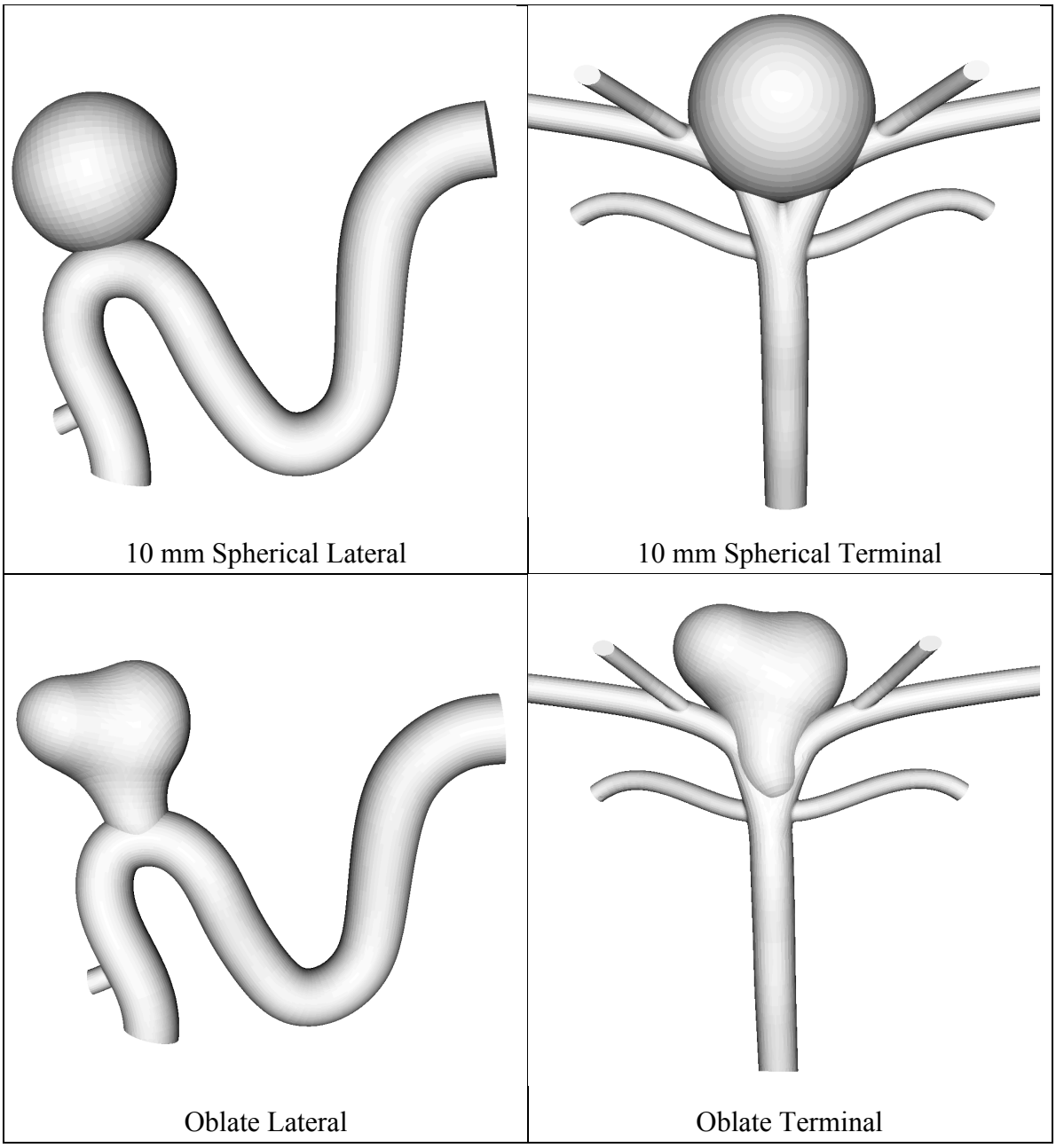

Figure 23 – continued

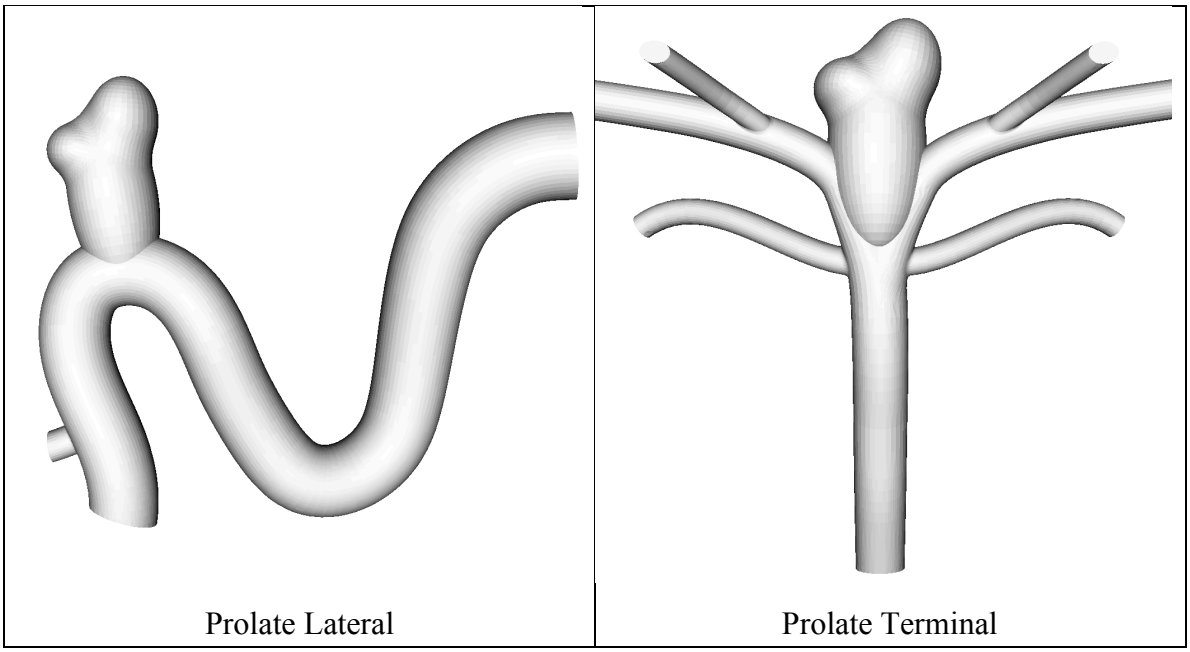

Prolate Lateral | Prolate Terminal

Figure 23 – continued

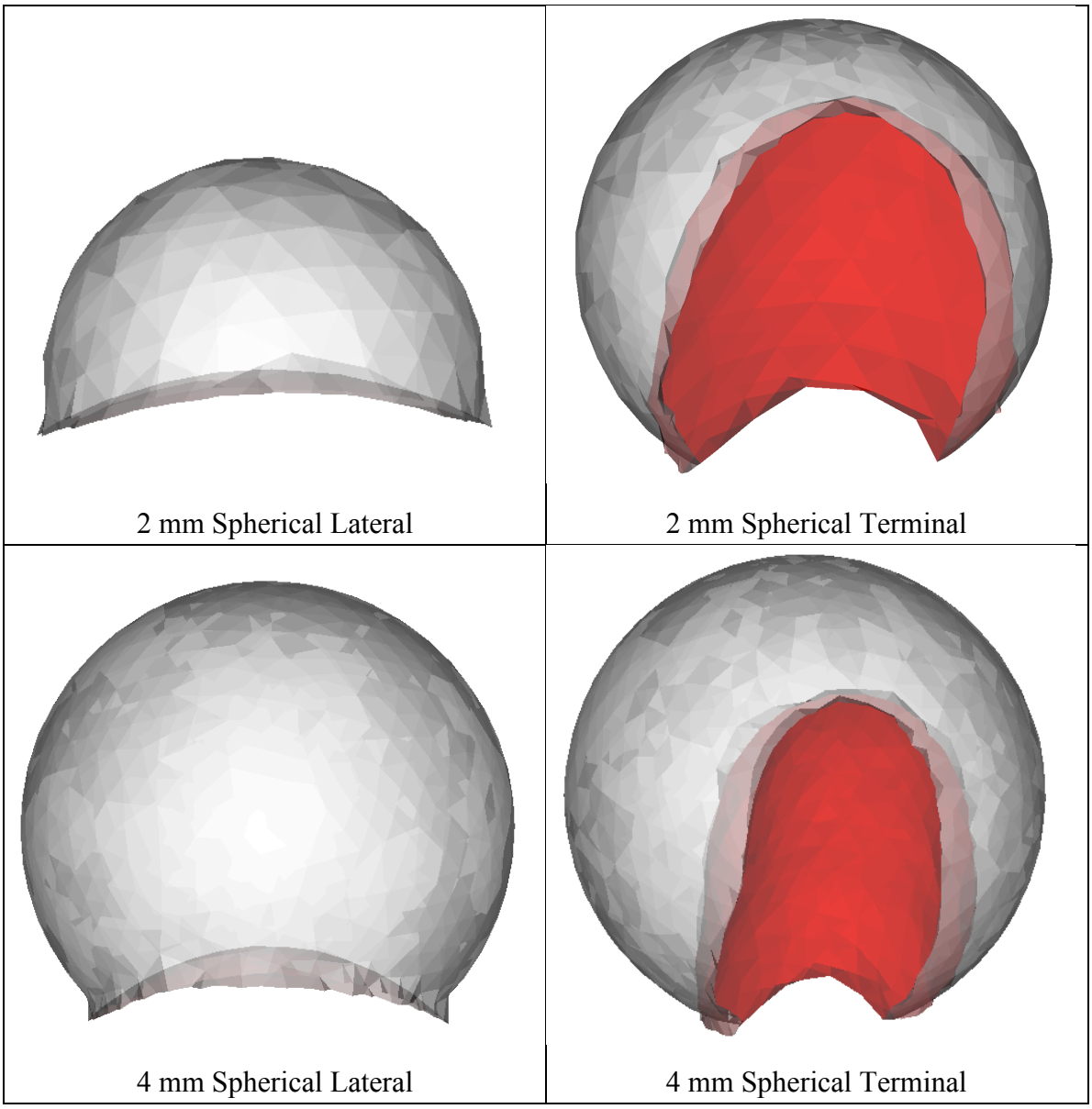

Figure 24. Isolated aneurysm geometries.

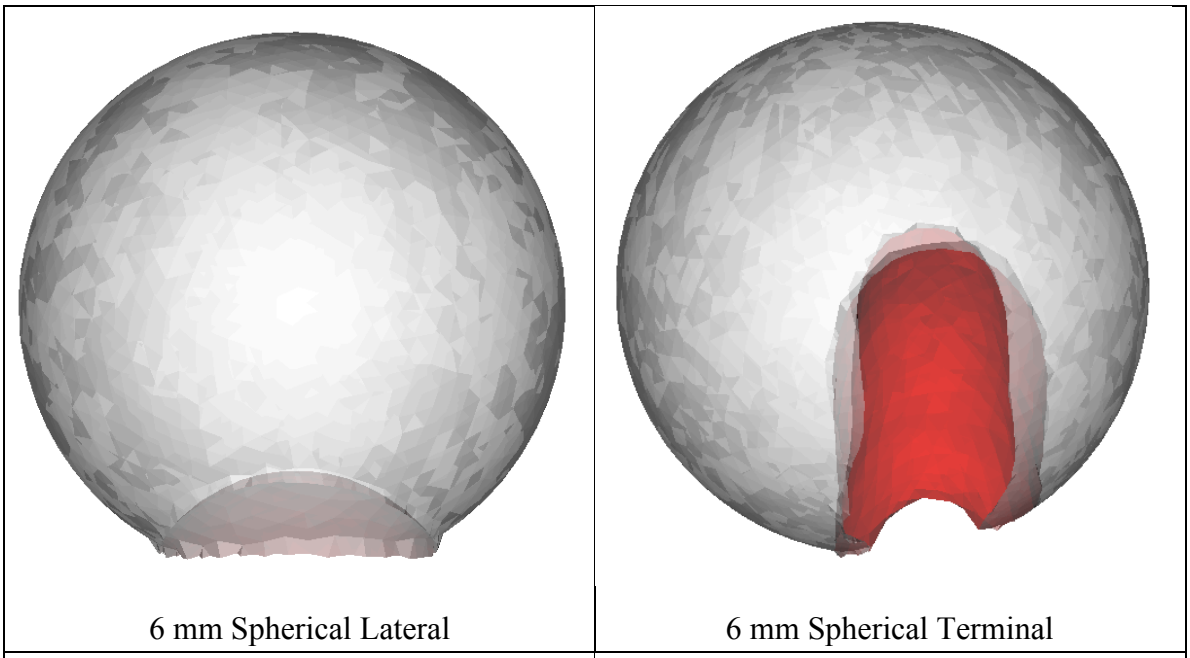

6 mm Spherical Lateral

6 mm Spherical Terminal

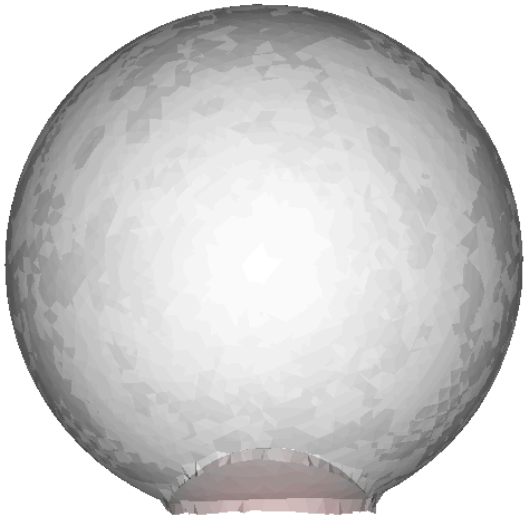

8 mm Spherical Lateral

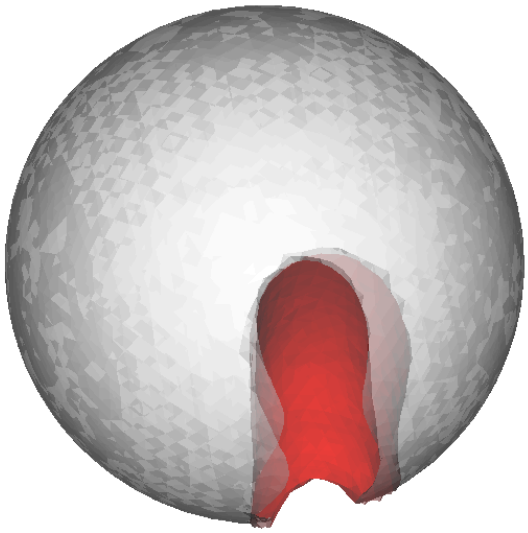

8 mm Spherical Terminal

Figure 24 – continued

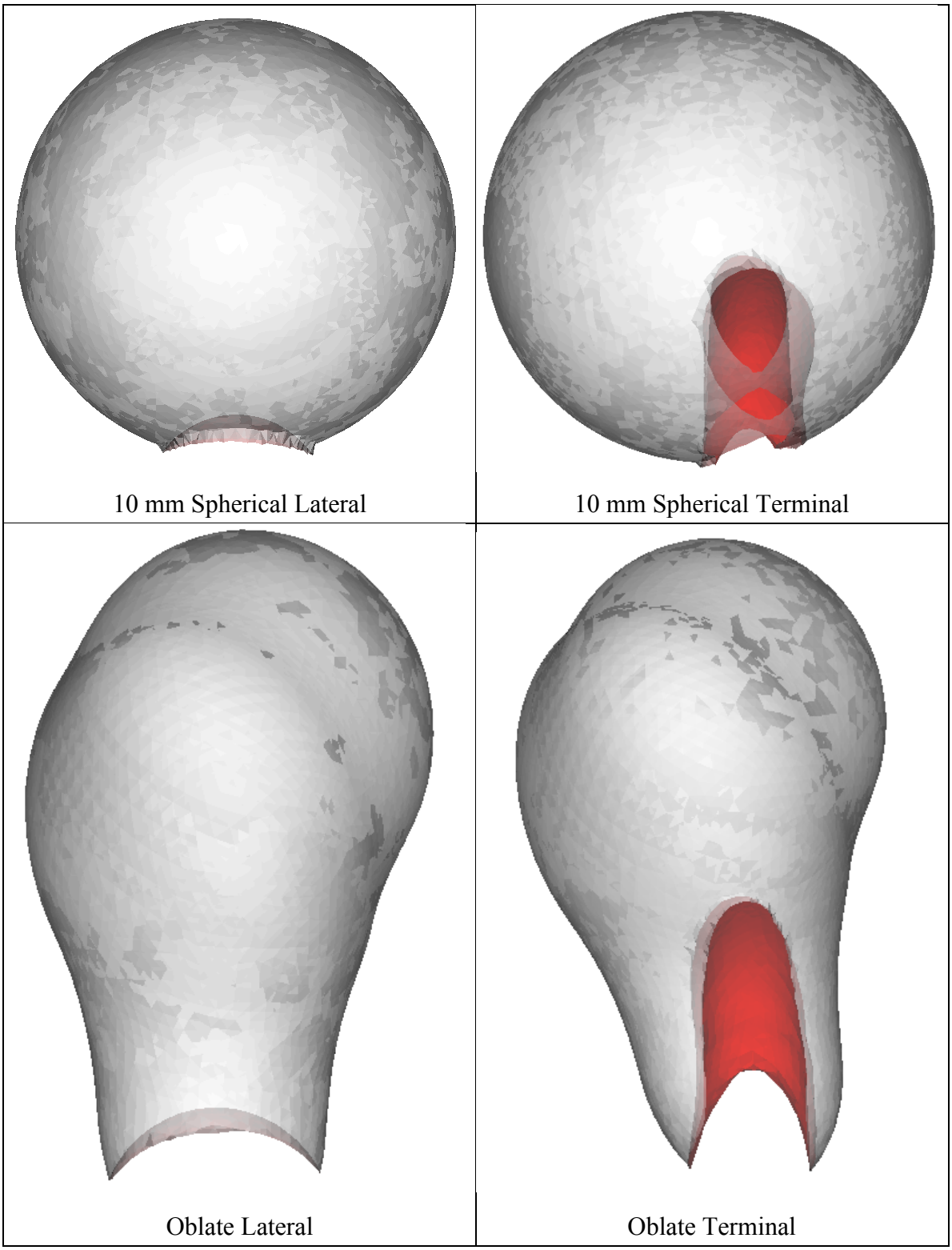

Figure 24 – continued

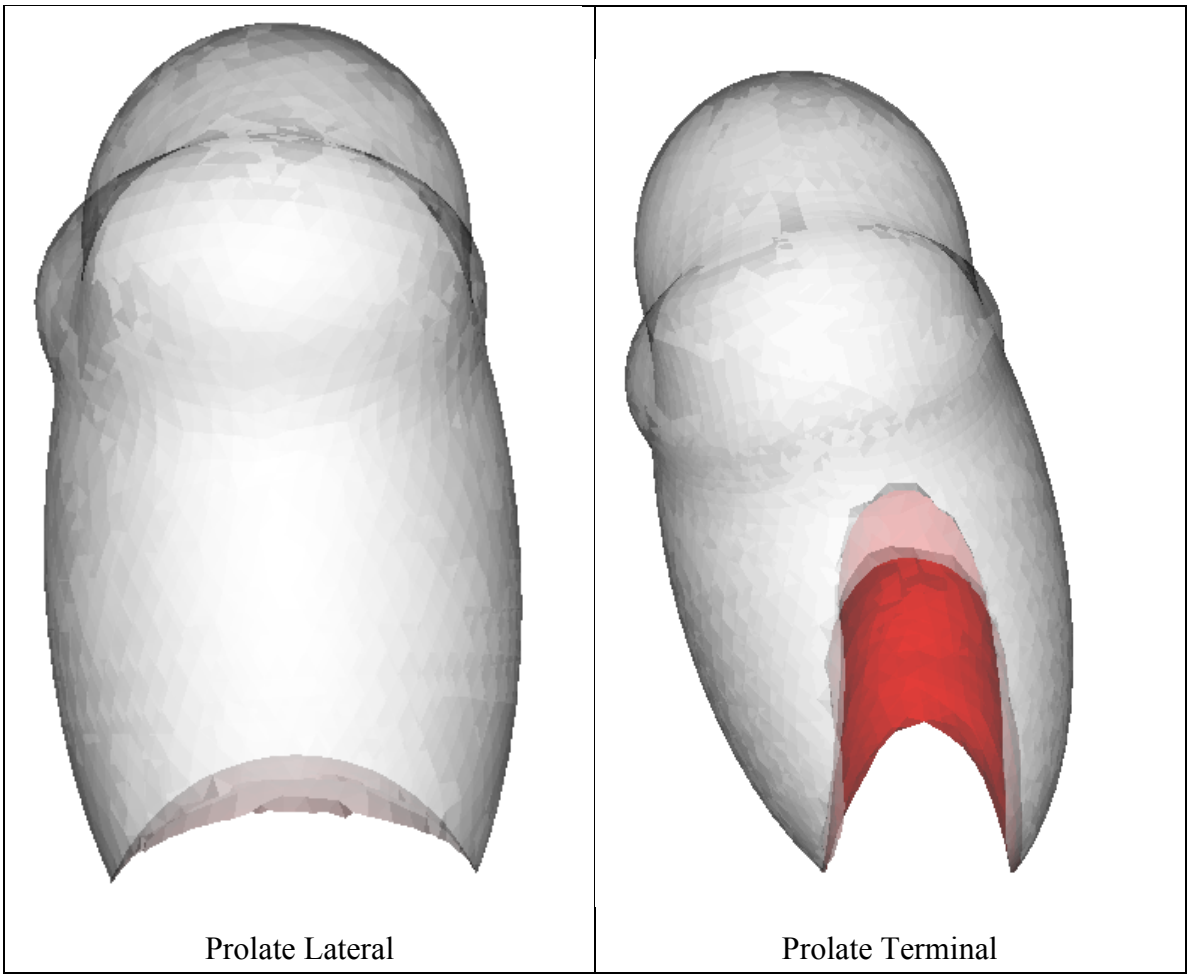

Prolate Lateral | Prolate Terminal

Figure 24 – continued

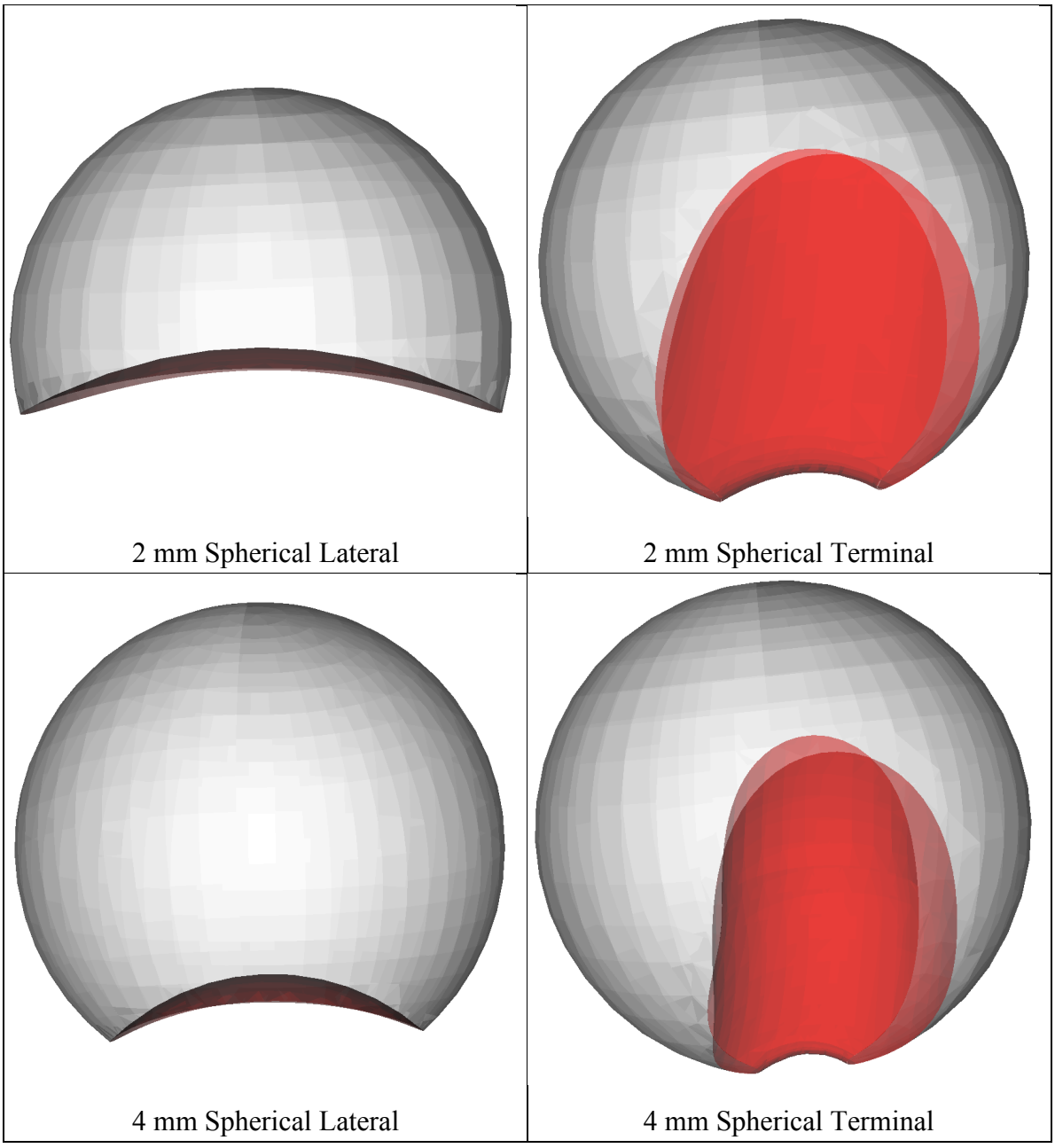

Figure 25. Known dome and neck geometry from Rhinoceros 3D.

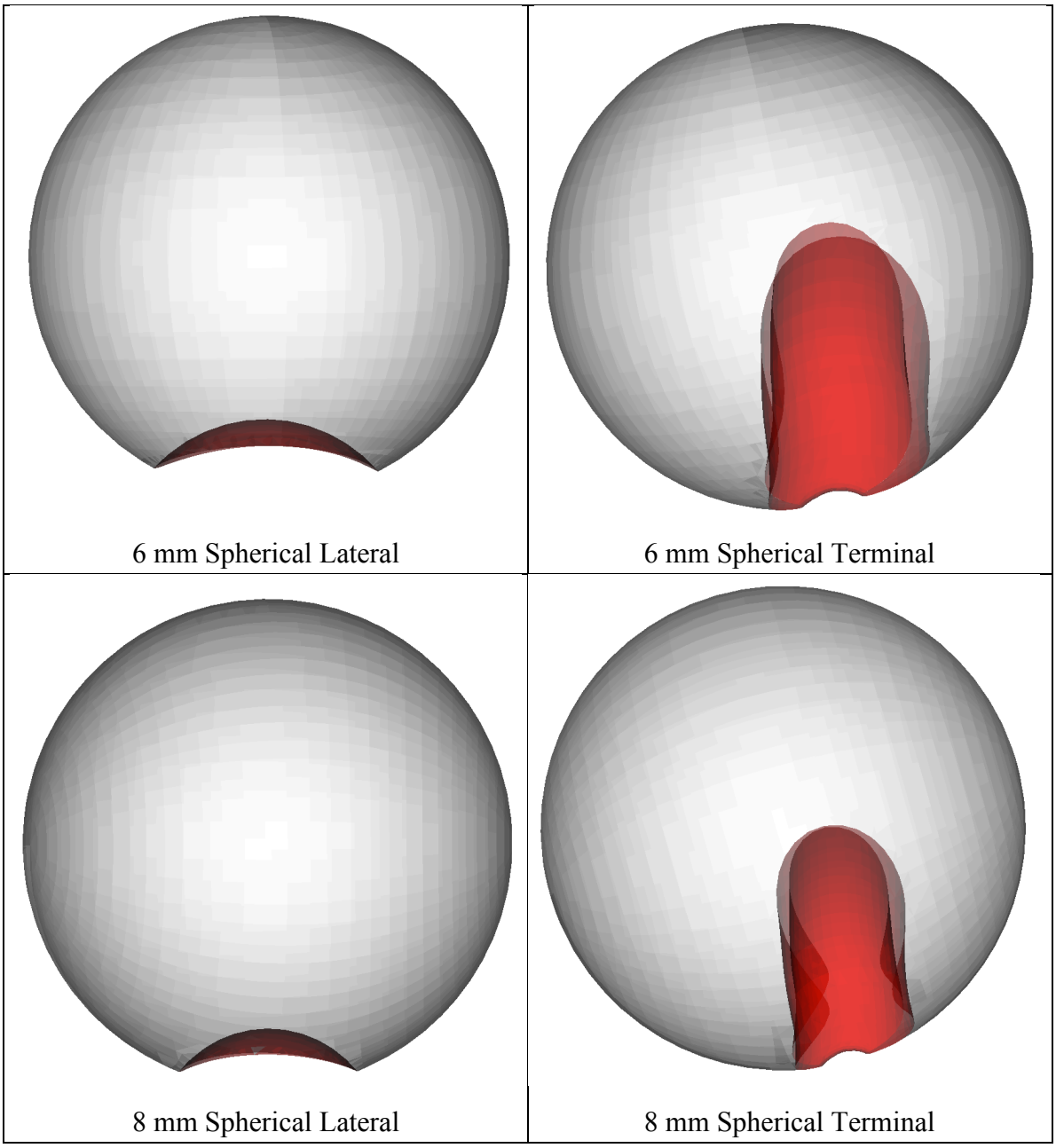

6 mm Spherical Lateral

6 mm Spherical Terminal

8 mm Spherical Lateral

8 mm Spherical Terminal

Figure 25 – continued

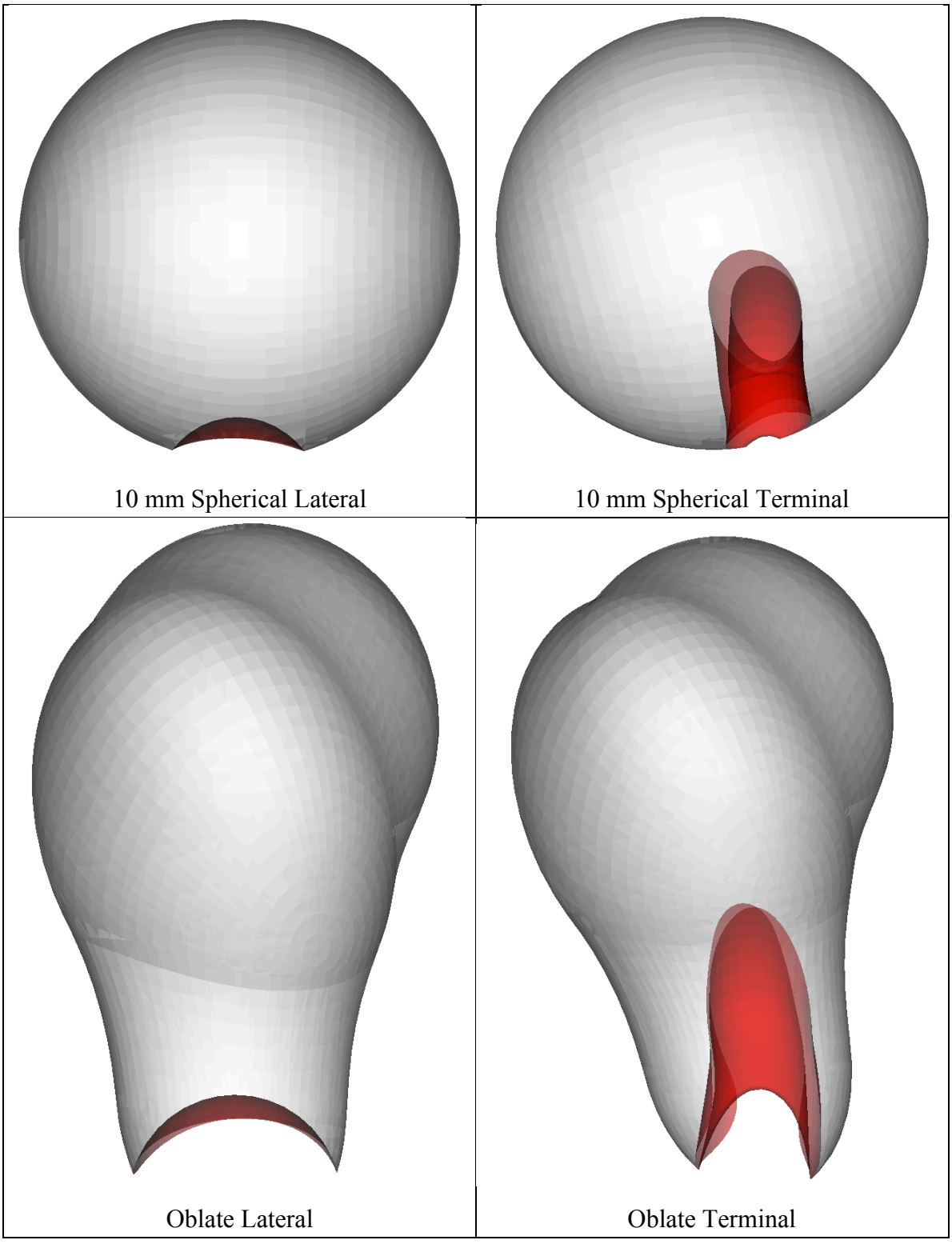

Figure 25 – continued

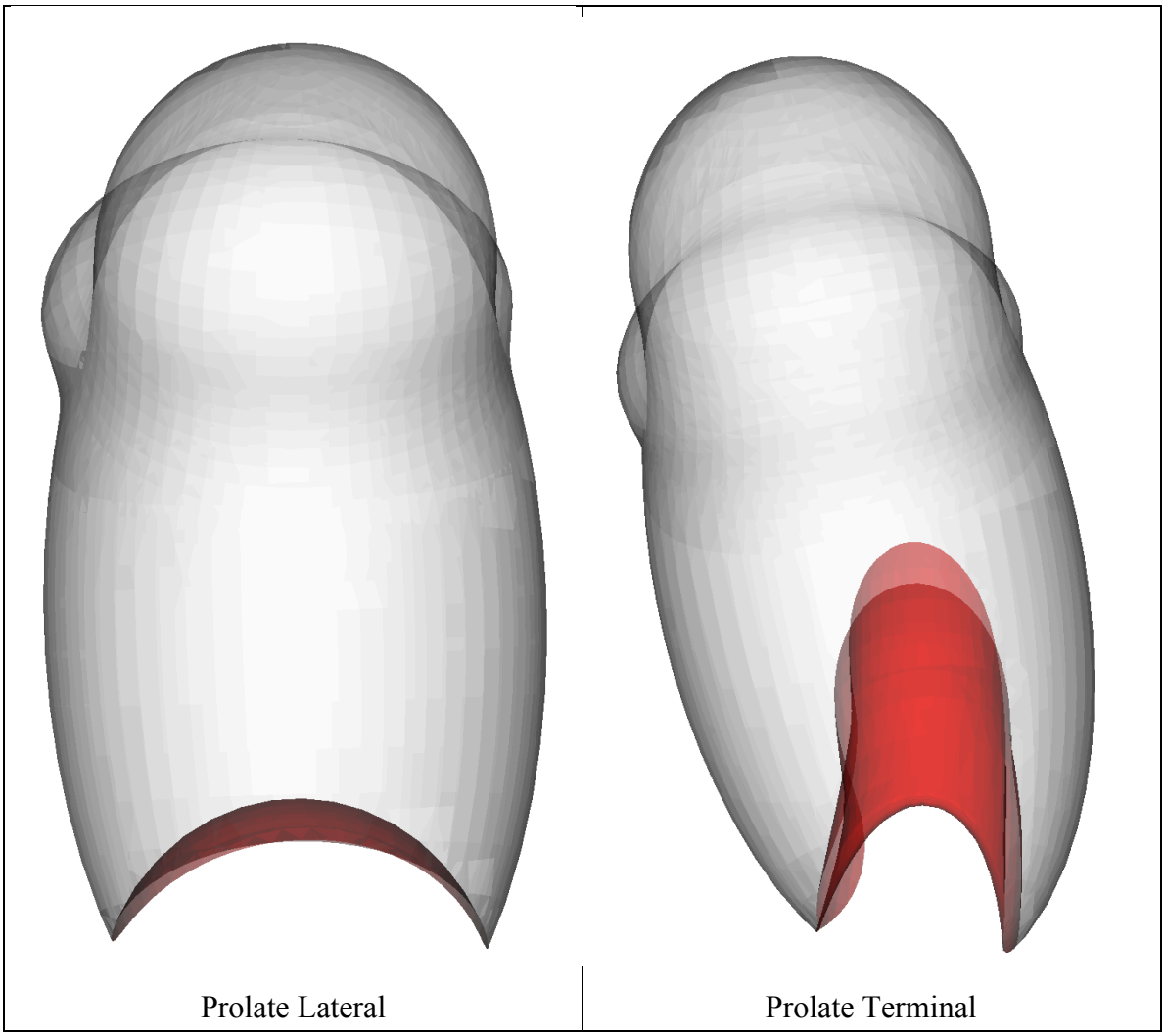

Figure 25 – continued

Table 3. Spearman's rank coefficient for lateral and terminal aneurysms comparing parent vessel reconstruction and Boolean isolation to direct model extraction from Rhinoceros 3D.

	Lateral Aneurysm Spearman's Rank Coefficient	**Terminal Aneurysm Spearman's Rank Coefficient**	**Combined Spearman's Rank Coefficient**
Vol	1.00	1.00	1.00
Max D	1.00	0.89	0.95
Neck D	0.89	0.96	0.93
Vessel D	N/A	N/A	1.00
BF	0.96	1.00	0.98
NVR	0.89	0.96	0.93
SR	1.00	0.89	0.95
TSR	0.99	0.99	0.98
EI	0.96	0.26	0.55
UI	0.82	0.79	0.67
NSI	0.96	0.13	0.57

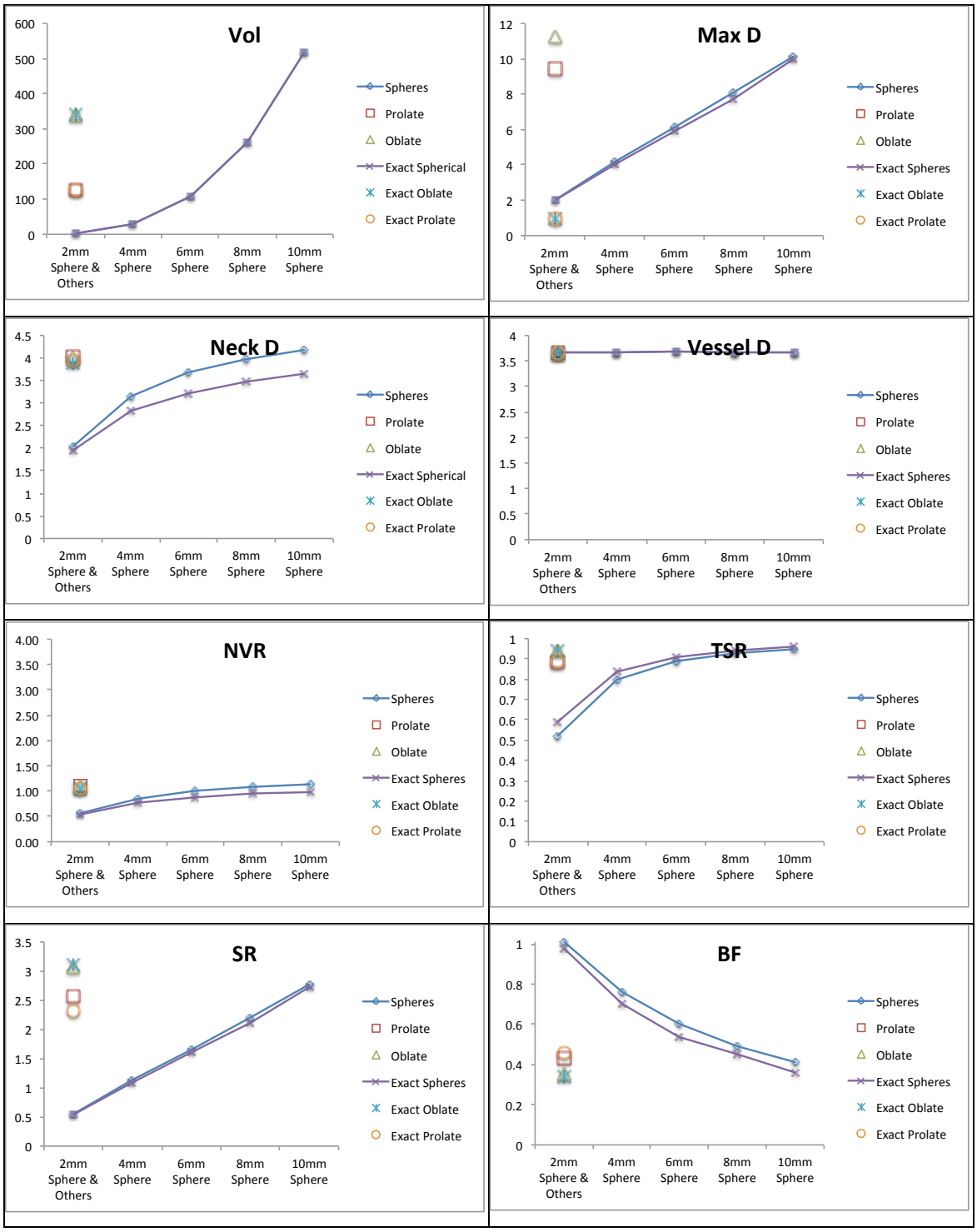

Figure 26. Morphometric index calculations for laterally oriented models.

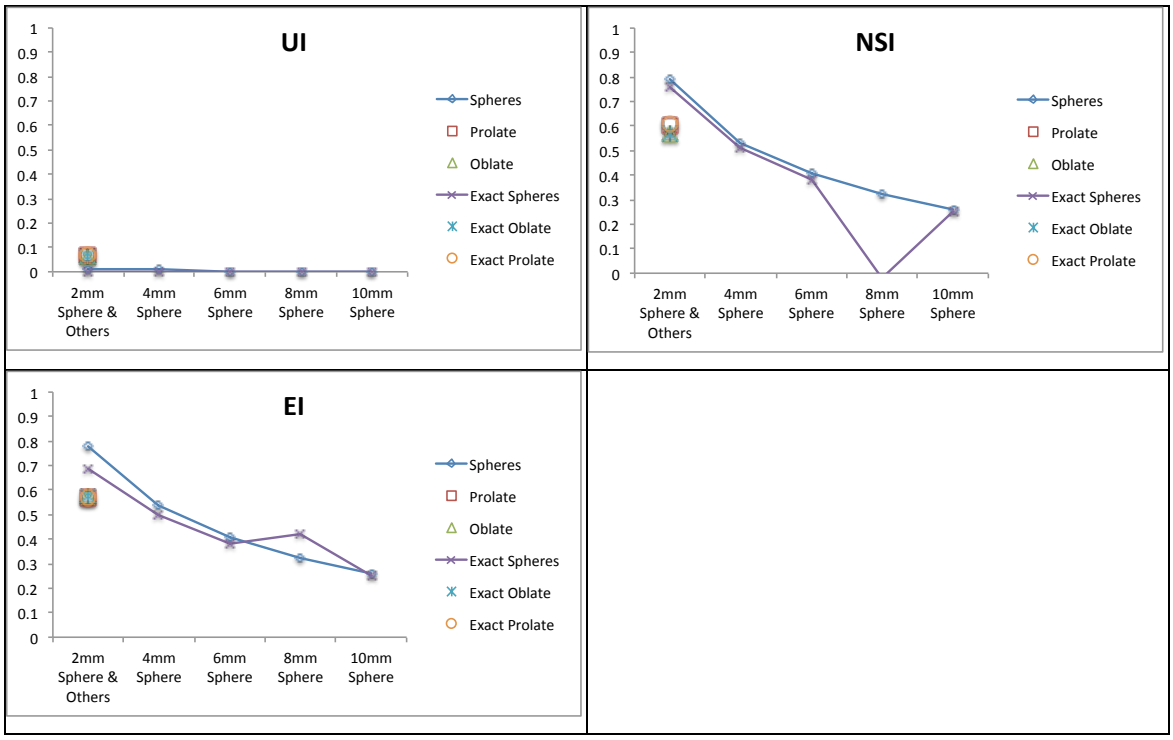

Figure 26 – continued

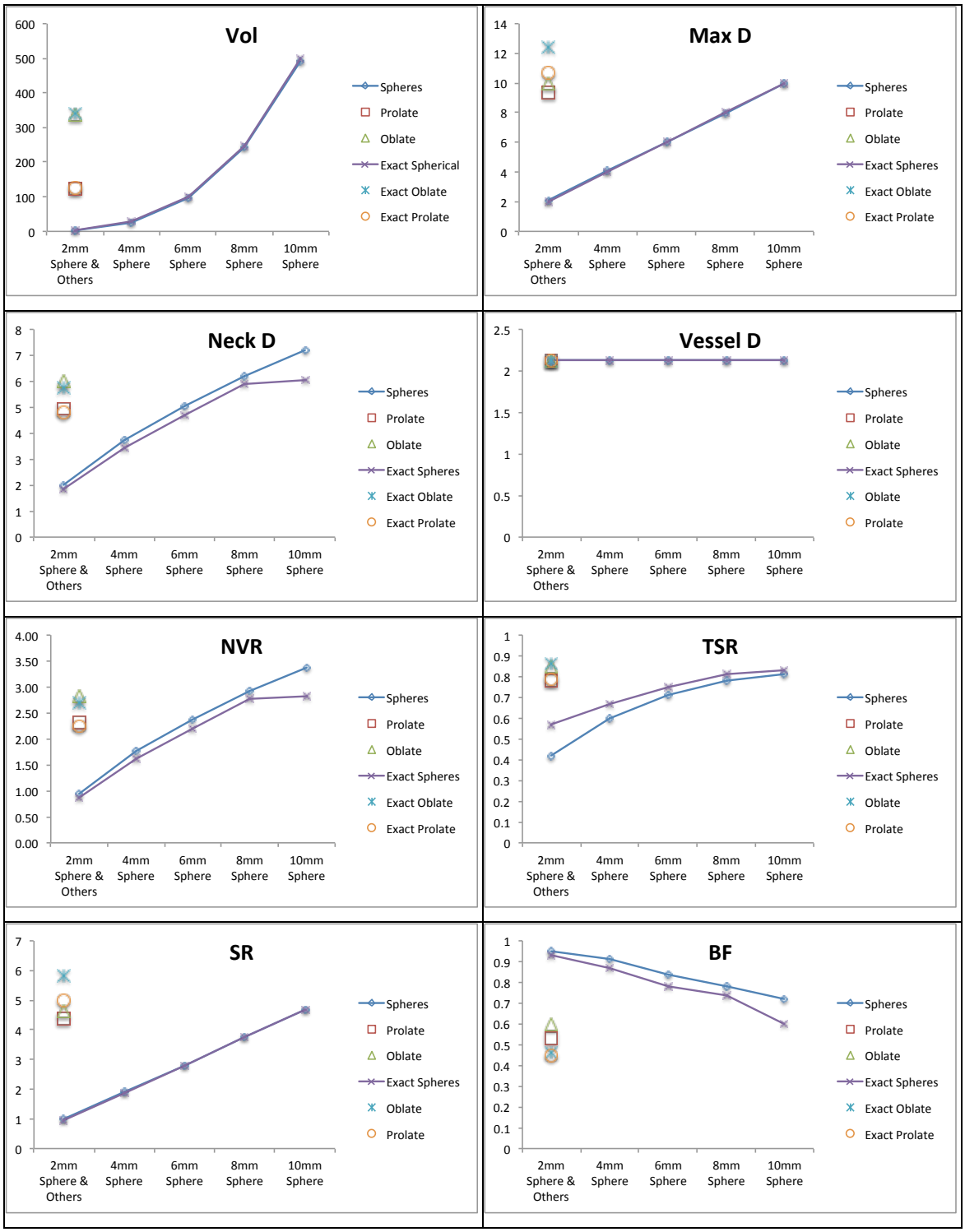

Figure 27. Morphometric index calculations in relation to spherical aneurysm model diameter in a terminal orientation.

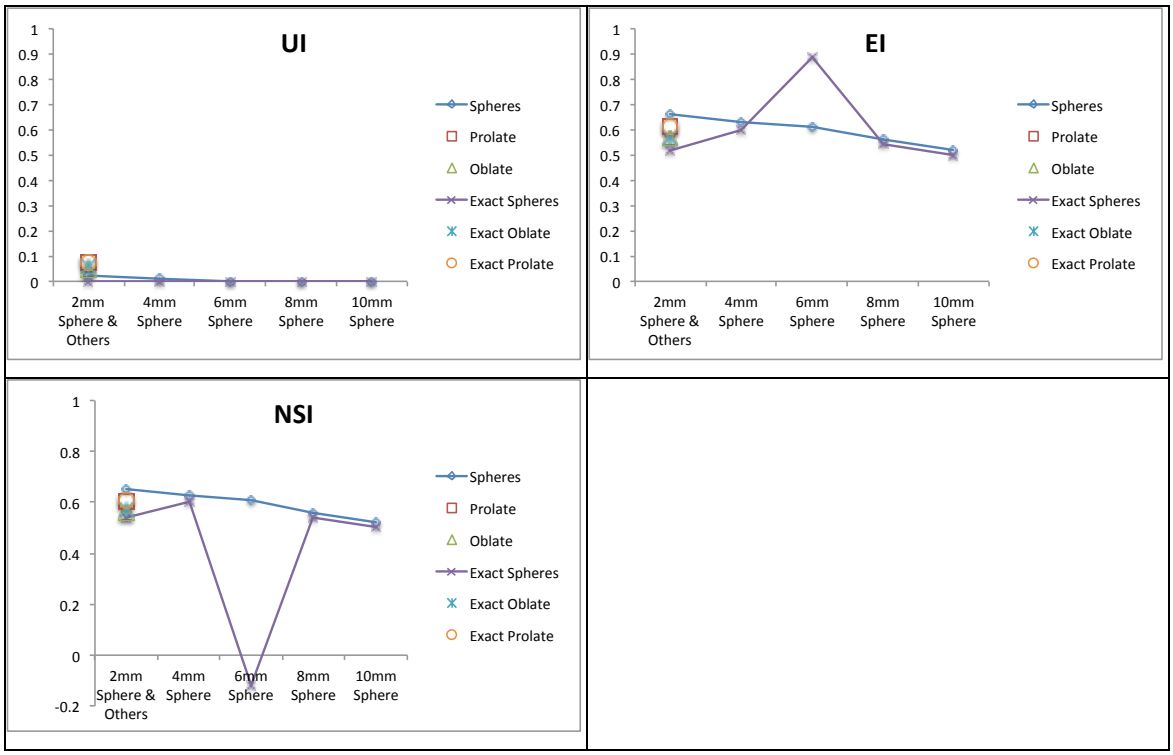

Figure 27 – continued

Discussion

Although each index is meant to eliminate bias for aneurysm size, certain indices such as NVR and SR are defined by the relationship between aneurysm sac size and parent vessel size, which is reflected in the results. Maximum diameter is very close to the prescribed diameters in all spherical cases, with any small fluctuations likely explained by variations caused by re-meshing. The parent vessel reconstruction in all cases resulted in a consistent vessel diameter (± 0.01 mm), reinforcing the efficacy of the Ford et al. algorithm in the case of a perfectly cylindrical vessel with relatively low curvature and an aneurysm with a well-defined neck. Additionally, Spearman's rank coefficient was high for all indices barring the NSI and EI for the terminal aneurysms. This was likely due to numerical errors due to the complex geometry near the sharp bifurcation at the basilar terminus, and numerical errors due to meshing. The Rhinoceros 3D meshing scheme produced noticeably skewed elements. This possibly resulted in errors where the points that defined the Voronoi diagram of these models were not close enough together to keep the Voronoi spheres completely internal to the surface. In meshes with skewed element geometries, this type of error commonly persists. Because of this, a re-meshing step had been added into the protocol in order to prevent high element aspect ratios. The 6 mm spherical terminal aneurysm that was isolated directly within Rhinoceros showed anomalies in the calculations of its NSI and EI values. This is likely because of errors caused by the calculation of the normal vectors near areas of high element skew, which resulted in a partially external Voronoi diagram from which the largest maximal inscribed sphere was derived.

Analysis of the Effects of Surface Mesh Resolution

The surface mesh resolution of a segmented model is a balancing act between processing time and accuracy of the analysis. As mesh resolution decreases computation

time becomes exponentially faster, and quicker computation time becomes increasingly important as the number of cases in a study increases. With some morphological studies reaching patient enrollment counts well into the thousands (Wiebers, 2003), this is not an issue to be taken lightly. However, decreased resolution also means decreased accuracy of the surface, and an increased possibility of obfuscating important morphological features. Additionally, the metrics described in this paper are mesh-dependent, and a change in mesh resolution could potentially have an effect on their value. It is therefore important to characterize the effect of surface mesh resolution on the outcome of the morphometric analysis.

Methods

In this study, two of the hypothetical idealized models created for the efficacy study - two spherical aneurysms, both of which were placed in a lateral configuration on an internal carotid artery vessel segment, were again used in this study. Each was re-meshed at four resolutions with triangular element target areas of 0.01, 0.05, 0.15, and 0.25 mm^2. Selected models are shown in Figure 28. The reconstructed parent vessel expansion model was also re-meshed with the respective target area for each individual model so that upon Boolean subtraction, mesh resolution would be consistent across the isolated aneurysm surface mesh. The morphometric indices were then evaluated for each surface mesh. The parent vessel reconstruction, sac isolation, and morphometric index analysis were timed in order to gain insight into the relationship between resolution and computation time. The computations were performed using an Apple Mac Pro with a 3.2 GHz Quad-Core Intel Xeon processor with 32 GB 800 MHz DDR3 ECC memory. Each Python process ran at up to 100% of 1 of 8 virtual cores.

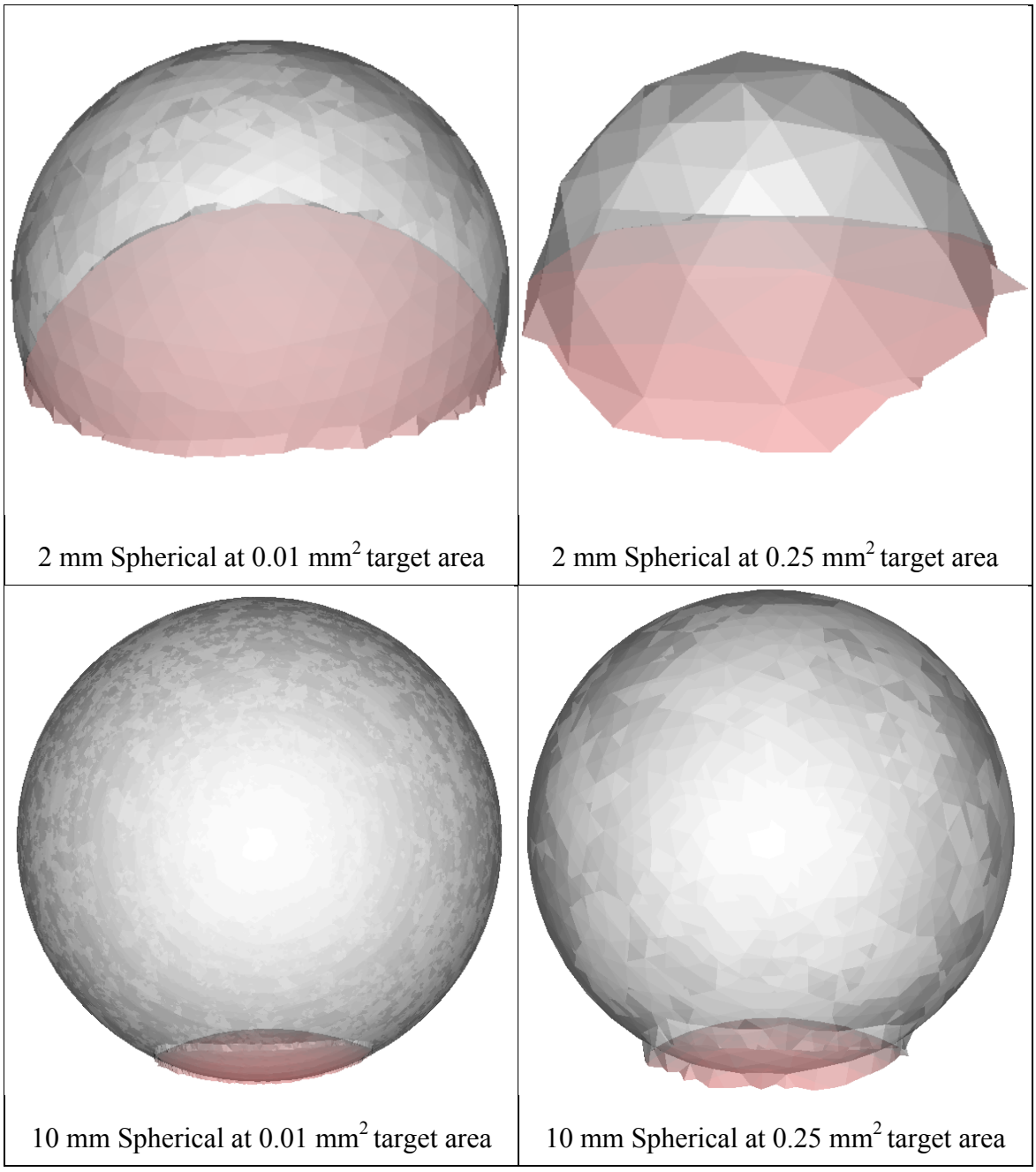

Figure 28. Effects of high and low resolution on differently sized aneurysm models. Dome is shown in grey, and neck is shown in red.

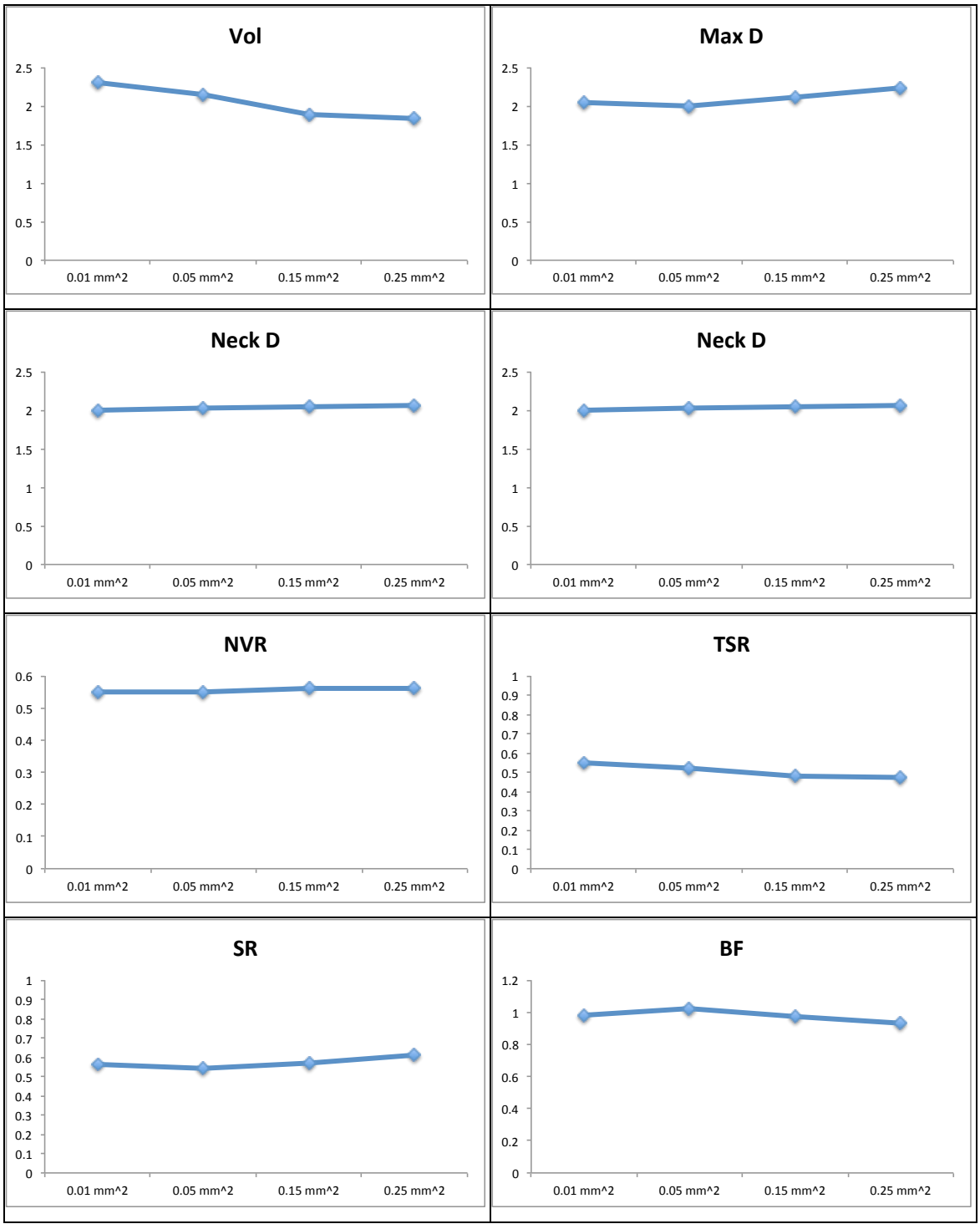

Figure 29. Morphometric indices for the 2 mm spherical aneurysm model plotted across decreasing resolution.

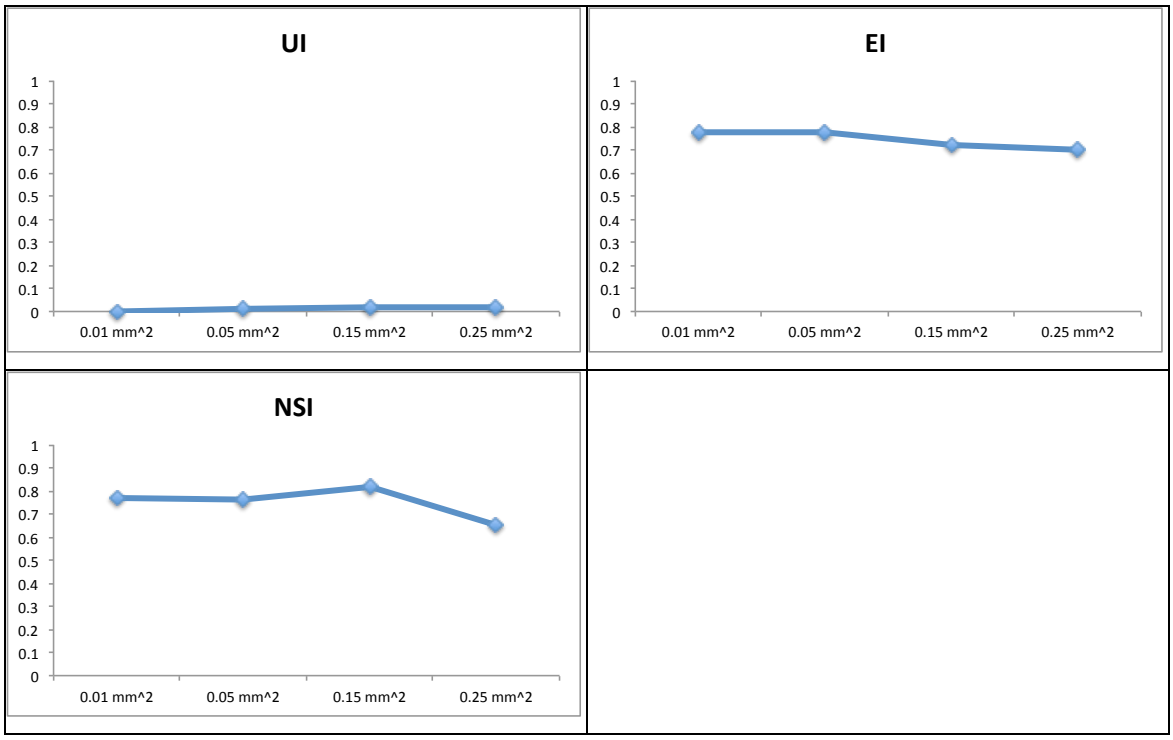

Figure 29 – continued

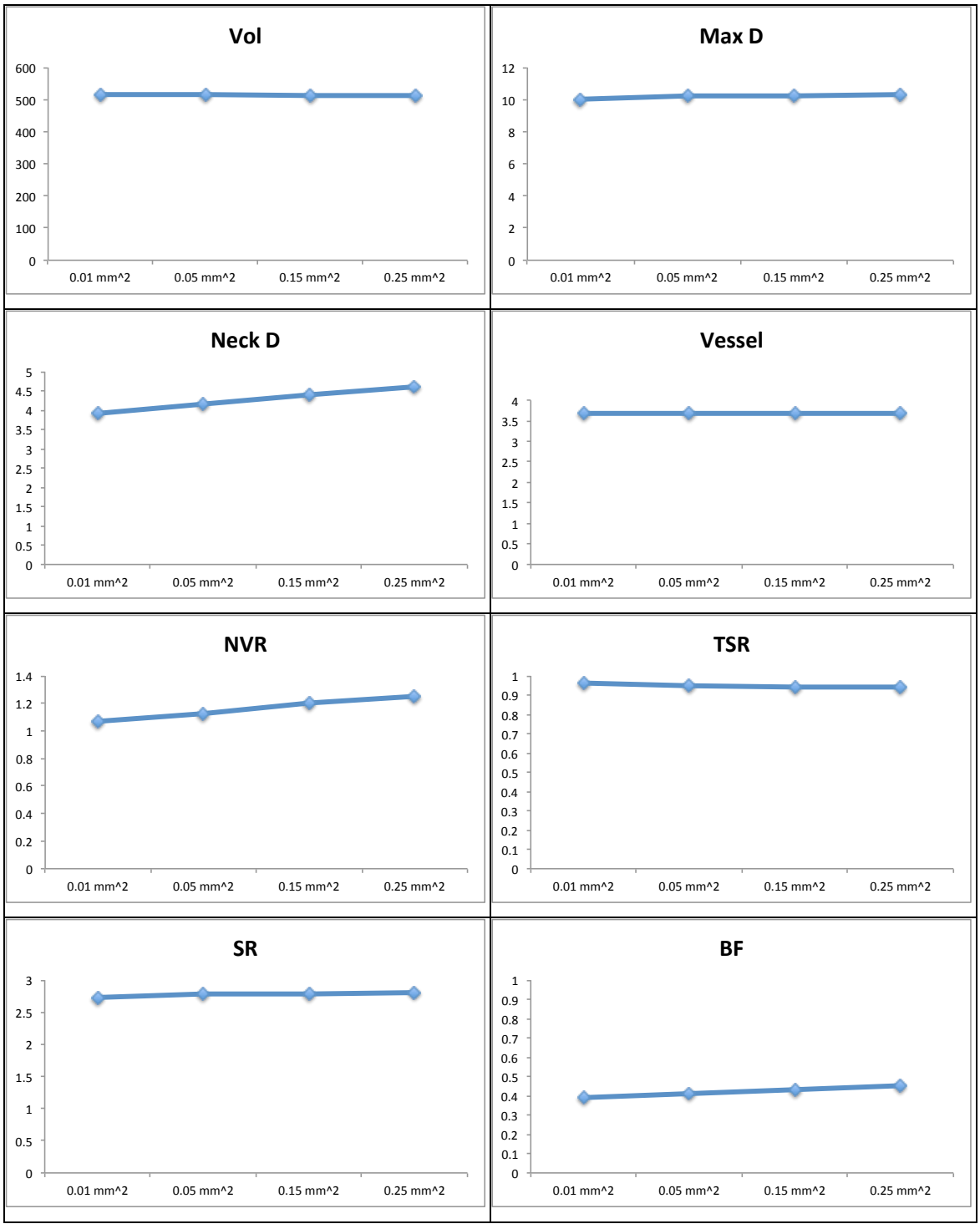

Figure 30. Morphometric indices for the 10 mm spherical aneurysm model plotted across decreasing resolution.

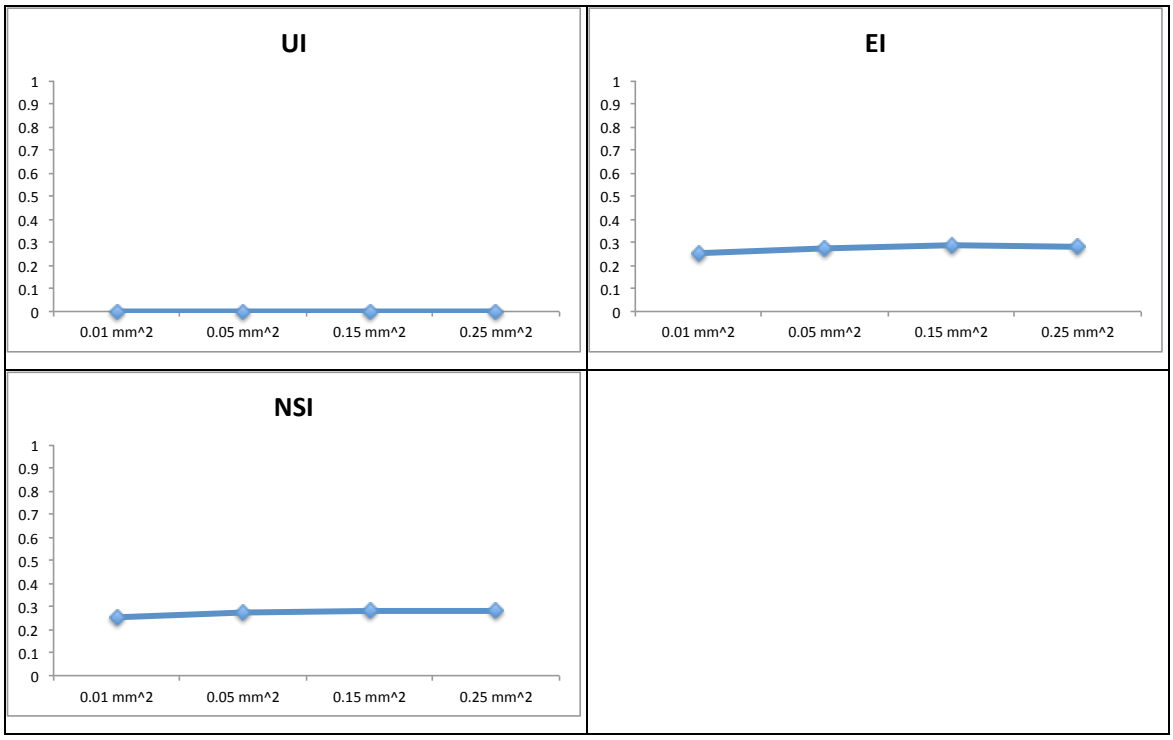

Figure 30 – continued

Results

The morphometric index calculations are shown in Figure 29 and Figure 30 for the 2 mm and 10 mm aneurysm models, respectively.

Discussion

Increased surface mesh resolution was seen to contribute to an exponential increase in computation time. Parent vessel reconstruction time was seen to be fairly similar between models of the same resolution, regardless of aneurysm size. This is to be expected as the Voronoi diagram of the aneurysm and parent vessel in the near is removed, and only the amount of removed parent vessel would affect the amount of computation needed for this step. The isolation and analysis processes, however, were greatly affected by both resolution and by aneurysm size. This is because of the large increase in the number of points that must be computed within the Voronoi diagram of the aneurysm sac for both processes between the 2 mm and 10 mm aneurysms. The large computational expense required for surface meshes of a resolution on the order of 0.01 mm^2 target element area (assuming an equilateral element geometry results in an edge length of approximately 0.15 mm) may be unnecessary, however, depending on the imaging modality, as the resolutions of most medical imaging modalities do not approach this number. Although perhaps still a higher resolution than necessary, a target element area of 0.05 mm^2 was used in all models in the previous two experiments. Assuming an equilateral element geometry, this results in an edge-length of 0.34 mm, which is reasonable considering the resolution of most modern medical imaging modalities. This resolution also provides a reasonable medium in computational time with an approximately 14 minutes for a small, 2 mm aneurysm on a mid-sized vessel segment and approximately 20 minutes for a 10 mm aneurysm on the same mid-sized vessel segment.

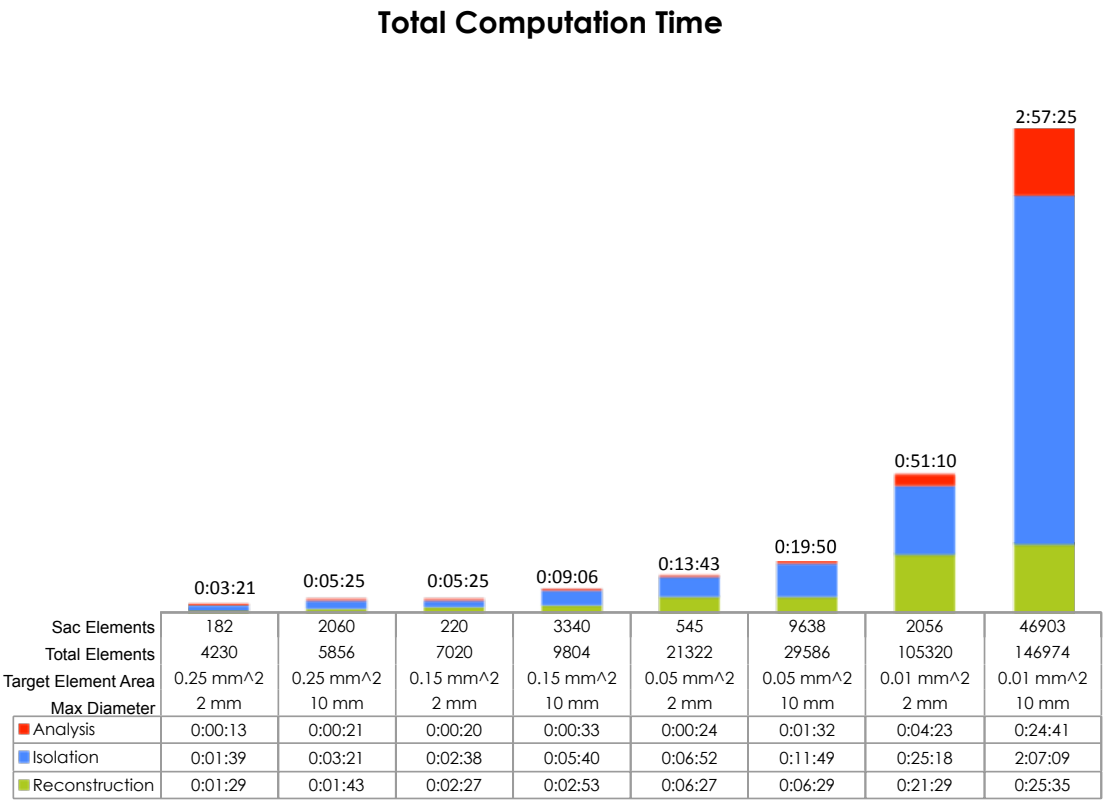

Sac Elements	182	2060	220	3340	545	9638	2056	46903
Total Elements	4230	5856	7020	9804	21322	29586	105320	146974
Target Element Area	0.25 mm^2	0.25 mm^2	0.15 mm^2	0.15 mm^2	0.05 mm^2	0.05 mm^2	0.01 mm^2	0.01 mm^2
Max Diameter	2 mm	10 mm	2 mm	10 mm	2 mm	10 mm	2 mm	10 mm
Analysis	0:00:13	0:00:21	0:00:20	0:00:33	0:00:24	0:01:32	0:04:23	0:24:41
Isolation	0:01:39	0:03:21	0:02:38	0:05:40	0:06:52	0:11:49	0:25:18	2:07:09
Reconstruction	0:01:29	0:01:43	0:02:27	0:02:53	0:06:27	0:06:29	0:21:29	0:25:35

Figure 31. Computation time for each aneurysm, stratified by process.

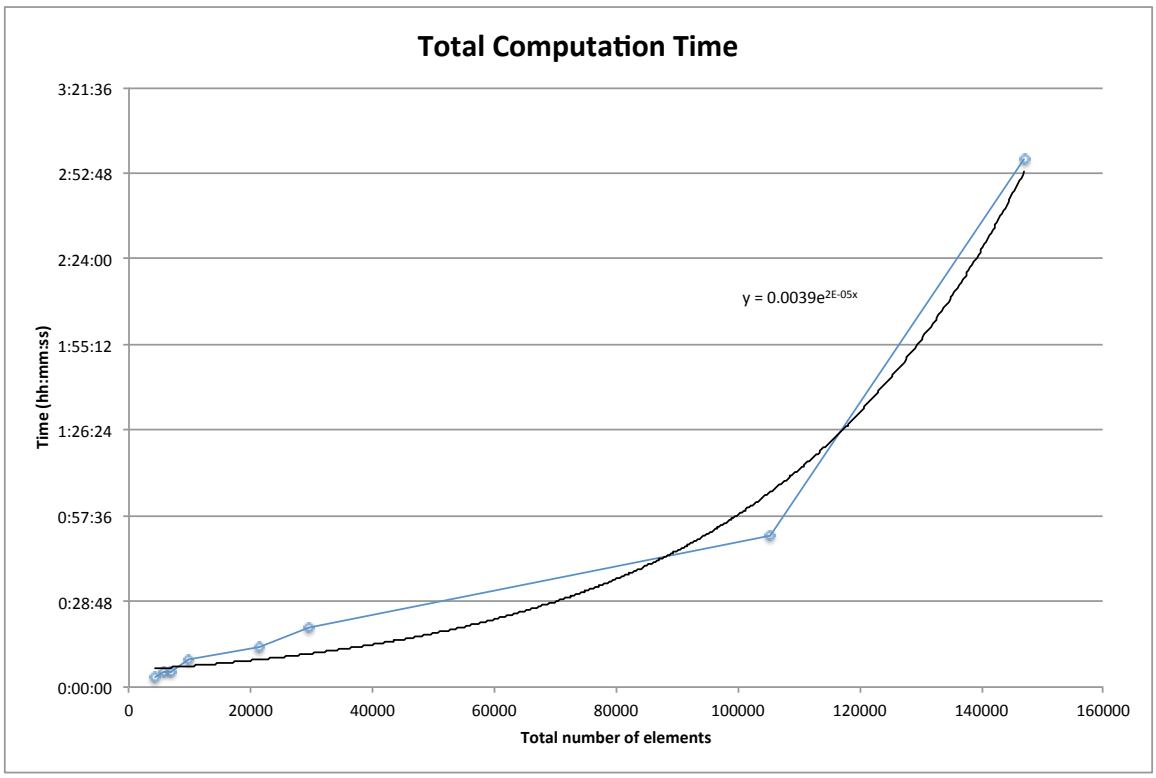

Figure 32. Resulting total computation time in relation to total number of elements in the original model, disregarding aneurysm size.

CHAPTER 5

CONCLUSIONS

Conclusions on Aneurysm Isolation

It was shown in the repeatability analysis that the Boolean isolation method introduced in this work provided no benefit in the reduction of user-induced variability compared to the current gold standard in the field, the two-dimensional user-placed cutting plane. This is assumed to be due to the large sensitivity of the resulting model to the size, orientation, and location of the parent vessel reconstruction. A change in average diameter of the parent vessel reconstruction or its location relative to the aneurysm sac will result in an even larger change in the resulting surface area of the neck.

However, value can still be garnered from this novel isolation process. Because of the cylindrical nature of the parent vessel and radial bulging caused by an aneurysm, a cutting plane is not always the best choice to extract all geometric features of an aneurysm sac. In many cases, a well-defined planar neck does not exist through which to place the cutting plane, leading to a large possibility for error in index calculation depending on what portion of the aneurysm sac is removed by necessity. With a Boolean isolation of the parent vessel, only the features unrelated to the sac geometry are removed. This leaves no sacrifice in geometry extraction, allowing for analysis of the entire sac.

Although only the P-value for NSI showed statistically significant differences between the index results of the two methods, it should be noted that this was a post-hoc analysis with low sample size. With higher sample size and greater variety in aneurysm geometry the possibility exists that larger statistical differences would be found, and further experimentation should be done to more thoroughly characterize the efficacy of this isolation method. However, this novel isolation method still provides an innate way

to isolate the entire body of the aneurysm as defined as the outward deviation from a healthy vascular geometry.

Conclusions on Aneurysm Morphology Analysis

The new measurement techniques for ascertaining maximum diameter, neck diameter, and vessel diameter introduced in this work are necessary to process the resulting geometries of the Boolean isolation method introduced in this work. The neck is no longer planar and represents an entirely different entity than that represented by a two-dimensional neck plane. This new idea of the aneurysm neck represents the hypothetical pre-lesion geometry of the aneurysm and its parent vasculature, and provides insight into the anatomical changes that may have occurred upon formation of the aneurysm. In this sense, TSR is a novel, appropriate morphometric index that should be tested in a prospective study to determine its value in discriminating low risk from high-risk aneurysms. Another novel index, NVR, is also worthy of further study. This index may be hemodynamically relevant, relating the mass flow of the feeding vessel to that at the ostium of the aneurysm sac. If the tissue mechanics and hemodynamics which lead to further aneurysmal disease progression can be simplistically characterized using morphological indices, then perhaps in the future relevant measures can be used by physicians to make diagnostic decisions.

Limitations

There are several possible sources for error in the methods. The dependence on the algorithm for parent vessel reconstruction (Ford et al., 2009) is a particular source for concern. This algorithm generally provides a very reasonable parent vessel approximation, and is a very effective tool in many aspects. However, a number of cases also exist in which this algorithm provides what appears upon visual inspection to be an obviously inaccurate or unrealistic reconstruction. This is particularly apparent in lesions appearing on vessels with high curvature within the reconstructed region, in which the

reconstruction does not remain within or follow the original curvature of the vessel. Because of this difference in the reconstructed versus original vasculature, upon isolation the neck region of the aneurysm acquires what may be described as a flanged shape. Although some morphological indices would be not be affected greatly by this error (particularly EI and NSI) the neck diameter and surface area could be significantly affected, leading to subsequent errors in calculation of BF, TSR, and NVR, and possible errors in UI as well.

Another drawback of the current isolation technique may be in cases of non-cylindrical vessel geometry. The reconstruction algorithm is meant only to reconstruct the parent vessel as interpolated between cylindrical portions of healthy vasculature. Blood vessels typically maintain a circular cross-section with any deviation generally referred to as an aneurysmal or a thrombotic lesion. However, non-cylindrical vessel geometry was encountered on some surface models in the user variability study. These irregularities were most likely a result of the lack of an image density gradient in near-skull regions. Because of this, a flanged region was present in the isolated aneurysm that is most likely an inaccurate geometrical feature.

It was also noticed in some cases that upon closer inspection of some isolated aneurysm surface meshes, unclosed edges were present near the neck-sac interface. Although no obvious missing or non-manifold elements were present, the presence of these edges could pose challenges if the geometry were to be re-meshed or mechanically analyzed with computational fluid dynamics (CFD) or finite element analysis (FEA). Additionally, errors may be present in volume and surface area calculations of open meshes. These errors may have been present in the presented data, however any inaccuracy was within reason of reality and was repeated exactly by multiple software algorithms.

Neck diameter is determined from an average of the point-wise radius measurement made from the average neck position. It was assumed that because the

mesh of the surface was evenly sampled with an approximately even point distribution across the entirety that the point-spread at the neck perimeter would be approximately even as well. However, upon closer inspection, it seems that this is not the case. A possible solution is to extract the perimeter utilizing the current technique and subsequently resample the points along that line using VMTK. This would prevent skewing of the centroidal calculation and radius average due to uneven point distribution.

Future Perspectives

Although many morphological indices have already been conceived, any number of shape features remains yet to be quantified in this regard. Additionally, some current morphological indices leave room for improvement in the efficiency with which they describe such shape features. For instance, the measure of surface undulation described

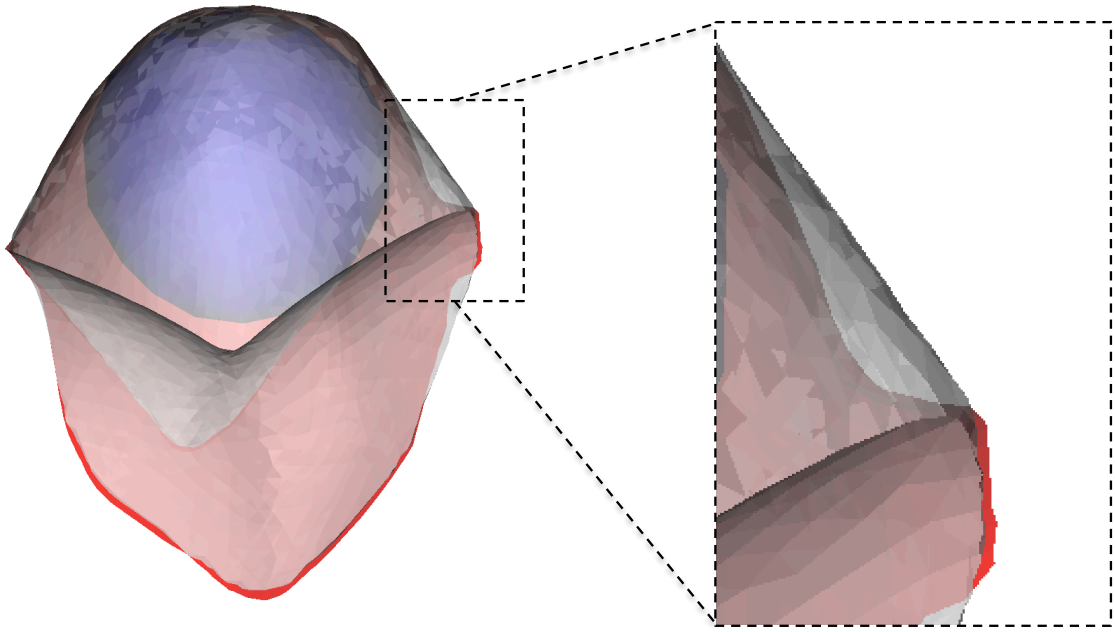

Figure 33. Artificial volume differences between the convex hull (grey) and the aneurysm dome (white) near the neck region of the aneurysm, leading to errors in the characterization of dome undulation.

by Raghavan et al. and Ma et al. in 2004 and 2005, respectively, is capable of describing

general geometric traits. However, upon any convexity near the neck boundary of the convex hull of an aneurysm, some volume differences may be artificially introduced as a result of natural curvature near the neck, as demonstrated in Figure 33. Because the index was conceived in order to describe undulations within the structure of the dome this results in inaccuracies in geometric characterization. Additionally, although the index does control for aneurysm size, because it is scaled by total volume the same magnitude of surface undulation in a large aneurysm would result in a lower indicial description than that of an aneurysm with lower volume. In order to account for this bias, a fractal-based approach such the box count method could be developed. Alternatively, a new method could easily be developed using a variation on the technique for undulation removal introduced by Piccinelli et al. as the Voronoi Diagram Core (VDC) (Piccinelli et al., 2012) simply by characterizing the differences between the undulation free surface (the VDC) and the original surface.

An improvement upon the Ford et al. algorithm would greatly improve the abilities of the method introduced in this paper to more accurately isolate the aneurysm sac geometry. As previously mentioned, in cases on which the aneurysm sits upon vessel regions of high tortuosity, the parent vessel reconstruction strays from the bounds of the vessel. These should, in subsequent work, be corrected. A more robust spline interpolation must be employed, taking into account that the spline and reconstructed Voronoi diagram should realistically not protrude externally to the diseased vasculature.

As previously mentioned in the introduction, cerebral aneurysm coiling procedures are growing in popularity as a treatment option. Much of the success of these operations depends greatly on the aneurysm sac and neck geometries, however, so perhaps a new study to determine the relationship of coiling success rate in relation to morphological features could be performed.

Additionally, a continuation of the prospective study by Ramachandran (Ramachandran, 2012) is an appropriate application of this work. This study investigated

the ability of the morphometric indices introduced by Raghavan et al. to predict aneurysm disease progression. The results of that study showed inconclusive evidence as to whether or not these morphometric indices could prospectively differentiate aneurysms that would continue on to grow or rupture from those that would not. However, perhaps the ability to capture a more full aneurysmal geometry in combination with novel and rethought geometric measures and morphological analyses could bring out morphological and mechanical characteristics of these aneurysms that would otherwise go unseen.

REFERENCES

Aneurysm. (2003). *Miller-Kean Encyclopedia and Dictionary of Medicine, Nursing and Allied Health*. Saunders.

Alyassin, A. M., Lancaster, J. L., & Downs, J. H. I. (1994). Evaluation of New Algorithms for the Interactive Measurement of Surface Area and Volume. *Medical Physics*, *21*(6), 741.

Antiga, L. (2002). Patient-Specific Modeling of Geometry and Blood Flow in Large Arteries.

Banatwala, M., Farley, C., Feinberg, D., & Humphrey, J. D. (2005). Parameterization of the shape of intracranial saccular aneurysms using Legendre polynomials. *Computer methods in biomechanics and biomedical engineering*, *8*(2), 93–101.

Berkowitz, B., & Raghavan, M. L. (2009). Interactive Computer Model of Cerebral Vasculature. *Biomedical Engineering Society Annual Meeting*. Pittsburgh, PA.

Bowker, T. J., Watton, P. N., Summers, P. E., Byrne, J. V., & Ventikos, Y. (2010). Rest versus exercise hemodynamics for middle cerebral artery aneurysms: a computational study. *American Journal of Neuroradiology*, *31*(2), 317.

Cieslicki, K., & Ciesla, D. (2005). Investigations of flow and pressure distributions in physical model of the circle of Willis. *Journal of Biomechanics*, *38*(11), 2302–2310.

Dhar, S., Tremmel, M., Mocco, J., Kim, M., Yamamoto, J., Siddiqui, A. H., Hopkins, L. N., et al. (2008). Morphology parameters for intracranial aneurysm rupture risk assessment. *Neurosurgery*, *63*(2), 185–96; discussion 196–7.

Federal Drug Administration. *Summary of Safety and Effectiveness Data (SSED)*. (2011). Retrieved from http://www.accessdata.fda.gov/cdrh_docs/pdf10/P100018b.pdf

Ford, M. D., Hoi, Y., Piccinelli, M., Antiga, L., & Steinman, D. A. (2009). An objective approach to digital removal of saccular aneurysms: technique and applications. *Br. J. Radiol.*, *82*, S55–S61.

Gonzalez, N., Sedrak, M., Martin, N., & Vinuela, F. (2008). Impact of anatomic features in the endovascular embolization of 181 anterior communicating artery aneurysms. *Stroke*, *39*(10), 2776.

Grunwald, I. Q., Papanagiotou, P., Struffert, T., Politi, M., Krick, C., Gül, G., & Reith, W. (2007). Recanalization after endovascular treatment of intracerebral aneurysms. *Neuroradiology*, *49*(1), 41.

Guglielmi, G., Viñuela, F., Sepetka, I., & Macellari, V. (1991). Electrothrombosis of saccular aneurysms via endovascular approach. Part 1: Electrochemical basis, technique, and experimental results. *Journal of neurosurgery*, *75*(1), 1.

Hademenos, G. J., Massoud, T. F., Turjman, F., & Sayre, J. W. (1998). Anatomical and morphological factors correlating with rupture of intracranial aneurysms in patients referred for endovascular treatment. *A Journal Devoted to Neuroimaging and Interventional Neuroradiology*, *40*(11), 755–760.

Hop, J. W., Rinkel, G. J., Alegra, A., & Van Gijn, J. (1997). Case-fatality rates and functional outcome after subarachnoid hemorrhage: a systematic review. *Stroke*, *28*(3), 660.

Kadasi, L. M., Dent, W. C., & Malek, A. M. (2012). Cerebral aneurysm wall thickness analysis using intraoperative microscopy: effect of size and gender on thin translucent regions. *Journal of NeuroInterventional Surgery*.

Kitware, I. (2006). *The VTK User's Guide*. (I. Kitware, Ed.) (Vol. 5). Kitware, Inc.

Lauric, A. (2011). Rupture Status Discrimination in Intracranial Aneurysms Using the Centroid-Radii Model. *IEEE Trans. Biomed. Eng.*, *58*(10), 2895–2903.

Lauric, A., Miller, E. L., Baharoglu, M. I., & Malek, A. M. (2011). 3D shape analysis of intracranial aneurysms using the writhe number as a discriminant for rupture. *Annals of biomedical engineering*, *39*(5), 1457–69.

Ma, B., Harbaugh, R. E., & Raghavan, M. L. (2004). Three-dimensional geometrical characterization of cerebral aneurysms. *Annals of biomedical engineering*, *32*(2), 264–73. Retrieved from http://www.ncbi.nlm.nih.gov/pubmed/15008374

Millán, R. D., Dempere-Marco, L., Pozo, J. M., Cebral, J. R., & Frangi, a F. (2007). Morphological characterization of intracranial aneurysms using 3-D moment invariants. *IEEE transactions on medical imaging*, *26*(9), 1270–82. doi:10.1109/TMI.2007.901008

Piccinelli, M., Steinman, D. a, Hoi, Y., Tong, F., Veneziani, A., & Antiga, L. (2012). Automatic Neck Plane Detection and 3D Geometric Characterization of Aneurysmal Sacs. *Annals of biomedical engineering*. doi:10.1007/s10439-012-0577-5

Raftopoulos, C., Goffette, P., Vaz, G., Ramzi, N., Scholtes, J.-L., Wittebole, X., & Mathurin, P. (2003). Surgical Clipping May Lead to Better Results than Coil Embolization: Results from a Series of 101 Consecutive Unruptured Intracranial Aneurysms. *Neurosurgery*, *52*(6), 1280–1290. doi:10.1227/01.NEU.0000064568.71648.EC

Raghavan, M. L., Ma, B., & Harbaugh, R. E. (2005). Quantified aneurysm shape and rupture risk. *Journal of neurosurgery*, *102*(2), 355–62. doi:10.3171/jns.2005.102.2.0355

Rahman, M. (2010). Size Ratio Correlates With Intracranial Aneurysm Rupture Status A Prospective Study. *Stroke*, *41*(5), 916–920.

Ramachandran, M. (2012). On The Role of Intracranial Aneurysm Morphology in Stable Versus Unstable Lesions, (May).

Rinkel, G. J., Djibuti, M., Algra, A., & Van Gijn, J. (1998). Prevalence and risk of rupture of intracranial aneurysms: a systematic review. *Stroke; a journal of cerebral circulation*, *29*(1), 251.

Ryu, C., Kwon, O., Koh, J. S., & Kim, E. J. (2011). Analysis of aneurysm rupture in relation to the geometric indices: aspect ratio, volume, and volume-to-neck ratio. *Neuroradiology*, *53*(11), 883.

Sluzewski, M., Menovsky, T., van Rooij, W. J., & Wijnalda, D. (2003). Coiling of very large or giant cerebral aneurysms: long-term clinical and serial angiographic results. *American Journal of Neuroradiology*, *24*(2), 257.

Ujiie, H., Tamano, Y., Sasaki, K., & Hori, T. (2001). Is the aspect ratio a reliable index for predicting the rupture of a saccular aneurysm? *Neurosurgery*, *48*(3), 495–502; discussion 502–3. Retrieved from http://www.ncbi.nlm.nih.gov/pubmed/11270538

Villablanca, J. P. (2002). Detection and characterization of very small cerebral aneurysms by using 2D and 3D helical CT angiography. *AJNR.American journal of neuroradiology*, *23*(7), 1187.

Wakhloo, A. K., Lanzino, G., Lieber, B. B., & Hopkins, L. N. (1998). Stents for intracranial aneurysms: the beginning of a new endovascular era? *Neurosurgery*, *43*(2), 377.

Wakhloo, A. K., Schellhammer, F., De Vries, J., Haberstroh, J., & Schumacher, M. (1994). Self-expanding and balloon-expandable stents in the treatment of carotid aneurysms: an experimental study in a canine model. *AJNR.American journal of neuroradiology*, *15*(3), 493.

Wiebers, D. O., Whisnant, J. P., & O'Fallon, W. M. (1981). The Natural History of Unruptured Intracranial Aneurysms. *New England Journal of Medicine*, *304*(12), 696–8.

Wiebers, D. O. (2003). Unruptured intracranial aneurysms: natural history, clinical outcome, and risks of surgical and endovascular treatment. *The Lancet*, *362*(9378), 103–110.

Wiebers, D. O. (2006). Unruptured intracranial aneurysms: natural history and clinical management. Update on the international study of unruptured intracranial aneurysms. *Neuroimaging clinics of North America*, *16*(3), 383.

van den Berg, R., Rinkel, G. J., & Vandertop, W. P. (2003). Treatment of ruptured intracranial aneurysms: implications of the ISAT on clipping versus coiling. *European Journal of Radiology*, *46*(3), 172–177.

Vega, C., Kwoon, J. V., & Lavine, S. D. (2002). Intracranial aneurysms: current evidence and clinical practice. *American Family Physician*, *66*(4), 601.

Yasuda, R., Strother, C. M., Taki, W., Shinki, K., Royalty, K., Pulfer, K., & Karmonik, C. (2011). Aneurysm volume-to-ostium area ratio: a parameter useful for discriminating the rupture status of intracranial aneurysms. *Neurosurgery*, *68*(2), 310–7; discussion 317–8.

APPENDIX

Aneurysm Sac Isolation Algorithm Flow Chart

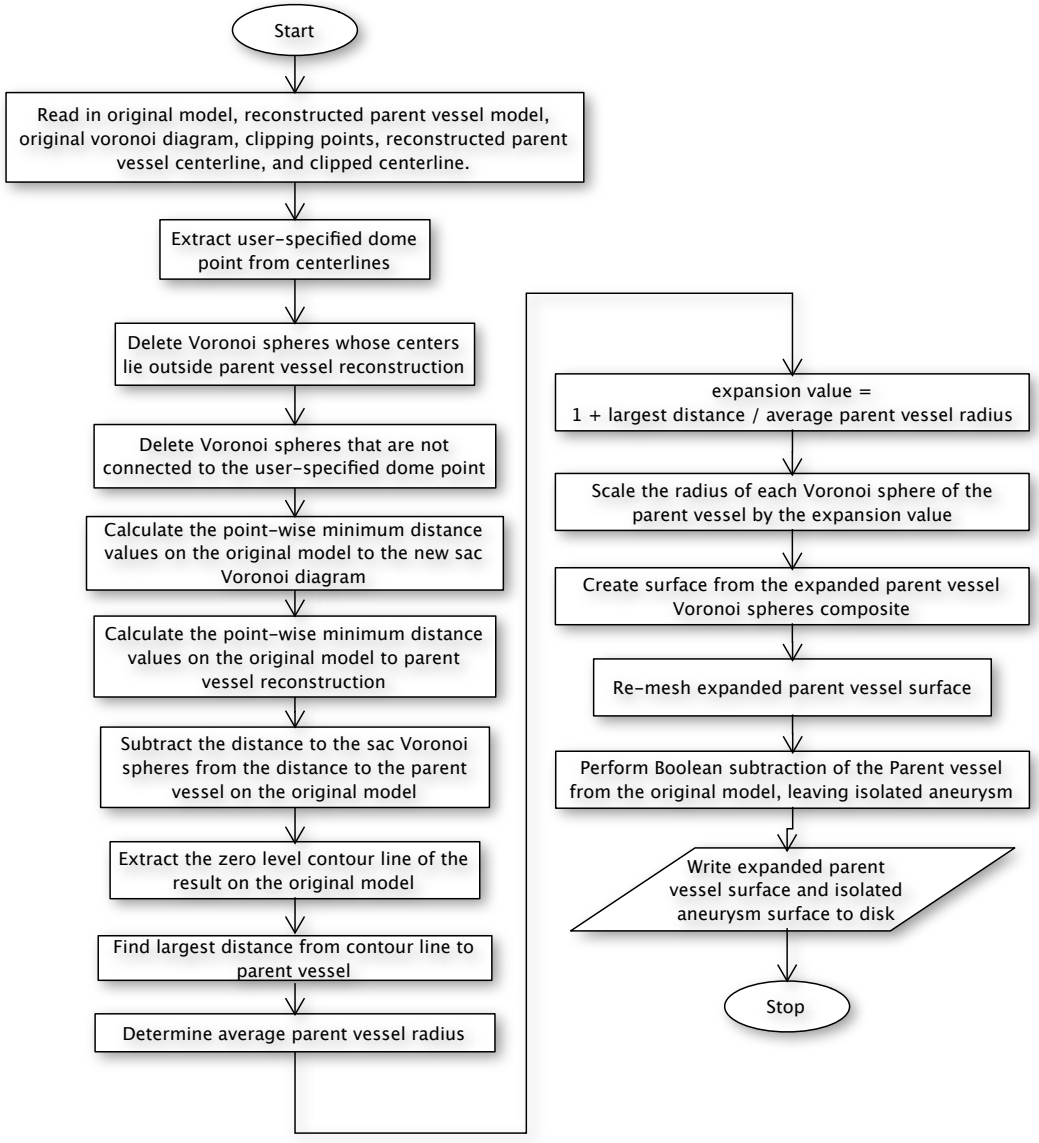

Figure A1. This flow chart takes the output files of the parent vessel reconstruction algorithm (Ford et al., 2009) as input.

Morphological Analysis Algorithm Flow Chart

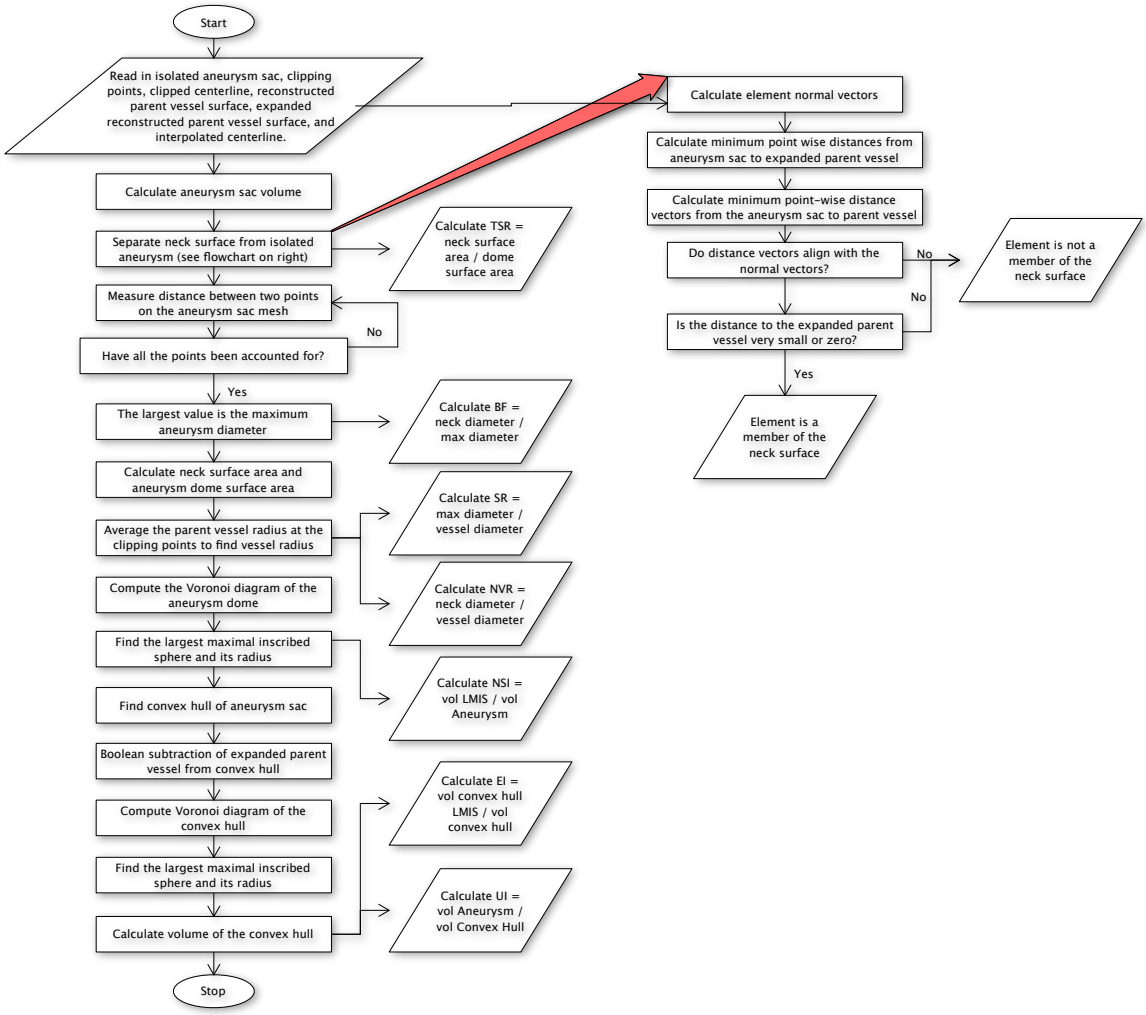

Figure 34. This flow chart takes the output files of the parent vessel reconstruction algorithm (Ford et al., 2009)and the aneurysm sac isolation algorithm as input.